ANALYSIS OF A THUNDERSTORM DOWNBURST

by

John Thomas Distefano

Submitted to the Department of
Meteorology and Physical Oceanography
in Partial Fulfillment of the
Degree of

MASTER OF SCIENCE

at the

MASSACHUSETTS INSTITUTE OF TECHNOLOGY

May 1983

Signature of Author _____
Department of Meteorology
and Physical Oceanography
May 1983

Certified by _____
Kerry Emanuel
Thesis Supervisor

Accepted by _____
Ronald G. Prinn
Chairman, Department Committee on
Graduate Students

ANALYSIS OF A THUNDERSTORM DOWNBURST

by

John Thomas DiStefano

Submitted to the Department of Meteorology
and Physical Oceanography on 15 April 1983 in partial
fulfillment of the requirements for the degree of

Master of Science in Meteorology

ABSTRACT

On 13 April 1981, a downburst occurred near Oklahoma City, Oklahoma. A downburst is a localized very intense downdraft that produces damaging winds, of a divergent character, at or near the surface. A synoptic scale analysis was undertaken to follow the events which led up to this occurrence. A more detailed picture of this downburst was then drawn using observations from a mesonetwork near Oklahoma City.

This analysis implies that the downdraft descended from the middle troposphere. A model based on a similarity theory for unsaturated downdrafts was then used to investigate the idea that downbursts result from evaporatively cooled penetrative downdrafts.

Thesis Supervisor: Kerry Emanuel
Title: Assistant Professor of Meteorology

TABLE OF CONTENTS

LIST OF FIGURES

1. GENERAL DISCUSSION OF DOWNBURSTS

Certain meteorological conditions which led to the crash of an airliner in New York were studied in depth by Fujita and Byers, 1976. They found in their investigation of the accident that the main cause of the crash was very sharp wind changes under a thunderstorm. Investigations were also undertaken for the August 7, 1975 airline accident at Stapleton Airport, Denver and the June 23, 1976 airline accident at Philadelphia International Airport (Fujita and Caracena, 1977). Found in these incidents were very strong downdrafts which were also reported by the pilots. To distinguish between an extremely intense downdraft and a regular downdraft, Fujita(1977) introduced the term 'downburst'. He defines a downburst in 'The Manual of Downburst Identification for Project Nimrod', as a "strong downdraft inducing an outward burst of damaging winds on or near the ground". Damaging winds, 40 M.P.H. or stronger, can be assessed using the F scale (Fujita, 1971). [Refer to Fig. 1.1-1.2]. This scale can be used to determine the classification of damage caused primarily by tornadoes and downbursts.

Another characteristic which distinguishes downbursts from other damaging wind events is that its wind field is highly divergent, in contrast to the damaging winds of a tornadic storm, which are strongly convergent. This wind field analysis has been the deciding factor in many cases in concluding whether a tornado or a downburst

had occurred in a given location. The downburst is associated with a highly localized high pressure disturbance within a thunderstorm. Another high pressure disturbance, occurring on a somewhat greater scale, is associated with the main thunderstorm downdraft. In contrast to the downburst, the damage-causing winds just behind the advancing gust front are only weakly divergent and straight-line.

Fujita (1981) points out that downbursts have diameters of up to 20 km. He distinguishes between downbursts that have path lengths of greater than and less than 5.1 km (3.16 miles), and refers to the latter as microbursts. Also recognized is a system within a downburst in which this system's path appears to resemble that of a tornado, with the exception that it is very divergent. This 'burst swath' has an average width of approximately 100 m. The divergent air flow is recognized as having a pair of cyclonic and anticyclonic circulations on both sides of the swath's centerline.

After reviewing the meteorological conditions during the three airline incidents, Fujita and Byers (1976) coined the term 'downburst' to describe the intense downdraft involved in the accidents. If we discuss the wind shear experienced by the airliners involved in the accidents, it will be found that the conditions were very similar. A landing aircraft will first experience a headwind, where the indicated airspeed increases and there is a gain in altitude, then a downdraft, where the aircraft will drop abruptly, and finally a tailwind. Here the indicated air speed drops and the aircraft loses altitude. Similar events will occur for an aircraft

just lifting off into a downburst. A crosswind shear from a downburst can also affect the maneuverability of the aircraft, causing it to drift to the right or left. The term 'downburst' was defined to describe a downdraft the speed of which is greater than or equal to the approximate rate of descent or climb of a jet aircraft on the final approach or take-off at a height of about 90 m above the ground. Fujita and Caracena (1977) defined 3.6 ms-1 at 90 m above the surface to be the lower limit of the vertical velocity of a downburst.

Downbursts appear to be frequently associated with mesocyclones. A mesocyclone is a rotating feature within a large thunderstorm also known as a supercell. The hook echo, often associated with the mesocyclone, appears to be associated with the "twisting downburst" (Fujita and Caracena, 1977). The damaging winds associated with this twisting downburst are characterized by curved outflow. Another probable indicator of the downburst, pointed out by Fujita (1979), is the "bow echo" (see Figure 1.3). The initial stage in the evolution of the bow echo, as illustrated in the figure, appears as a tall echo region within the thunderstorm preceded by a gust front along its leading edge. In the next stage, the downburst seems to extend from the tall echo and distorts the line echo into a bow-shaped bulge. In the mature stage, the bow echo may take the shape of a "spearhead echo" (Fujita and Byers, 1977). This type of radar echo is characterized by a pointed appendage extending toward the direction of the echo motion. The appendage moves faster than

the parent echo which is drawn into the appendage. During its mature stage, the appendage becomes a major echo and the parent echo loses its identity. The downburst weakens within a short period of time after it has pushed ahead of its parent echo. At this time, it would appear that a mesoscale circulation dominates the area of the bow echo. In the final stage, the bow echo may turn into a comma-shaped echo which gradually disappears along with the mesoscale circulation (Fujita, 1981).

It should be of interest to compare the vertical velocities associated with downbursts and the velocities of downdrafts observed in the Thunderstorm Project, which was conducted in Florida and Ohio during 1946-47. According to the project statistics, the mean downdraft values increased from zero at the surface to approximately 3.1 ms^{-1} at the 4000 ft. level. The high values here are three times that of the mean vertical values (Byers and Braham, 1947). We know that the vertical velocities measured in a downburst of approximately 3.6 ms^{-1} at a level of about 90 m above the surface (minimum value by definition) are about ten times the mean downdraft speed that has been estimated from the data compiled during the Thunderstorm Project.

There appears to be some controversy concerning the source height of downbursts. Fujita and Caracena (1977) considered the possibility of a long distance descent of cloud top air possibly triggered by the collapsing phase of an overshooting cloud top. Lemon and Doswell (1979) proposed that a pressure-induced rear-flank

downdraft originates at or near the jet stream level. Emanuel (1981) used penetrative downdrafts to help explain downbursts. In a severe thunderstorm, a penetrative downdraft may occur when cool, dry air overlying cloudy air of high liquid water content is driven downward by evaporative cooling.

This thesis is concerned with the analysis of a downburst which occured in Oklahoma on 13 April 1981. The large-scale meteorological situation, including surface and upper air analysis, which accompanied this downburst, is discussed in Chapter III. Chapter IV looks at a mesoscale analysis of the downburst over a mesonetwork of observational recording stations in the Oklahoma City area. This mesonetwork and also the data used in the analysis of this case is introduced in Chapter II. The idea regarding the downburst as a penetrative downdraft (Emanuel, 1981) is implemented in Chapter V by means of a similarity model for a penetrative thermal. Some conclusions are drawn in the final chapter.

F-SCALE DAMAGE SPECIFICATIONS

F0 18-32 m/s (35-63 kts), (40-72 mph): LIGHT DAMAGE
Some damage to chimneys; break branches off trees; push over shallow rooted trees; damage sign boards.

F1 33-49 m/s (64-97 kts), (73-112 mph): MODERATE DAMAGE
The lower limit (73 mph) is the beginning of hurricane wind speed; peel surface off roofs; windows broken; mobile homes pushed off of foundations or overturned; some trees uprooted or snapped; moving automobiles pushed off the roads.

F2 50-69 m/s (98-136 kts), (113-157 mph): CONSIDERABLE DAMAGE
Roofs torn off frame houses leaving strong upright walls; weak buildings in rural areas demolished; mobile homes demolished; railroad box cars pushed over; large trees snapped or uprooted; light-object missiles generated; cars blown off highway.

F3 70-92 m/s (137-179 kts), (158-206 mph): SEVERE DAMAGE
Roofs and some walls torn off well constructed houses; trains overturned; steel-framed hanger-warehouse type structures torn; heavy cars lifted off ground and thrown; most trees in forest uprooted, snapped, or leveled.

F4 93-116 m/s (180-226 kts), (207-260 mph): DEVASTATING DAMAGE
Whole frame houses leveled, leaving piles of debris; steel structures badly damaged; structures with weak foundations blown off some distance; trees debarked by small flying debris; cars and trains thrown some distances or rolled considerable distances; large missiles generated.

F5 117-142 m/s (227-276 kts), (261-318 mph): INCREDIBLE DAMAGE
Strong frame houses lifted off foundations and carried considerable distance to disintegrate; steel-reinforced concrete structures badly damaged; automobile-sized missiles generated; trees debarked; incredible phenomena will occur.

F6 143 m/s to Mach 1: INCONCEIVABLE DAMAGE
Maximum wind speeds of tornadoes and downbursts are not expected to reach the F6 wind speeds.

Figure 1.1

DAMAGING WIND SCALE BY FUJITA

Scale	m / sec	Knots	mph	Expected Damage
F 0	17.8- 32.6	35- 63	40- 72	LIGHT DAMAGE
F 1	32.7- 50.3	64- 97	73-112	MODERATE DAMAGE
F 2	50.4- 70.3	98-136	113-157	CONSIDERABLE DAMAGE
F 3	70.4- 91.9	137-179	158-206	SEVERE DAMAGE
F 4	92.0-116.6	180-226	207-260	DEVASTATING DAMAGE
F 5	116.7-142.5	227-276	261-315	INCREDIBLE DAMAGE

From SMRP Research Paper Number 91.

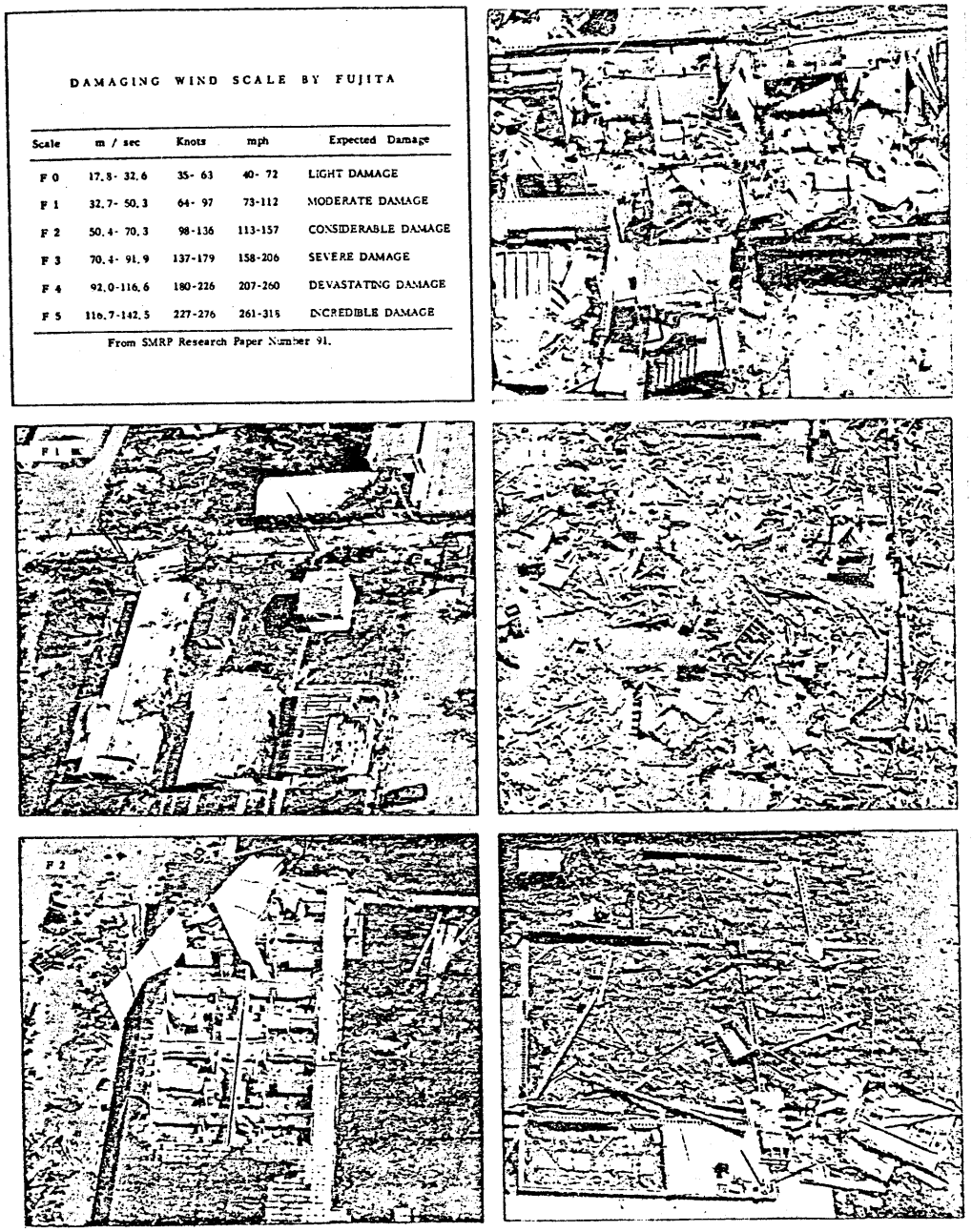

Figure 1.2

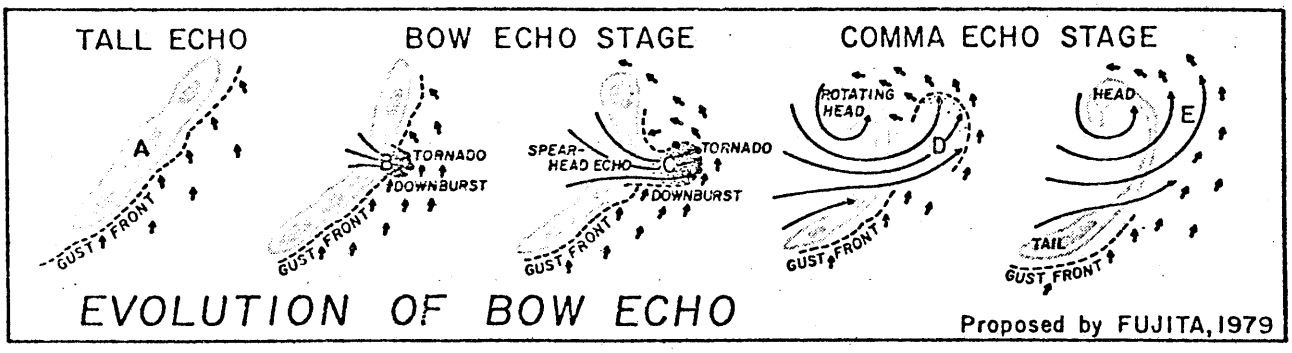
TALL ECHO
BOW ECHO STAGE
COMMA ECHO STAGE
A
B
C
D
E
GUST FRONT
TORNADO
DOWNBURST
SPEAR-HEAD ECHO
ROTATING HEAD
HEAD
TAIL
EVOLUTION OF BOW ECHO
Proposed by FUJITA, 1979

Figure 1.3

2. DATA SOURCES

In order to analyze the synoptic situation, we used hourly surface weather reports from 2000 GMT on 13 April 1981 to 0400 GMT on 14 April 1981 within, approximately, an area of 1550 square km, centered around Oklahoma. Upper air analyses were constructed using observations reported at 850, 500, and 300 mb with a centered time of 0000 GMT on 14 April 1981. A radar summary for 2335 GMT on 13 April 1981 was used for comparison with surface observations.

For the mesoscale analysis, the 1981 National Severe Storms Laboratory (NSSL) mesonetwork (MESONET), Figure 2.1, was utilized. Centered in the mesonet is Oklahoma City, which is surrounded by numerous recording stations (which are numbered) and within a smaller radius by several FAA operated stations, which are marked by directional coordinates. Norman, Oklahoma is located in the southeast corner of the mesonet, while Tuttle is approximately 8 km to the north-northeast of station number 26 in the southwest corner of the mesonet and another recording station, the KTVY-Tower, is located more than 8 km to the northwest of station number 3. This mesonet has an area of approximately 45 squared kilometers.

The numbered stations recorded data from 0100-1000 GMT on 14 April 1981 for each minute of every hour. Data which were useful in the analysis included temperature (DRY BULB and WET BULB), equivalent potential temperature (calculated using the wet bulb temperature), pressure, wind speed and direction, maximum wind speed over a one

minute's time interval and relative humidity. The FAA stations give only wind direction and speed. The data from these stations were taken from 2122 CST (0322 GMT) to 2148 CST (0348 GMT) on 14 April 1981 (GMT). Approximately seven reports were made every minute. During analysis of these lettered stations, a one-minute average centered about the specified time was taken. The KTVY-Tower reported temperature (dry bulb) and wind speed and direction, at elevations of 26, 45, 90, 177, 266 and 444 meters, as well as at the surface. Wet bulb readings were taken at the surface, 90, 266, and 444 meters. Pressure was measured at the surface. Data were recorded from 0245 GMT on 14 April 1981 through 0425 GMT on 14 April 1981 at a rate of up to forty observations per minute. Again, the data were averaged over one-minute intervals.

Obtained from NSSL were soundings for Tuttle and Edmond, Oklahoma, at 0205 and 0323 GMT for the former and 0130 and 0324 GMT for the latter. The Edmond soundings were not used due to very obvious recording errors. The Oklahoma City sounding of 0000 GMT on 14 April 1981, was useful in the investigation of this case study.

The actual data that were used in the model of the penetrative thermal were taken from the NSSL sounding at Tuttle at 0205 GMT on 14 April 1981.

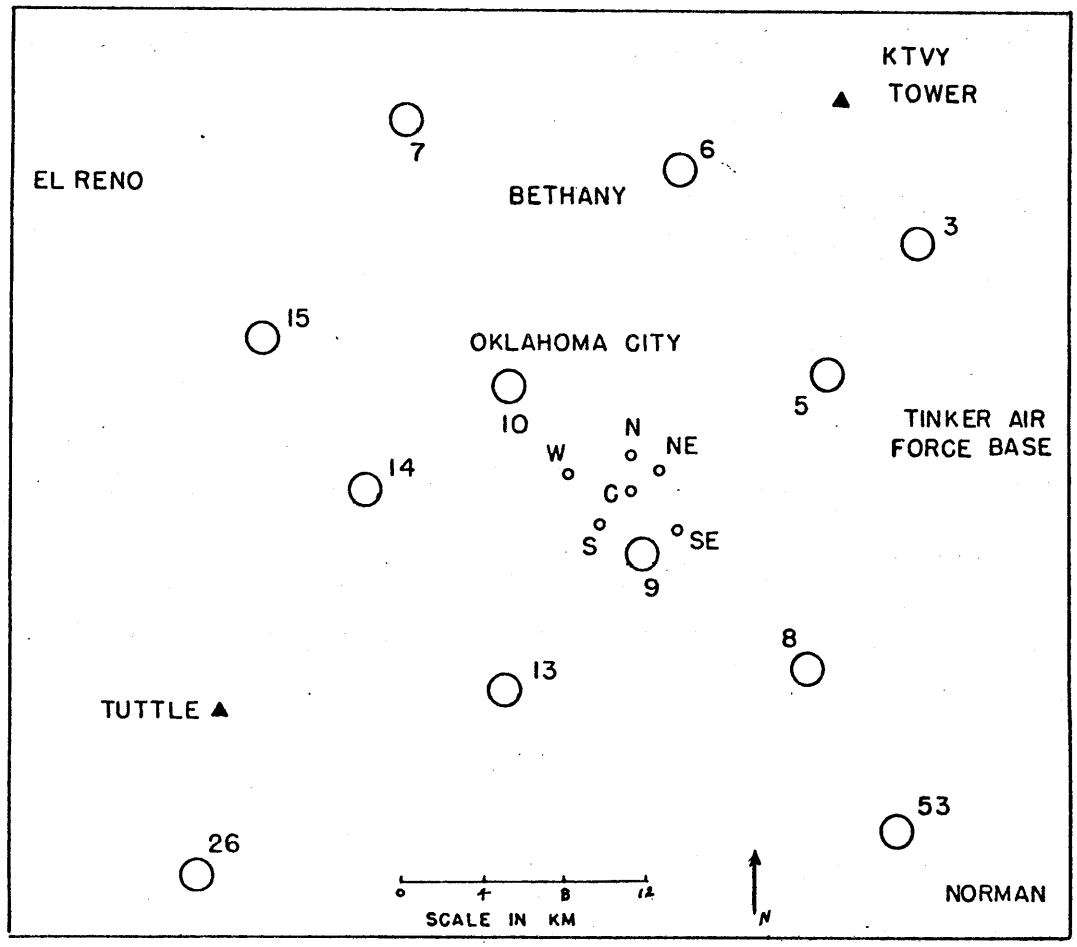
KTVY
TOWER
7
6
EL RENO
BETHANY
3
15
OKLAHOMA CITY
5
10
N
W
NE
TINKER AIR
FORCE BASE
14
C
S
SE
9
8
13
TUTTLE
53
26
0
4
8
12
SCALE IN KM
N
NORMAN

Figure 2.1

3. LARGE SCALE ANALYSIS

a. Surface Analysis

At 2100 GMT, just a little more than six hours prior to the arrival of the severe weather in the Oklahoma City area, the main feature on the surface map (Figure 3.1) in the central and south-central plains region is a cold front which extends from northern Iowa, southwestward through the northwestern corner of Missouri into northeastern Kansas and then continues southwestward into the Texas and Oklahoma panhandle and west-northwestward through northwestern New Mexico and southern Colorado. The lowest pressure, in the vicinity of the front, appears to be in the northeastern part of Kansas extending into northwestern Missouri. The pressure is just under 1008 millibars in this area. In advance of the front, the component of the wind is mainly from the south. Temperatures here are predominantly in the upper 20's and lower 30's (degree C). Dewpoints are in the upper teens to lower 20's (degree C) in the area eastward from the Texas-Oklahoma panhandle and southward from this region.

This air is at some stations close to saturation, though the dewpoints are much lower in New Mexico. Behind the front, the wind veers sharply into the north and northwest and is quite strong (gusts to near 30 kts.). Temperatures start to fall off upon passage of the front from the upper 20's (degrees C) to the lower teens about 400 km

behind the front. Some light rain is falling in the Texas panhandle and thunderstorms are occurring in New Mexico and also in southeastern Iowa. The air dries out behind the front with no reports of precipitation.

Three hours later, (Figure 3.2) 0000 GMT, 14 April 1981, the front has progressed about 50 km to the southeast into Iowa, northwestern Missouri and eastern Kansas. In this area, its movement has been at approximately 10 kts. Further to the southwest, the front has pushed through Gage, Oklahoma and Amarillo, Texas. This part of the front progressed at more than 25 kts to the south and southeast. From just south of Amarillo, the front curves off to the northwest through northwestern New Mexico as a stationary front. Temperatures and dewpoints preceeding the front varied little in three hours. A strong windshift of up to 180 degrees accompanied the frontal passage. A rather strong temperature gradient has developed, and reaches magnitudes, in some places, of approximately 10 degrees C per 100 km. The radar summary for 2335 GMT, 13 April 1981, (Figure 3.4), shows echoes along the cold front from Iowa southwestward through Kansas and into the Texas-Oklahoma panhandle. A tornado watch was issued for the frontal region in southern Iowa, northwestern Missouri and northeastern Kansas and thunderstorms were reported in this area at the time of the 0000 GMT surface analysis. Radar also showed developing showers to the northwest of the tornado watch area extending into eastern Nebraska. More important to the Oklahoma City area is a severe thunderstorm watch that was issued for

the Texas panhandle southward to San Angelo, Texas. Cloud tops of up to 52,000 ft. are associated with these thunderstorms. This band of thunderstorms moved to the northeast at 20 kts and its leading edge reached Oklahoma City at or about 0300 GMT on the 14th.

By 0300 GMT, Figure 3.3 shows the positions of the fronts. Temperatures over the entire region have dropped several degrees C, due to the absence of solar heating, whereas the dewpoints have held nearly steady over the last three hours. The cold front accelerated somewhat to a speed of about 30 kts. A windshift of up to 180 degrees is still quite evident at the front. There is very strong low-level convergence along the front, especially in Oklahoma. Thunderstorms are in evidence just to the west of Oklahoma City, where observations indicate that lightning was visible to the southwest of the city extending northward and moving to the east. A short time later, Oklahoma City experienced a very strong thunderstorm with heavy rains, strong winds and a windshift accompanied by at least a 7 degree C drop in temperature within several minutes.

b. Upper Air Analysis

The 850 mb chart for 12Z, 13 April 1981 (Figure 3.5), shows a trough of low pressure with its axis extending from Hudson's Bay southward through Minnesota and then southwestward into Nebraska and Kansas then into Colorado. A large split-centered ridge of high

pressure dominates the eastern third of the nation. This ridge is associated with southerly winds through Texas and into Oklahoma. Twelve hours later, (Figure 3.6), the 850 mb analysis shows that the axis of the trough has moved east-northeastward at approximately 15 kts., to a position over Hudson's Bay extending southward through Lake Superior and Wisconsin and then southwestward through the Texas-Oklahoma panhandle. Cyclonic vorticity is evident at this level in the panhandle region, and the ridge of high pressure is still the dominant feature in the east as it continues to bring a moist flow over Texas and on toward Oklahoma. By 12Z on 14 April 1981 (Figure 3.7), the trough has continued to move to the east and northeast.

The 500 mb chart for 12Z, 13 April 1981 (Figure 3.8), shows a short wave trough over the northern and central Rocky Mountain area. Meanwhile a ridge dominating the southeastern quarter of the nation, is associated with the flow of very moist air from New Mexico, northwestern Mexico and western Texas into Oklahoma. Twelve hours later (Figure 3.9), the 500 mb analysis shows that the short wave trough has progressed eastward at some 25 kts to a position over the northern plains. The southeastern ridge still dominates that part of the country, with a continuation of a moist flow in nearly the same area as that shown earlier in the 12Z analysis. By 12Z, 14 April 1981, the 500 mb analysis (Figure 3.10) reveals that the short wave has progressed further to the east. The 500 mb vorticity pattern for the sequence covering 12Z, 13 April 1981-12Z, 14 April 1981 (Figures 3.11-3.13) shows anticyclonic vorticity advection over

the Oklahoma City area early in this period, and cyclonic vorticity advection over this area for the remainder of the period beginning at approximately 0000 GMT. This cyclonic vorticity shows up well, in this area, on the 500 mb wind field analysis at 00Z and 12Z on 14 April 1981 (Figures 3.9, 3.10).

A 48 hour sequence of 300 mb analyses, centered at 00Z, 14 April 1981 (Figures 3.14-3.16), shows a trough with an associated jet over the northwestern United States at 00Z, 13 April 1981. This trough continues to progress to the east at approximately 25-30 kts. The flow over the Oklahoma region is rather steady through the period, with west to southwest winds averaging 40 knots or more.

The Tuttle sounding for 0205 GMT, 14 April 1981 (Figure 3.17) shows deep conditional instability and a moist surface boundary layer. Also evident, is the presence of a dry air mass above the surface boundary layer which could provide the potential for downdrafts due to evaporative cooling. Also notice a stable layer (an inversion) above the moist surface boundary layer. This inversion will prevent deep convection from occurring until there appears a mechanism for removing this "cap". A likely mechanism in this case is vertical motion associated with the strong surface cold front. In the vertical, there is veering with height of the wind, but the vertical shear is modest. Another sounding (Figure 3.18) taken at Tuttle at 0323 GMT, 14 April 1981 shows that the inversion has been broken and that the sounding is almost totally within cloud.

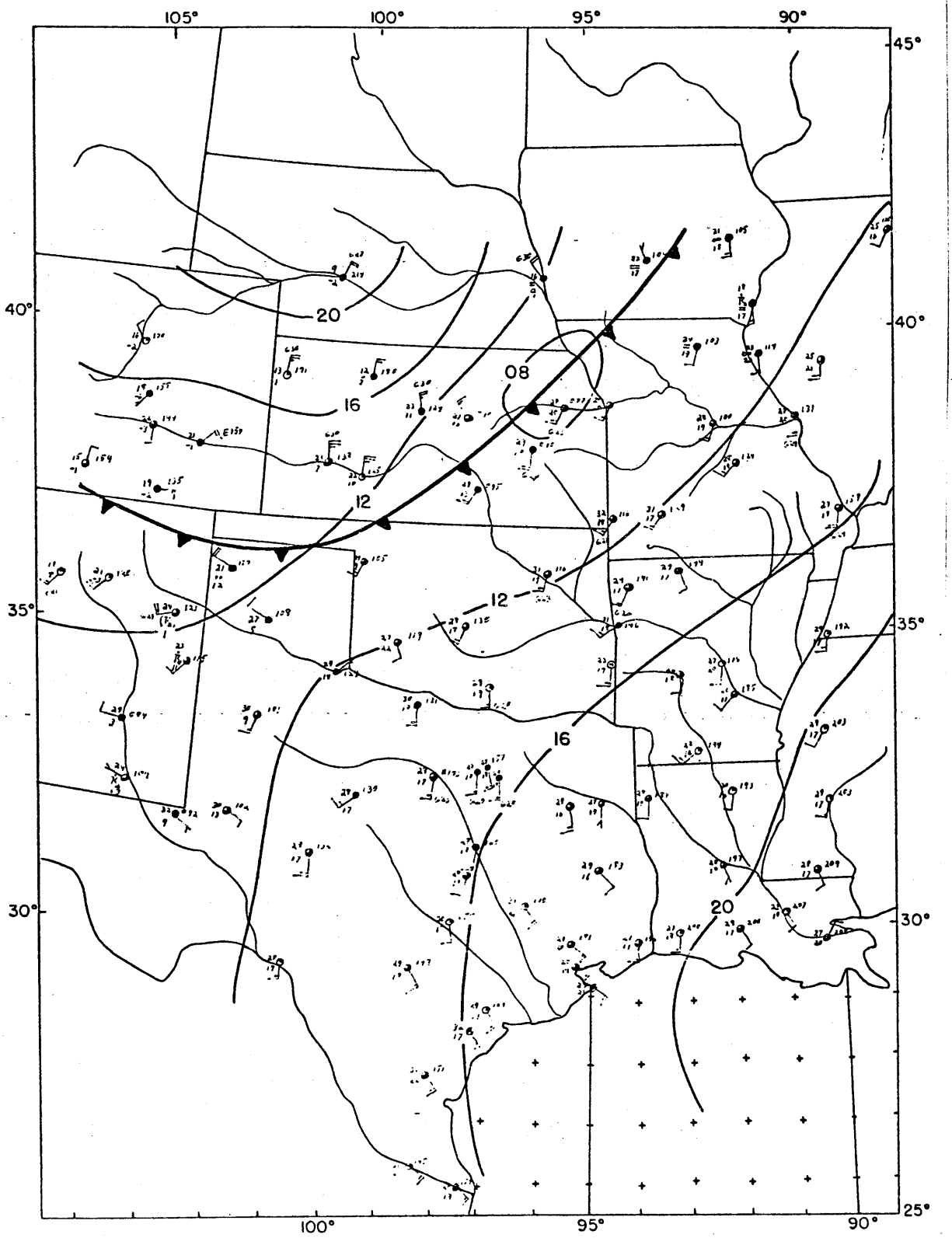

Figure 3.1

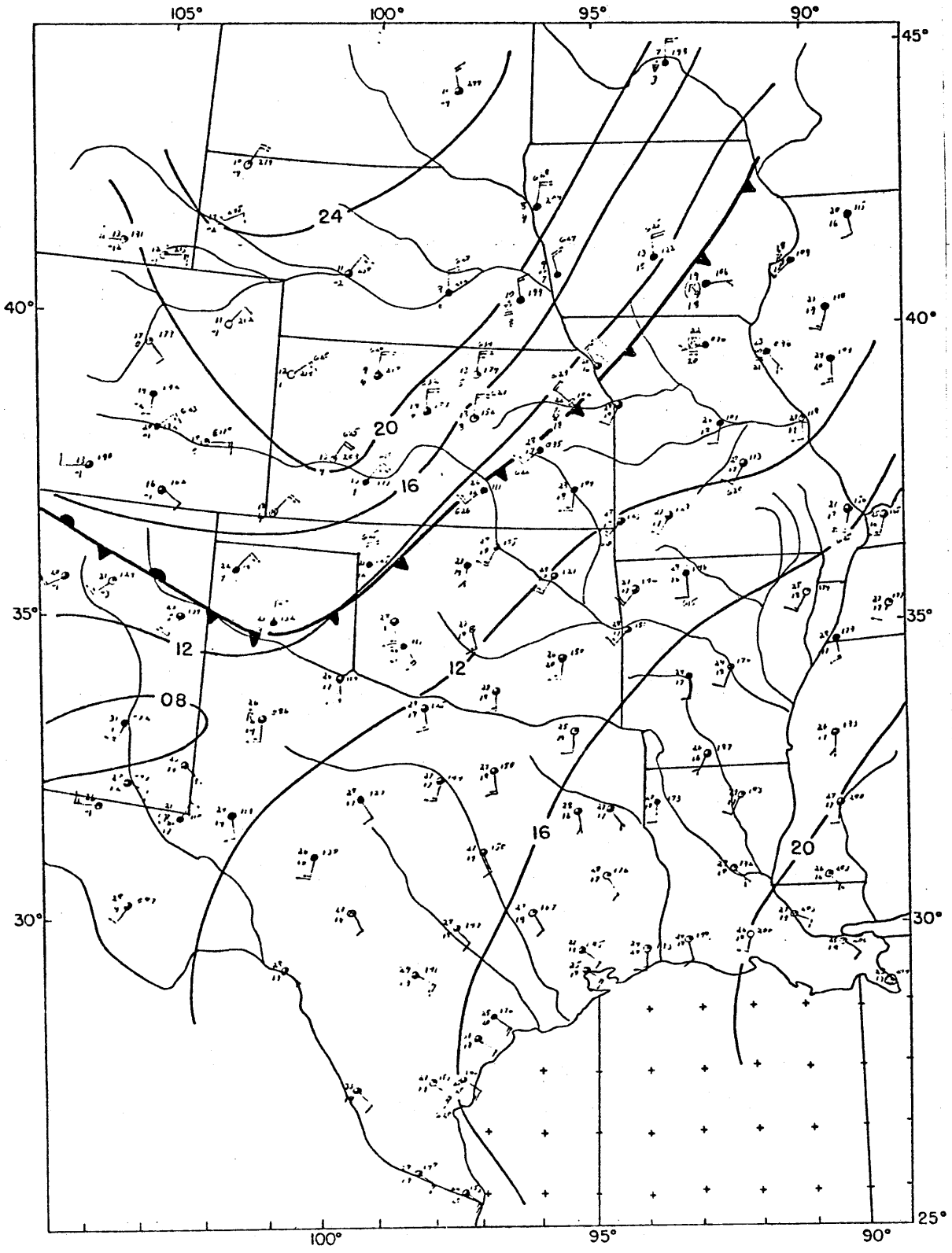

Figure 3.2

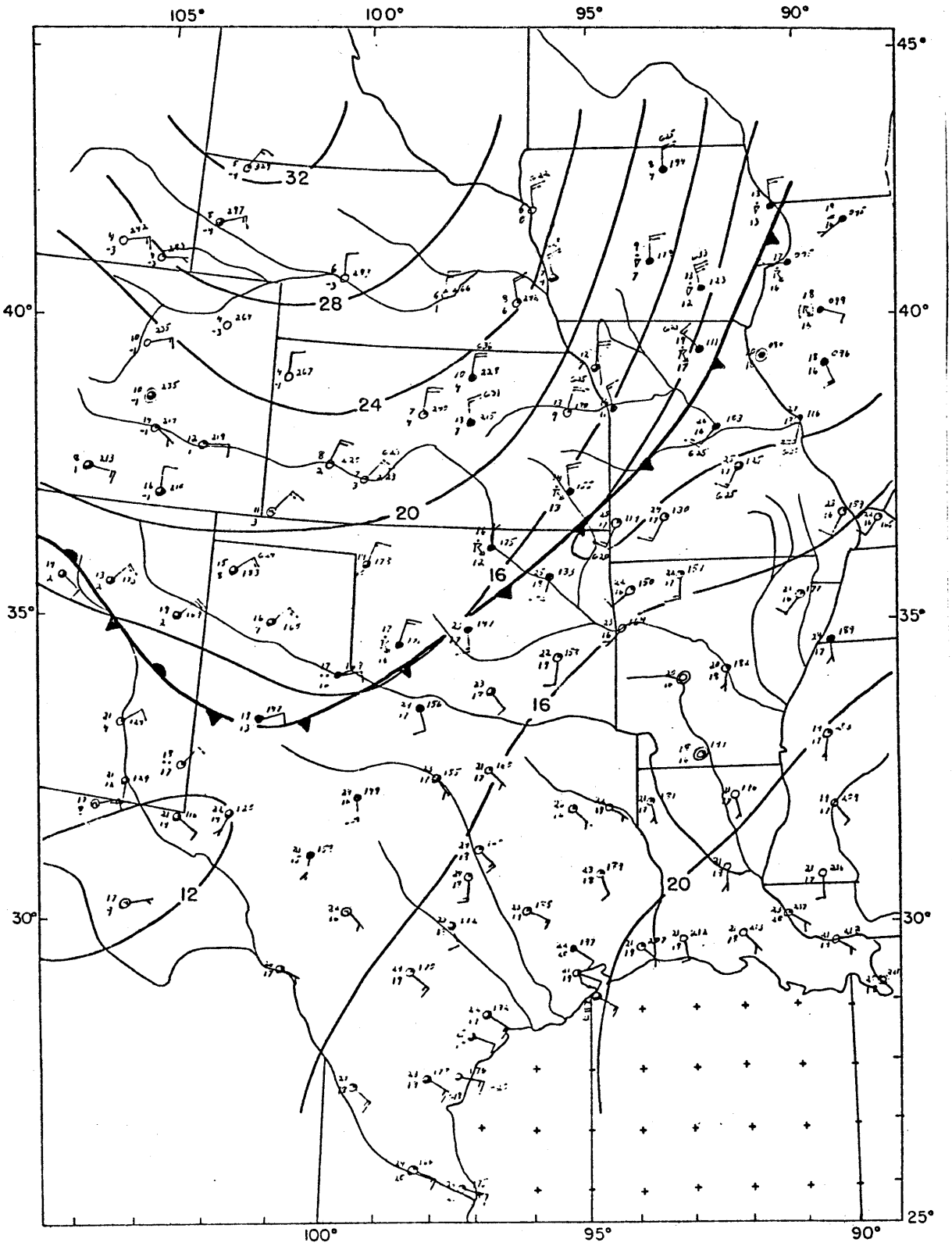

Figure 3.3

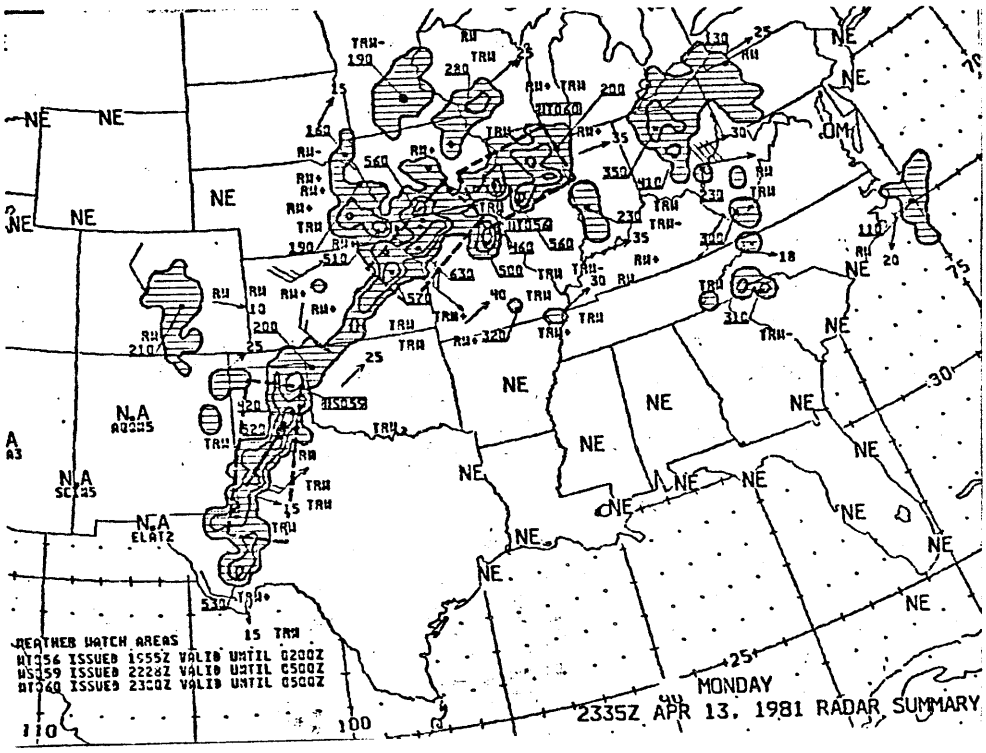

Figure 3.4

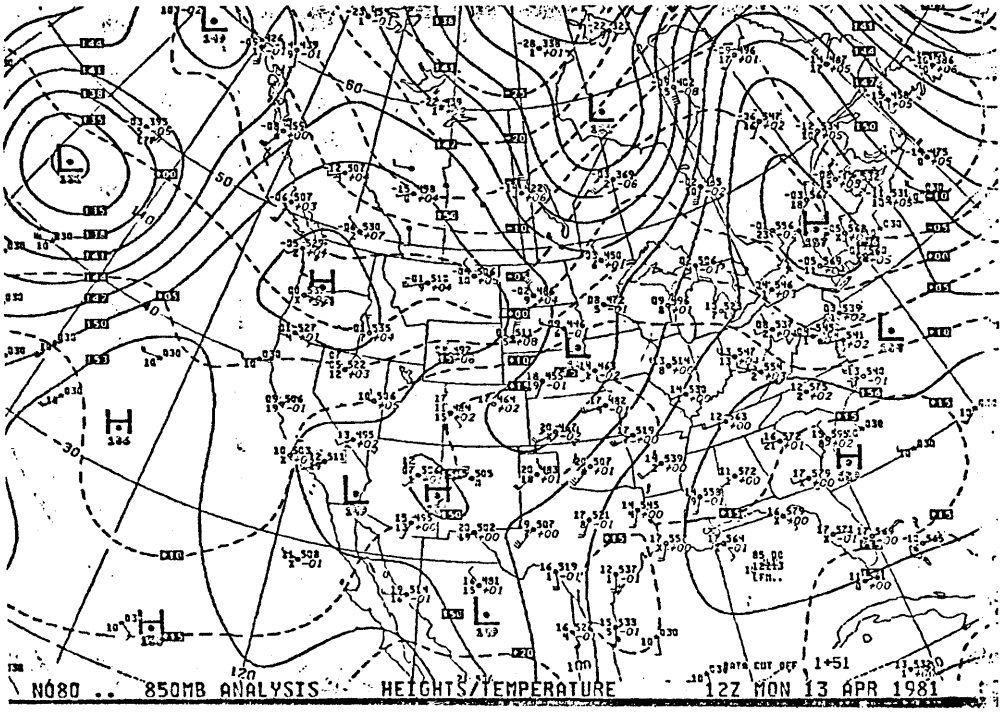

Figure 3.5

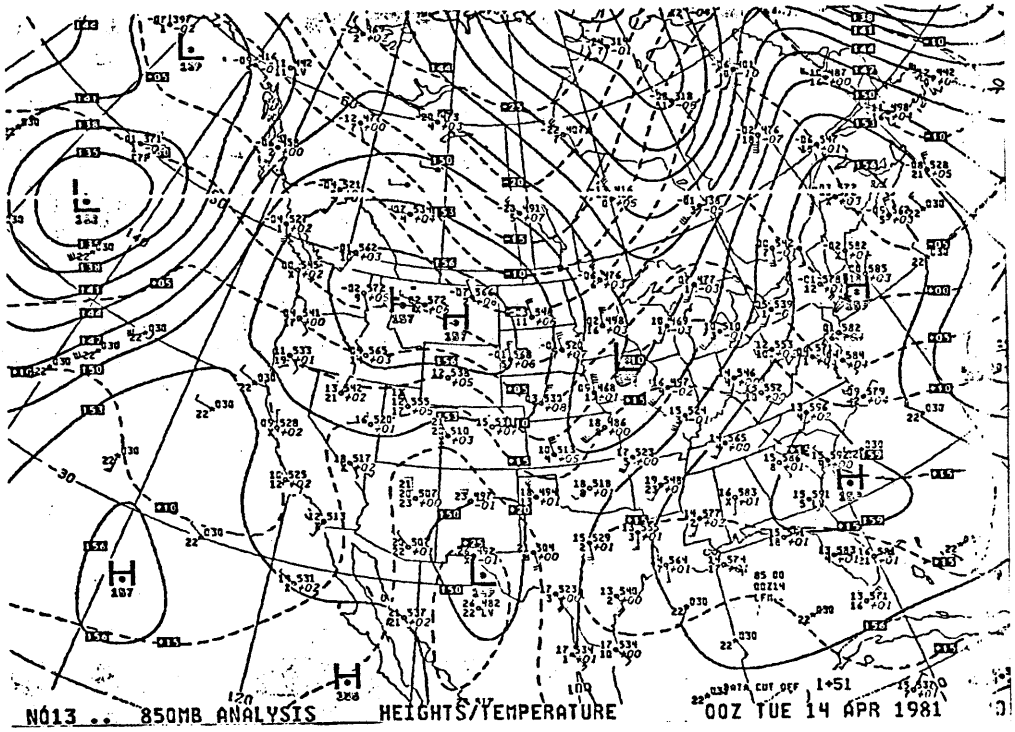

Figure 3.6

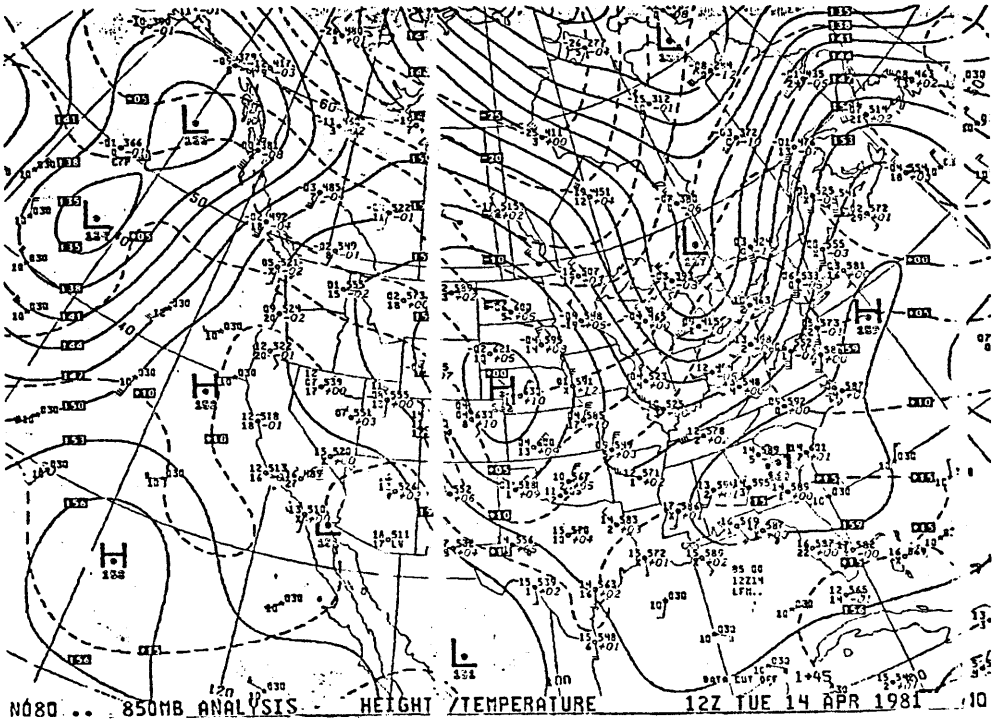

Figure 3.7

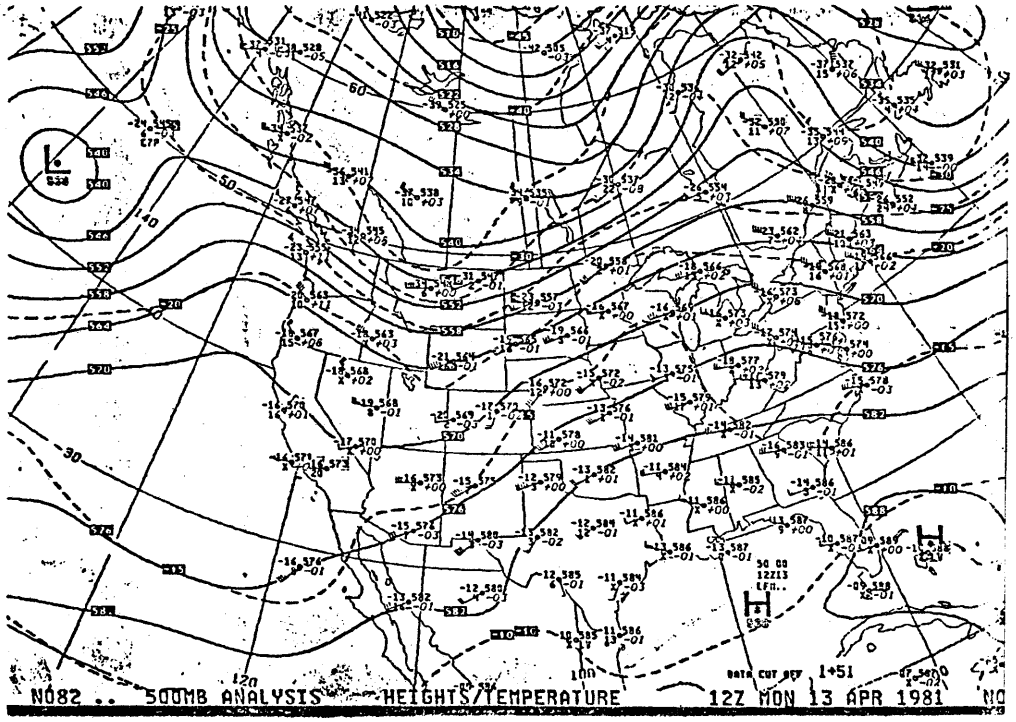

Figure 3.8

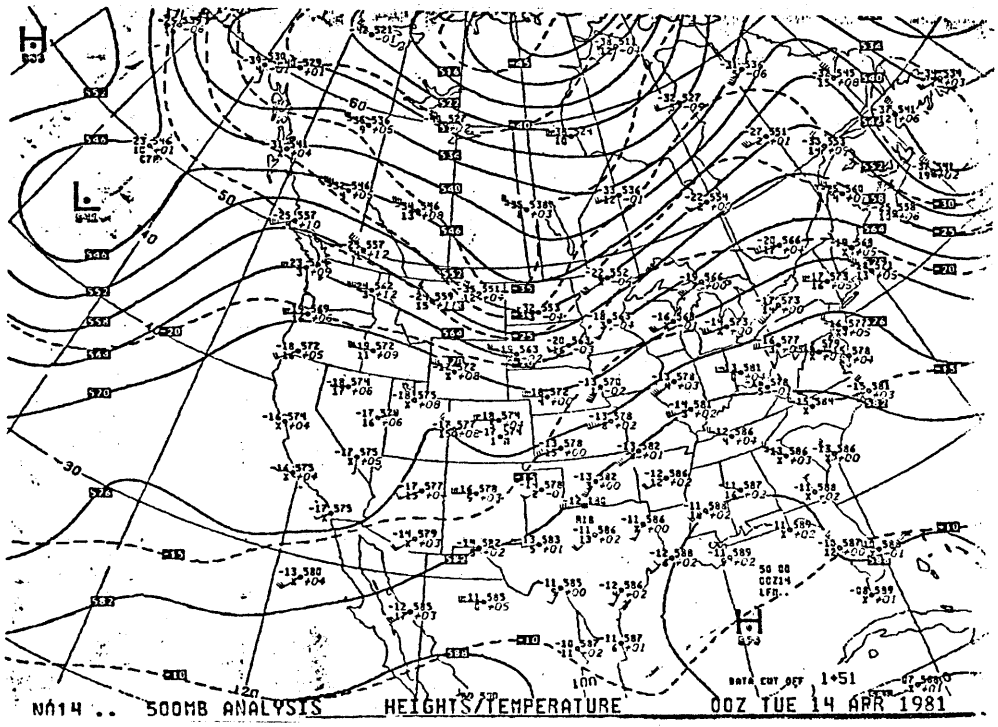

Figure 3.9

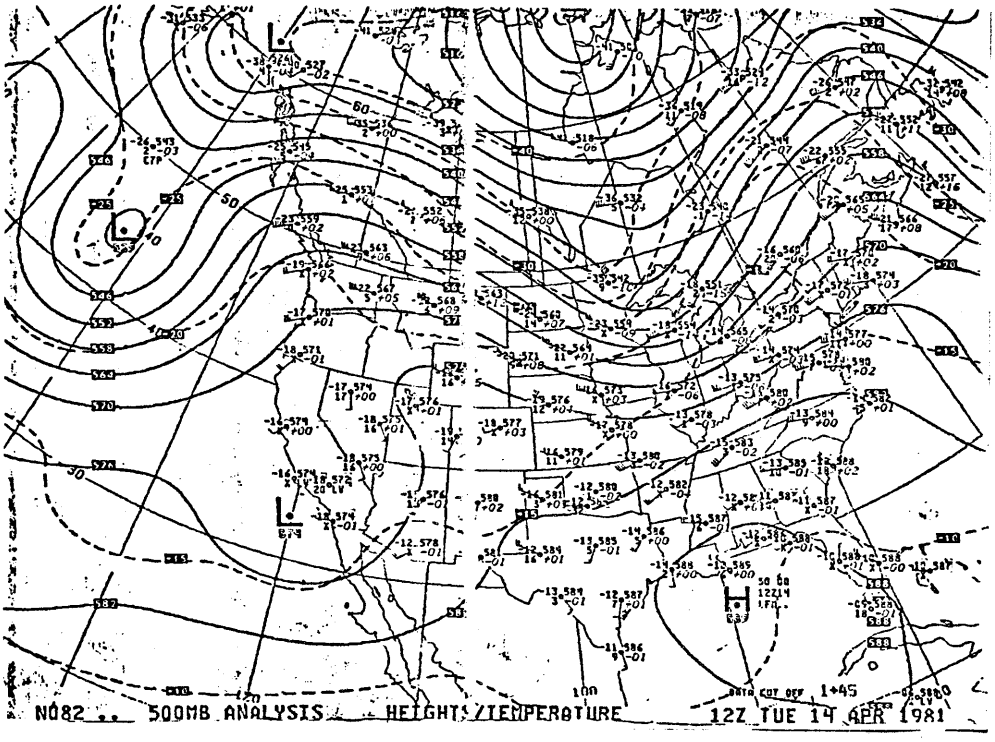

Figure 3.10

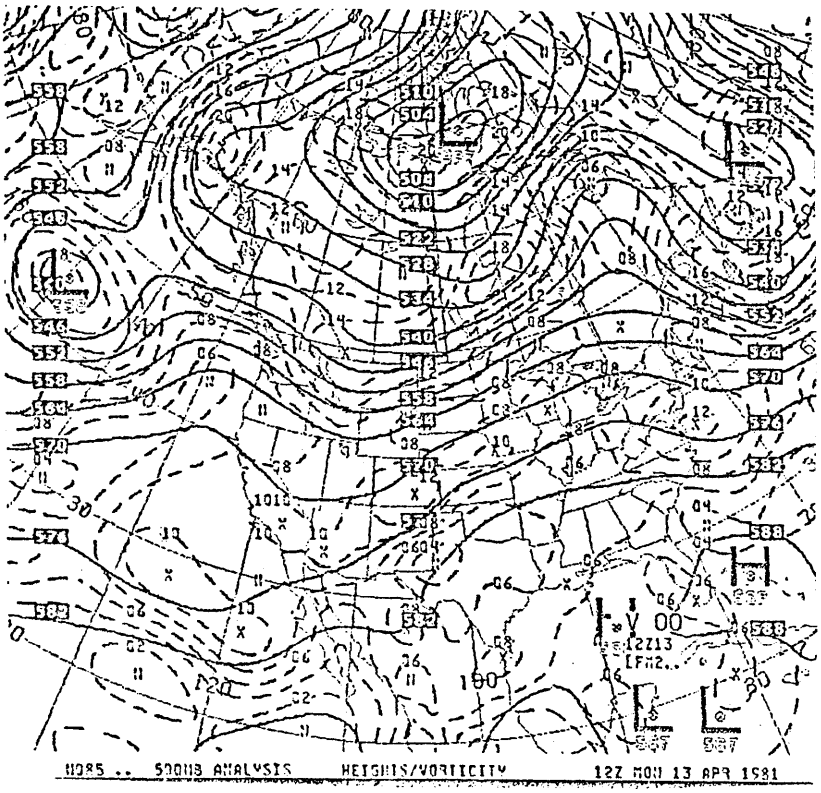

Figure 3.11

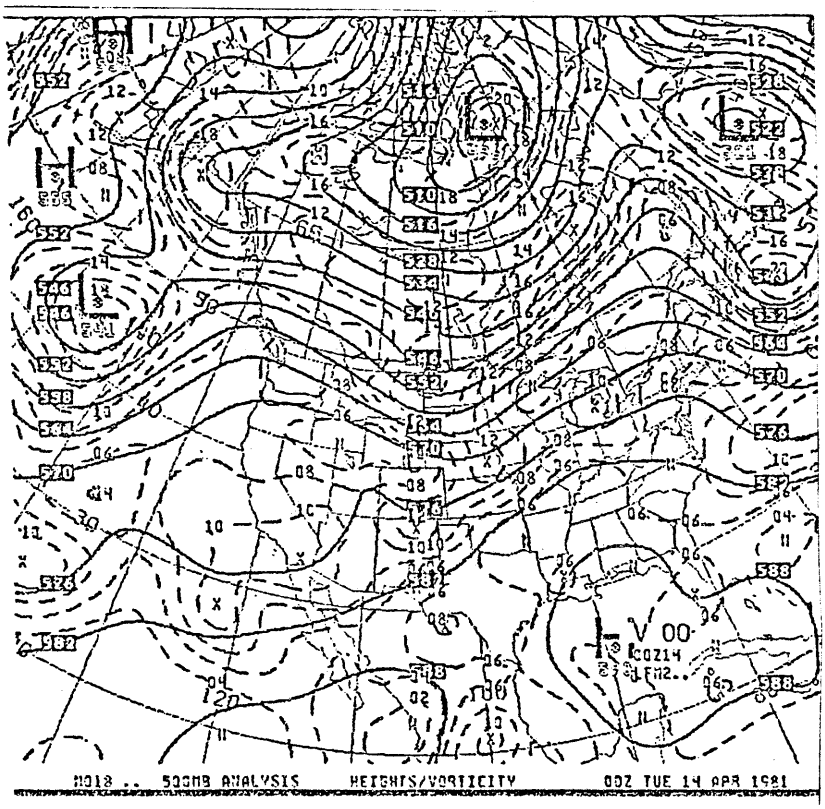

Figure 3.12

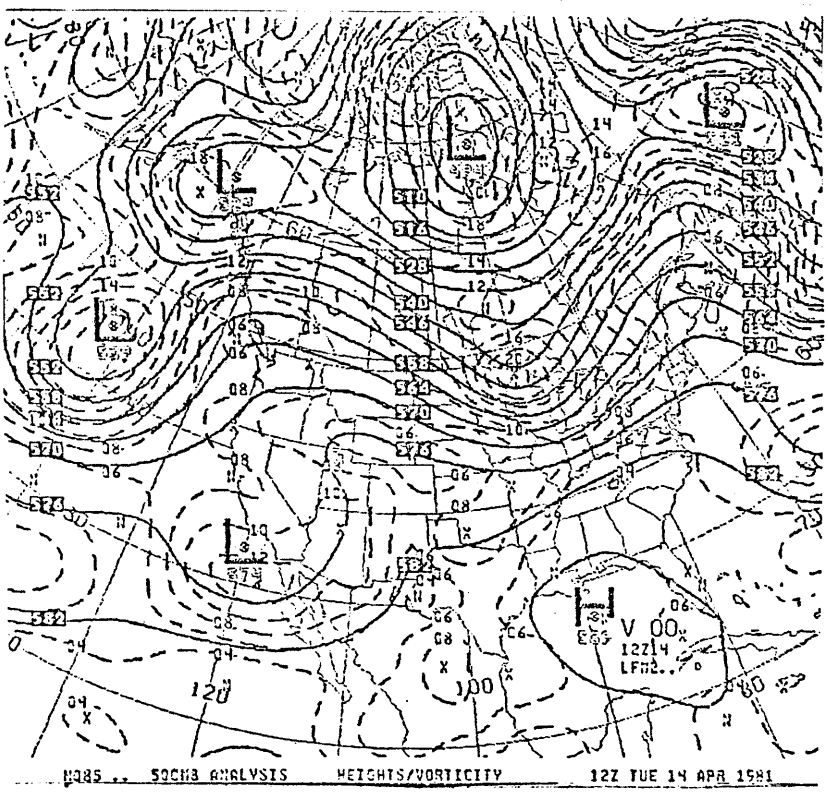

Figure 3.13

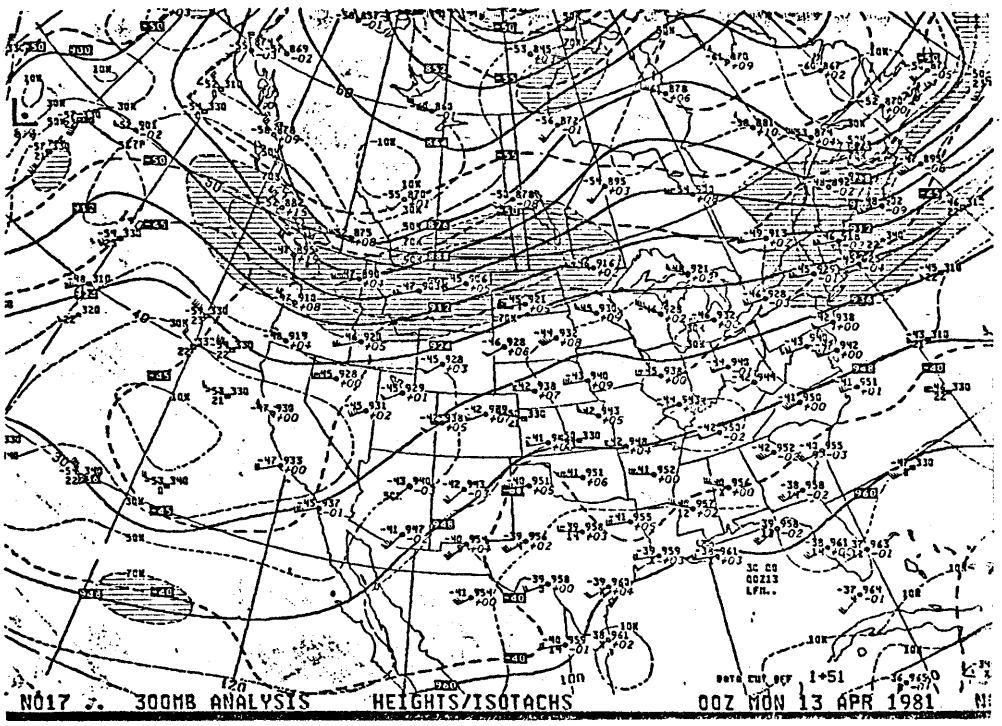

Figure 3.14

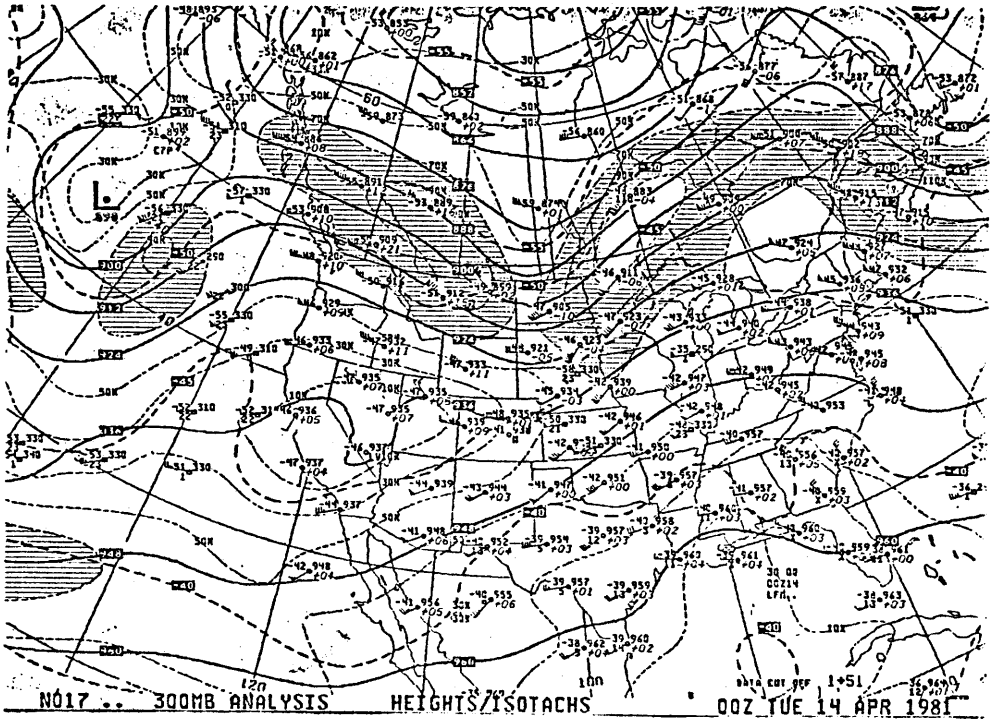

Figure 3.15

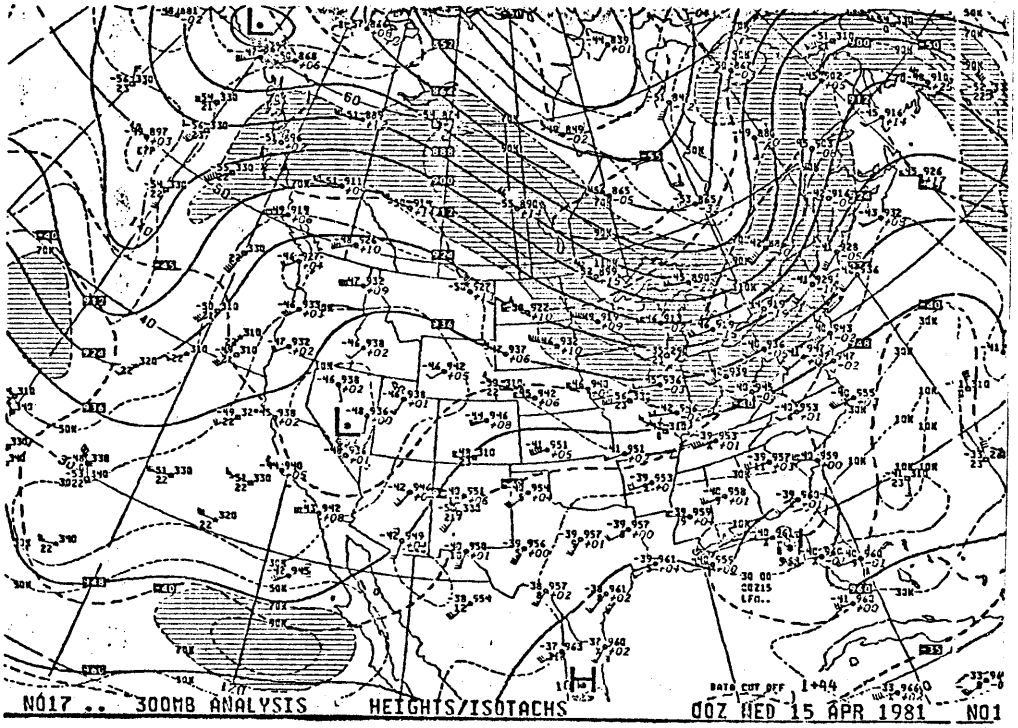
N017 .. 300MB ANALYSIS HEIGHTS/ISOTACHS
00Z WED 15 APR 1981
N01

Figure 3.16

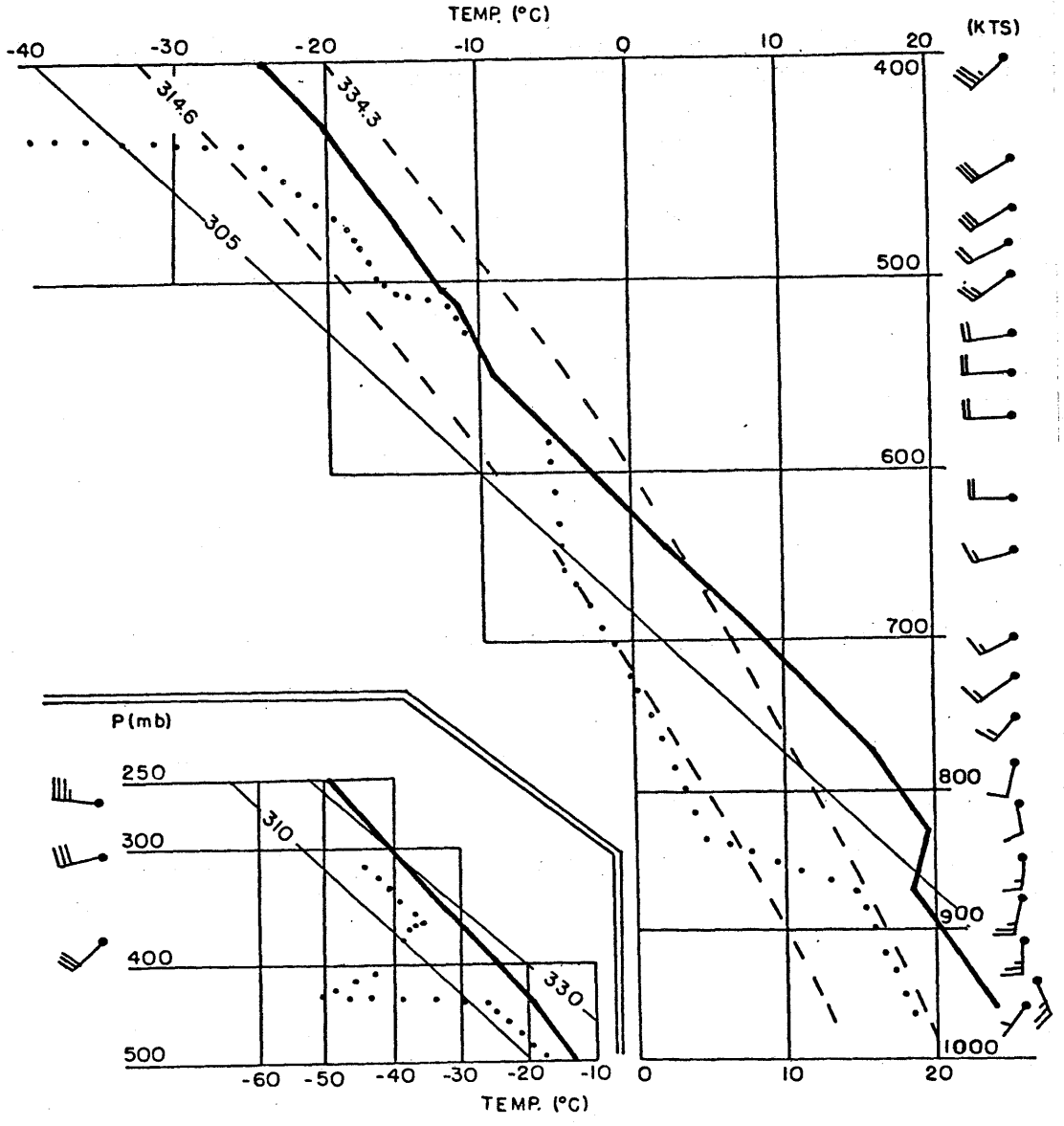
TEMP. (°C)
-40
-30
-20
-10
0
10
20
(KTS)
400
500
600
700
800
900
1000
314.6
334.3
305
P(mb)
250
300
400
500
310
330
-60
-50
-40
-30
-20
-10
0
10
20
TEMP. (°C)

Figure 3.17

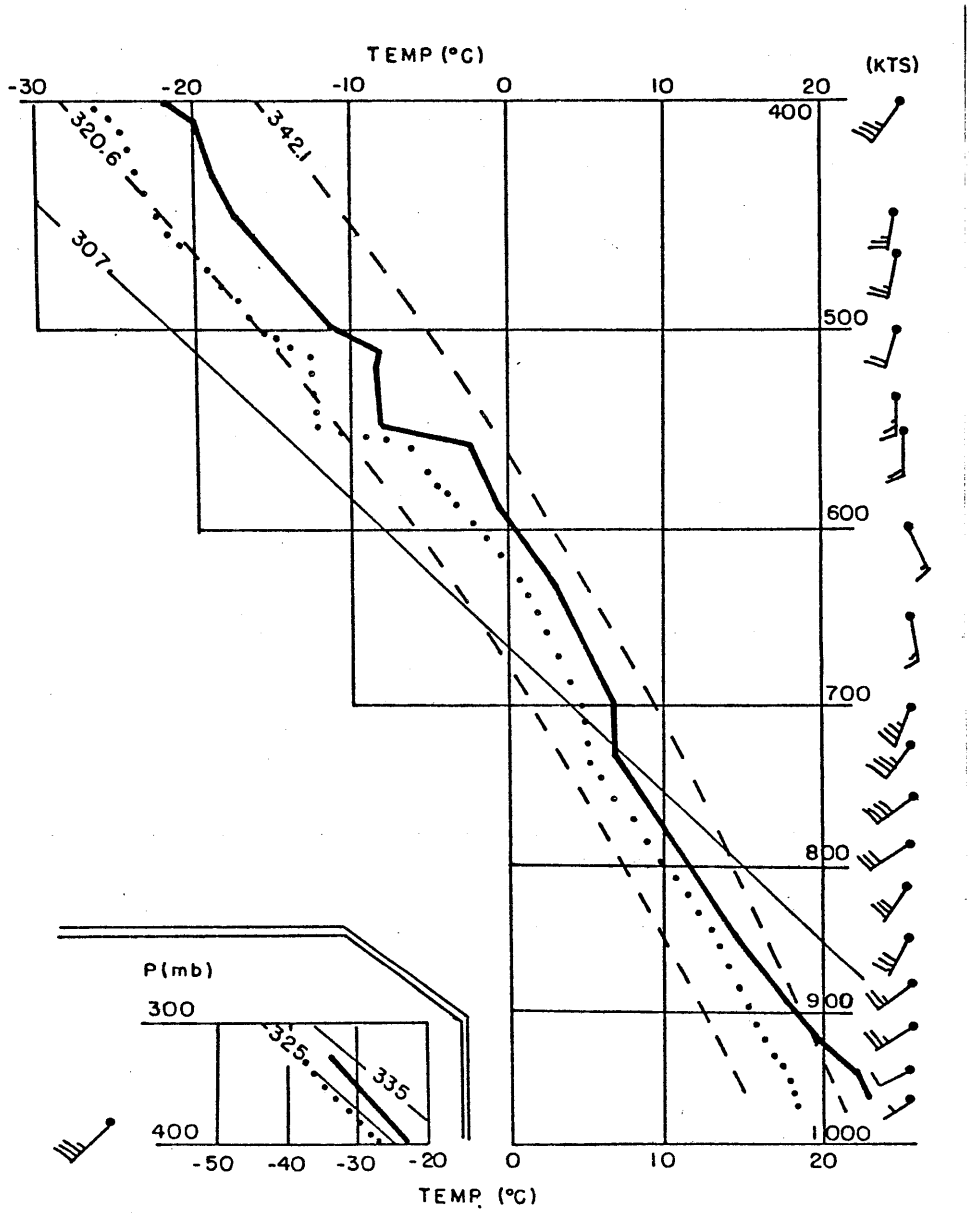
TEMP (°C)
(KTS)
-30
-20
-10
0
10
20
400
500
600
700
800
900
1000
320.6
342.1
307
P(mb)
300
400
325
335
-50
-40
-30
-20
0
10
20
TEMP (°C)

Figure 3.18

4. MESOSCALE OBSERVATIONAL ANALYSIS

a. Wind Field Analysis Over the Mesonet

At 0305 GMT on 14 April 1981, the wind velocities over the mesonet (Figure 4.1) range from 3-9 (ms^{-1}) and the direction is mainly from the south except in the northwest corner of the mesonet where the winds are from the southwest and west. Also notice a protrusion in the velocity field as shown by the 5 and 7 (ms^{-1}) contours around station number 15. It is in this area, in the mesonet, that the downburst first becomes noticeable. Also apparent in this figure is a region of high velocity near the KTVY-Tower, in the northwest section of the mesonet. This maximum seems to be the result of a system that is leaving the area toward the north and northeast, as evidenced in Figures 4.2, 4.3 by a decrease in the velocities in this region. Possible evidence of this separate system may be seen in Figure 3.3 as a thunderstorm is positioned to the north-northeast of Oklahoma City. Five minutes later, Figure 4.2 shows the protrusion near station number 15 to be the main feature over the mesonet. Average velocities have increased upward to 17 ms^{-1} in this area and by 0315 GMT, Figure 4.3, the velocity field has smoothed out somewhat, as the maximum in this field has moved off to the northeast, now showing up as a 20 (ms^{-1}) contour near station number 7. Abatement in the velocities are already evident at station number 15. Five minutes later, 0320 GMT, Figure 4.4 shows a more

evenly spaced set of contours over most of the mesonet with a somewhat tighter gradient appearing near Bethany, showing that the downburst or what remains of the downburst is still moving to the northeast and east. With this stronger gradient comes a windshift from the south, into the west and northwest. After 0325 GMT, (Figure 4.5) the analysis is enhanced by the addition of reports from the FAA stations (lettered points) in the center of the mesonet. There is a definite bulge still evident in the wind field, with the strongest gradient appearing in the northeast quadrant of the area. The area enclosed by the 15 ms-1 contour has increased dramatically in size compared with Figure 4.4. It is conceivable that another downburst cell, less intense than that which was previously seen 10-15 minutes prior to this time, has appeared. Figure 4.6 and 4.7 show that the velocities have increased further to the south and southeast in the mesonet, apparently due to the passage of the cold front. The velocity field has weakened markedly in the 15 minutes prior to the time of Figure 4.6. The maxima now showing up in the velocity field in the area of the lettered stations appears to be very inconsistant with what the trend has been and should be ignored (Figures 4.6-4.9). Their tendencies appear correct but their magnitudes seem too large. Figures 4.8-4.11 (0340-0400 GMT) show that the velocity field is becoming more tranquil and the major perterbations, seen earlier, have moved off.

Figure 4.12 shows the maximum velocities recorded over the mesonet for the time from 0305-0350 GMT on 14 April 1981. The strongest velocities occur in the northwestern section, where speeds of more than 27 ms^{-1} appear at station number 7. This is consistant with the fact that the plotted one-minute mean velocity field (Figures 4.2-4.3) shows the same pattern. The isochrones of the maximum average velocities (Figure 4.13), show the motion of the system to be to the east-northeast and east-southeast from the area around station number 15. It appears that the strongest velocities occurred by 0325 GMT. Figure 4.14 demonstrates that the maximum gusts reported over the mesonet were quite strong in the northwestern quadrant, where reports ranged from 25 to close to 40 (ms-1). The isochrones of the maximum gusts (Figure 4.15) resembles those of the mean velocities (Figure 4.13).

b. Equivalent Potential Temperature Analysis

The equivalent potential temperature (EPT) is a quantity which is conserved through dry-and saturated- adiabatic processes in the atmosphere, and is thus an appropriate quantity to use in analyzing the source of the downburst. The data for station number 53 was not available for this part of the analysis. Figures 4.16 and 4.17 show a rather unperturbed EPT field, with values around 335 degrees K over the mesonet. However, by 0310 GMT (Figure 4.18), a large negative anomaly has protruded into the northwest corner of the mesonet. EPT

values dropped markedly around station number 15, from 334 degrees K to near 321 degrees K within a few minutes. Looking back at the velocity analysis for this same time (Figure 4.2), notice the striking resemblance between the contours, especially in the northwest quadrant of the mesonet. At 0315 GMT (Figure 4.19), there is still a resemblance between the EPT field and that shown in Figure 4.2 except that the gradient of the EPT is slightly stronger with even lower values appearing near station number 15. Five minutes later, (Figure 4.20), this anomaly in the EPT field has radially spread over a large part of the mesonet. A minimum of less than 316 degrees K appeared at station number 15. This represents a drop of approximately 20 degrees K in less than 15 minutes. Over the next twenty minutes (Figures 4.21-4.24), the same process, of air of lower EPT spreading out over the mesonet and replacing the air of higher EPT, continued, until by 0400 GMT (Figure 4.27) the EPT field was once again flat over the mesonet. But unlike in Figures 4.16 and 4.17, this was air of much lower EPT.

One possibility is that the air of low EPT which first appeared at the surface near station number 15 on the mesonet was horizontally advected into this area. To check this, a surface analysis of EPT was conducted on a larger scale, which encompassed the area described in Chapter II for the surface synoptic analysis. Figure 4.28 shows the synoptic view of the EPT field for 2100 GMT on 13 April 1981. Notice that the leading edge of the strong EPT gradient corresponds

with the position of the cold front, as shown previously in Figure 3.1, at the same time. An isolated minimum shows up in the form of a closed 325 degree K contour line over sotheastern Iowa and western Illinois, probably the result of air of lower EPT value being transported down from higher levels by thunderstorm downdrafts in that area. To the south and southeast of the leading edge of this gradient, there is a rather broad area of high EPT. There appears to be an anomalously warm region in a small area in southwestern Oklahoma, which is observed through 0100 GMT on 14 April 1981. Three hours later, 0000 GMT, 14 April 1981, Figure 4.31 shows the tighter gradient of EPT more established further to the southwest through the Texas-Oklahoma panhandle. Again, the leading edge of this gradient is represented by the cold front, as viewed in Figure 3.2. Between 2100 GMT and 0000 GMT, the 320 degree K contour progressed south and southeastward at a speed of just under 30 kts. By 0300 GMT (Figure 4.34), the leading edge of the tighter EPT gradient, again correlating with the frontal system as it appears in Figure 3.3, has moved toward central Oklahoma. The higher values in the EPT field ahead of this leading edge have dropped off slightly over the past few hours, primarily as a result of decreased solar heating. The 320 degree K contour accelerated between 0000 GMT and 0300 GMT, to 30-34 kts and continued to move toward the south and southeast. For the air with EPT less than 320 degrees K to be horizontally advected into the mesonet at the surface level, by 0315 GMT, it would have to have

been moving at approximately 120 kts, and this clearly could not be the case. Figure 4.35 portrays the EPT field at 0400 GMT. An interesting feature at this time is the bulge in this EPT field over the Oklahoma City area. It is likely that this air of lower EPT was brought down to the surface from some higher level. A possible mechanism for bringing this air down will be discussed in the next chapter. Figure 4.36 shows a time trace of the 327 degree K EPT contour, which was sweeping across the mesonet at approximately 33 kts. This speed is consistant with that of the 320 degreé K contour of the large scale EPT analysis through 0300 GMT, but between 0300 and 0400 GMT, the 320 degree K contour appears to have an average speed of close to 50 kts. This acceleration is not evident until after the onset of the thunderstorm producing downburst in the area of the mesonet. The shape of the 320 degree K contour in Figure 4.35 (in the Oklahoma City area) is consistent with the notion that the air was transported from above. In other words, this speed of 50 kts is just an apparent speed. If it were not for the coincidence of this probable transportation of air from upper levels to the surface, this bulge in the EPT field would not show up. Figures 4.37-4.39 show the upper air analyses of the EPT field on the 850, 700 and 500 mb surfaces. These three levels do not give a complete picture of the EPT field in the vertical, but one can see that the 320 degree K contour is positioned in a southwest to northeast direction over Gage, Oklahoma. To get a better idea of the EPT distribution in the

vertical, Figure 4.40 shows the vertical profile of EPT over Tuttle, approximately an hour before the occurrance of the downburst just to its north. Here one can see a minimum of about 322 degrees K at the 430 mb level, and other minima of slightly higher values appearing at 500, 550 and 660 mb. In the following chapter, this sounding will be examined in order to find a possible source height for the downburst. The 0000 GMT sounding (Figure 4.41) for Oklahoma City, on 14 April 1981, is not as complete a sounding as is the Tuttle sounding, but nevertheless, it shows the major features of the latter. Figure 4.42 shows the vertical profile of EPT over Oklahoma City for 0000 GMT on 14 April 1981, and exhibits a definite minimum around 600 mb of approximately 320 degrees K. Both the Tuttle and the Oklahoma City soundings show low values of EPT at upper levels, and since neither sounding shows EPT as low as is reported over the mesonet (~ 316 degrees K), the downburst must have originated in air that moved in from the west of the mesonet. Nevertheless, we feel that these EPT profiles are qualitatively representative of the type of air that the downburst originated in.

c. KTVY-Tower Analysis

The KTVY-Tower, as mentioned in Chapter II, records data in the lower half kilometer of the atmosphere. Figure 4.43, a time vs. height cross-section of the wind field at the tower from 0310-0410 GMT, shows a wind shift from the south-southwest to west by 0320 GMT,

at all levels. An east-west oriented gust front, as analyzed using doppler velocities and reflectivities by Wolfson (1983), is apparently responsible for the wind shift. Figure 4.45, a time vs. height cross-section of the Tower's vertical velocities, shows that between 0315 and 0320 GMT, the dominant feature is upward motion, which occurs ahead of the gust front. Another wind shift is evident by 0330 GMT (Figure 4.43). This might be due to the passage of an occluded gust front, as discussed by Wolfson (1983). Figures 4.45 and 4.46 also show evidence of this gust front in the strength of the upward motion around the time of 0330 GMT. The next maximum in the upward motion of the vertical field occurs at about 0335 GMT (Figure 4.46) and also at this time there is an increase in the horizontal velocities (Figure 4.43). This probably represents the passage of the cold front. The shaded or hatched areas, in Figures 4.45 and 4.46 denote downward velocities which are associated with passage of the fronts, and downdrafts from imbedded showers and thunderstorms. Recalling the definition given for a downburst, it would be quite evident in looking at the velocity fields (Figures 4.43-4.46), that a downburst did not exist over the KTVY-Tower. It would appear that instead, the tower experienced what remained of the downburst which occurred further to the west. Represented in Figure 4.47 is a time vs. height cross-section of EPT where the pressure at each level is assumed constant after 0325 GMT. It is interesting that the minimum values, at 0330 GMT and 0337 GMT, which occur at these low levels

seem to spread out from these points. The perterbation in the EPT field which shows up between 0327 and 0330 GMT is coincident with the approach of the occluded gust front.

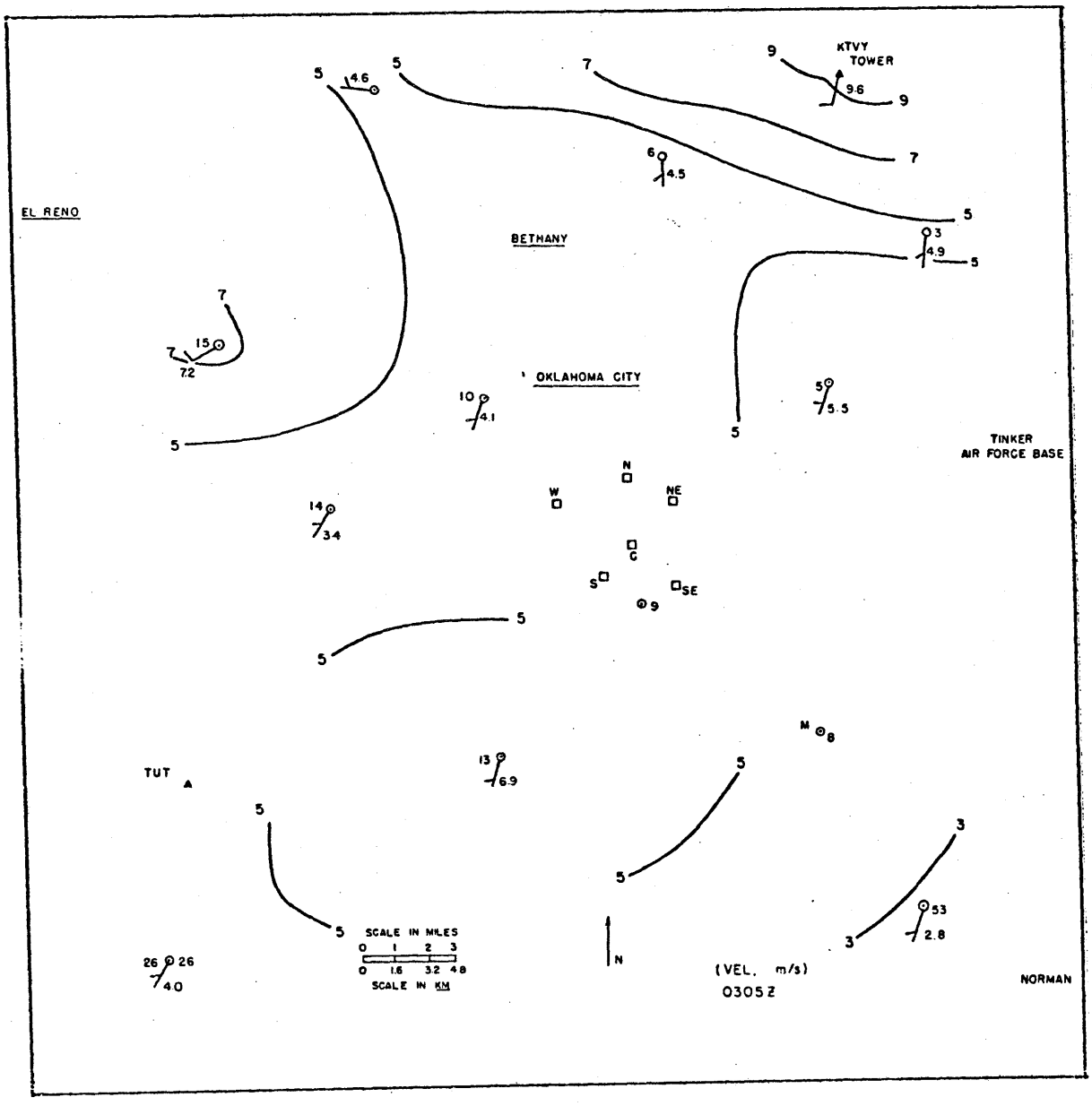
KTVY
TOWER
9.6
EL RENO
BETHANY
OKLAHOMA CITY
TINKER
AIR FORCE BASE
TUT
NORMAN
4.6
4.5
4.9
7.2
4.1
5.5
3.4
6.9
2.8
4.0
N
W
NE
C
S
SE
SCALE IN MILES
0 1 2 3
0 1.6 3.2 4.8
SCALE IN KM
(VEL. m/s)
0305Z

Figure 4.1

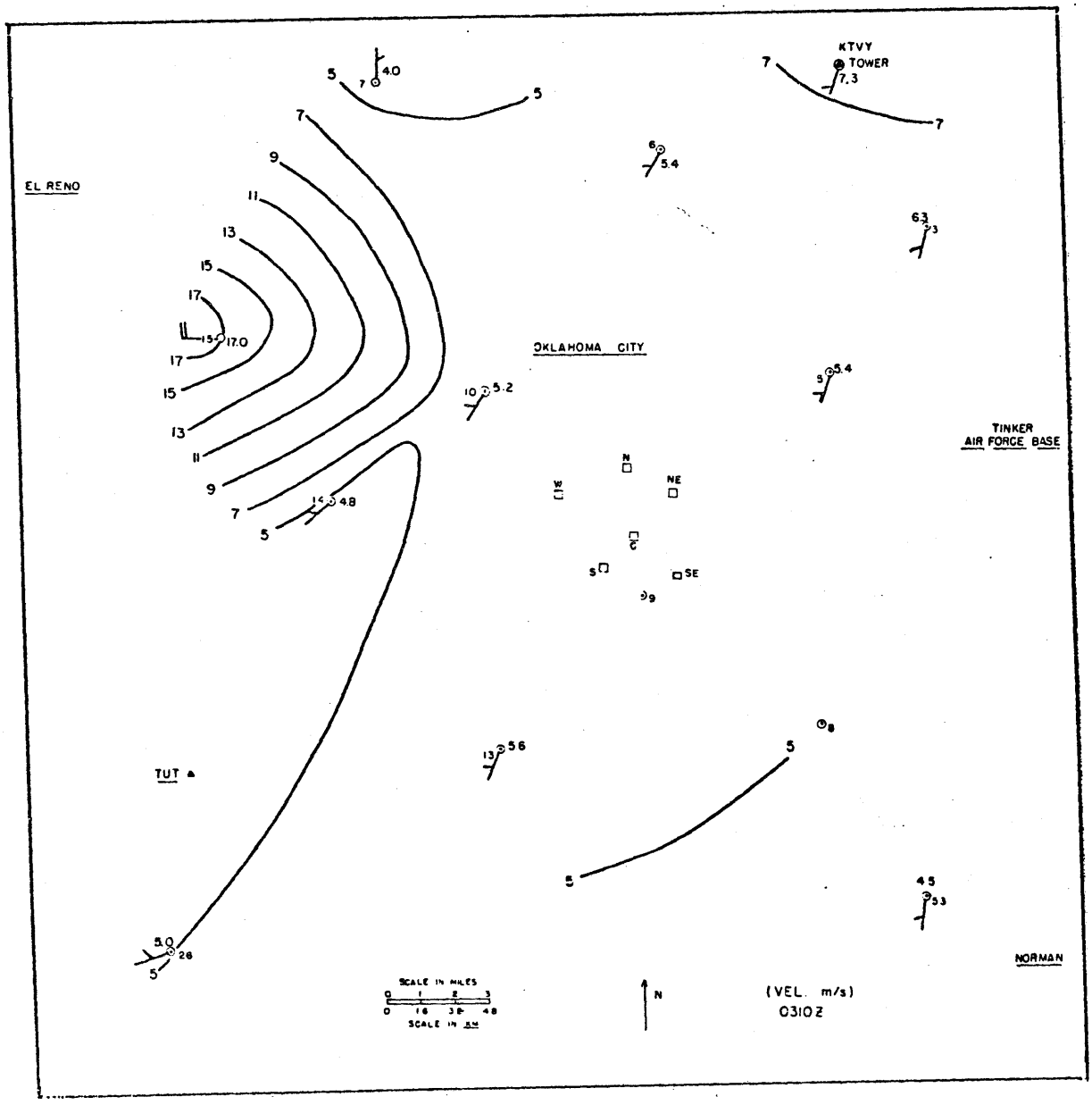
KTVY
TOWER
7.3
EL RENO
OKLAHOMA CITY
TINKER
AIR FORCE BASE
NORMAN
TUT
NE
SE
SCALE IN MILES
SCALE IN KM
N
(VEL. m/s)
0310Z

Figure 4.2

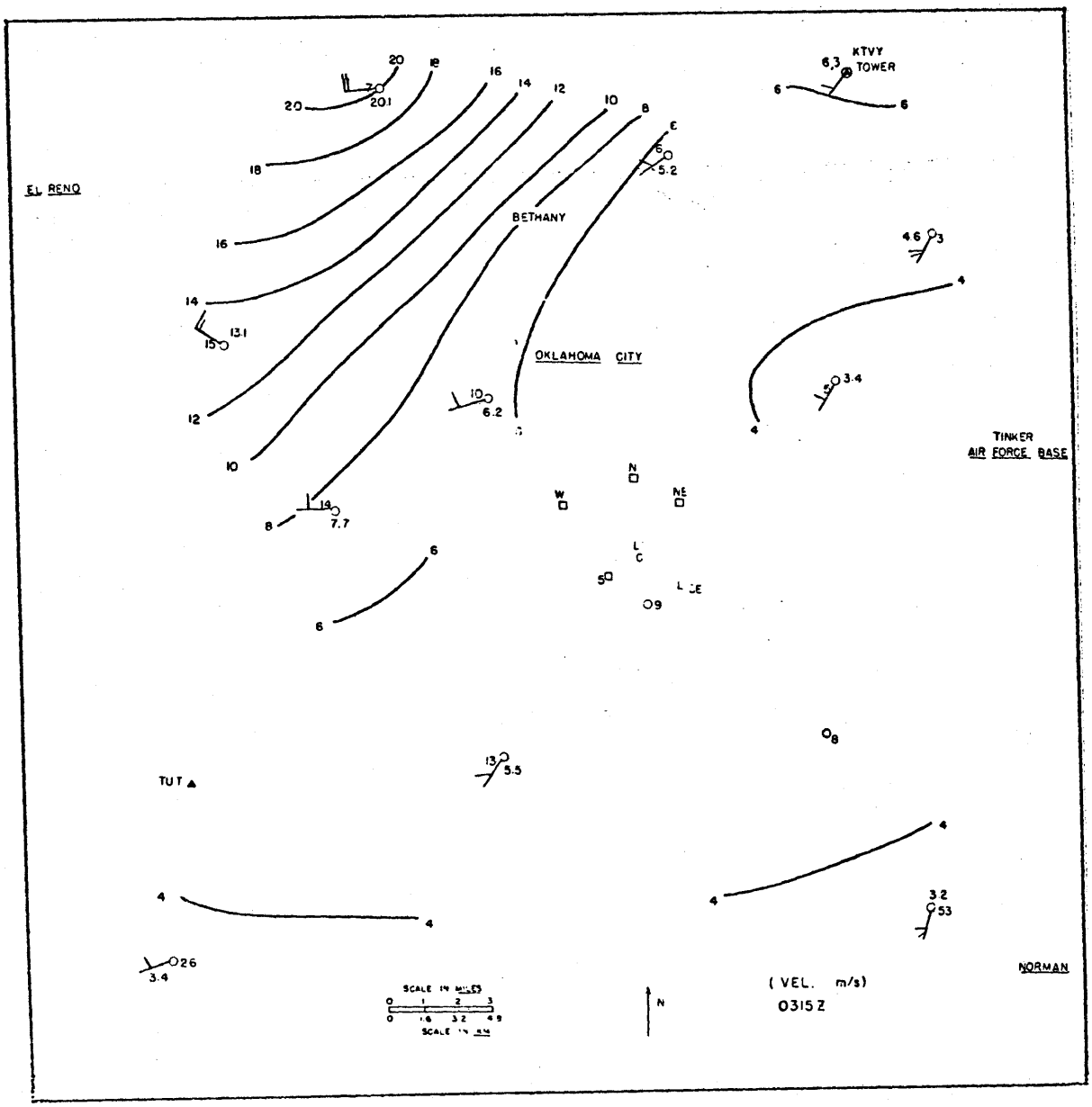
EL RENO
OKLAHOMA CITY
BETHANY
KTVY TOWER
TINKER AIR FORCE BASE
NORMAN
TUT
(VEL. m/s)
0315Z
N
SCALE IN MILES

Figure 4.3

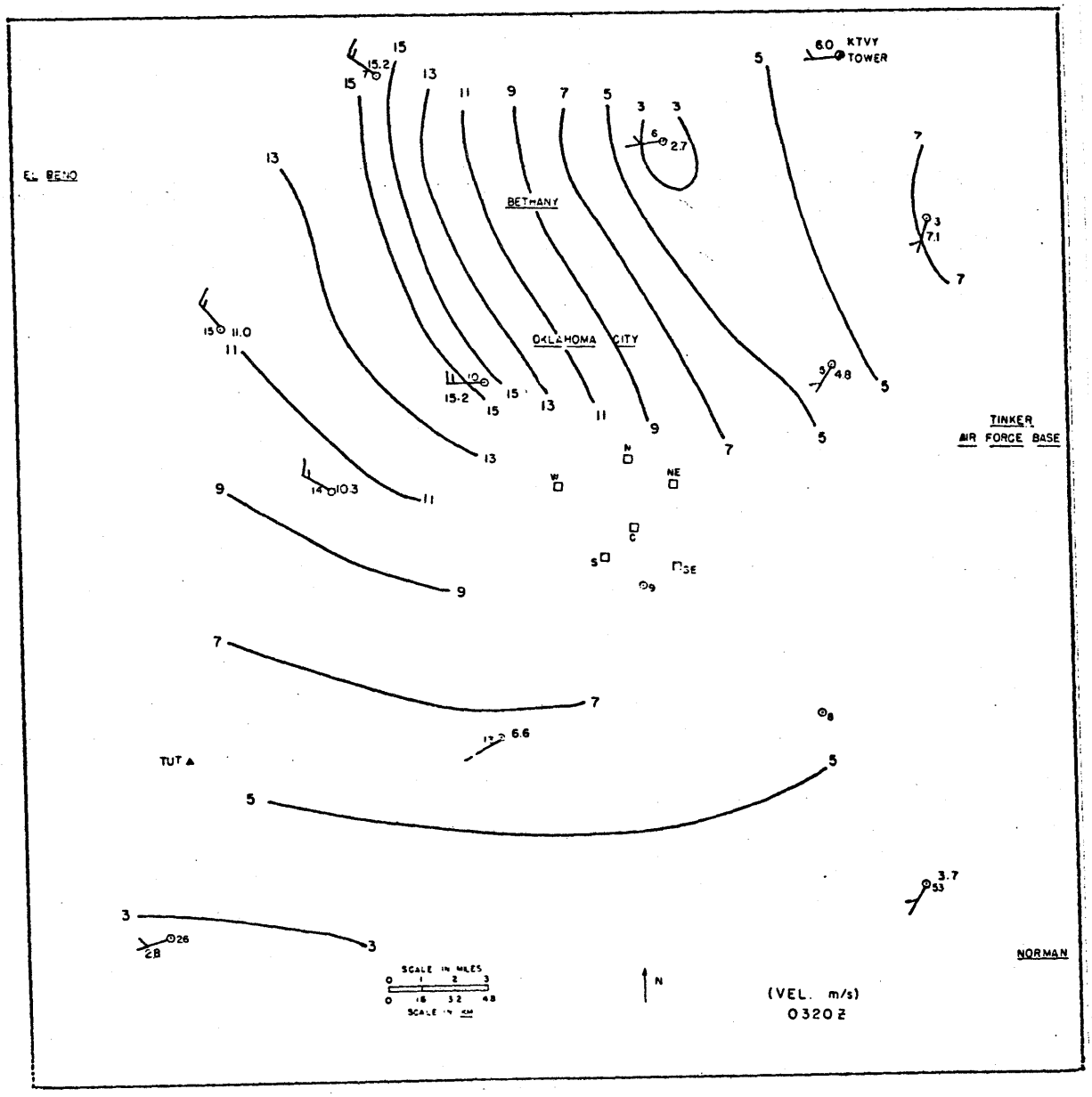
EL RENO
BETHANY
OKLAHOMA CITY
TINKER
AIR FORCE BASE
NORMAN
TUT
6.0 KTVY
TOWER
SCALE IN MILES
0 1 2 3
0 1.6 3.2 4.8
N
(VEL. m/s)
0320Z

Figure 4.4

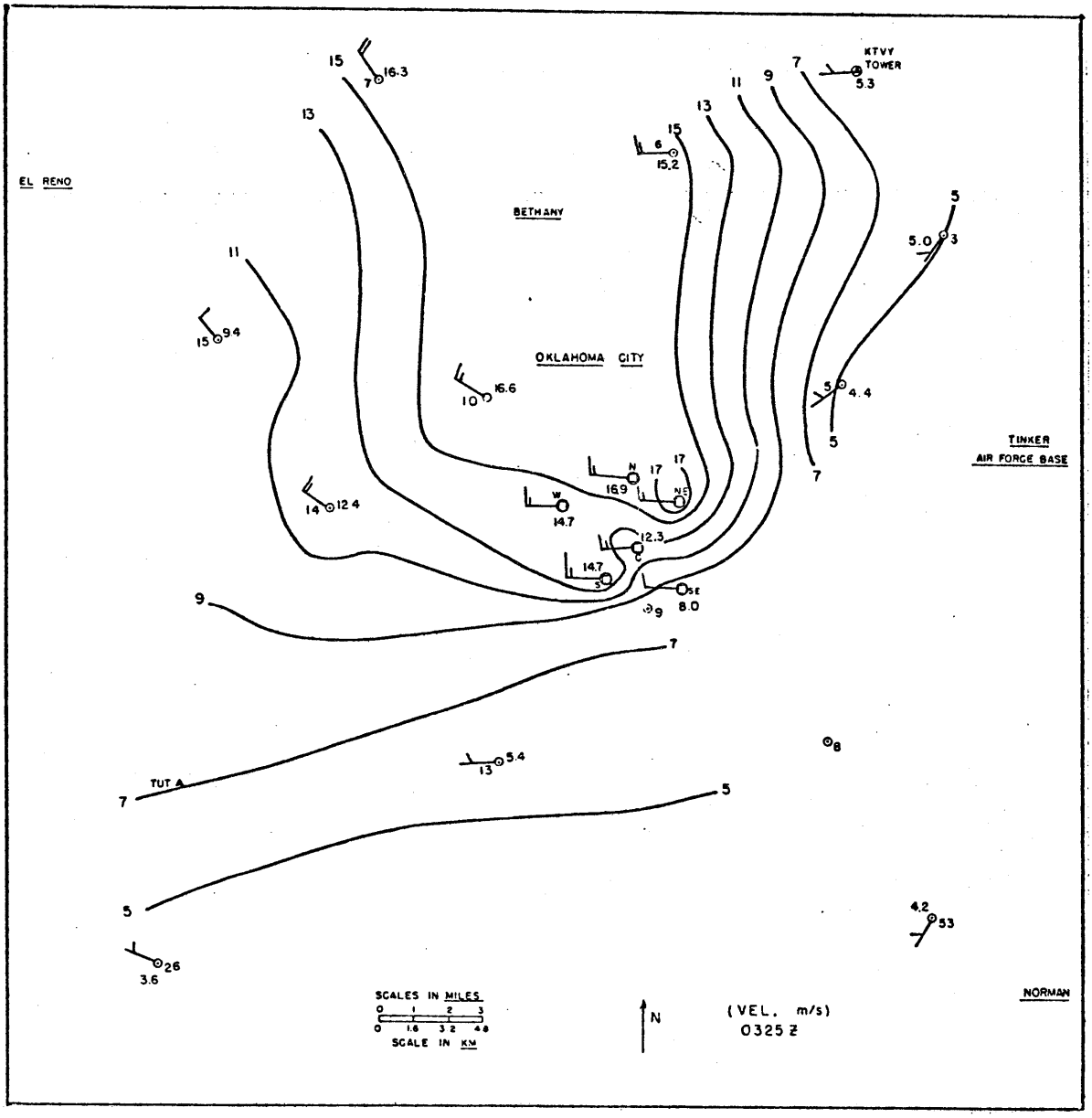
EL RENO
BETHANY
OKLAHOMA CITY
TINKER
AIR FORCE BASE
NORMAN
KTVY
TOWER
5.3
TUT A
SCALES IN MILES
0 1 2 3
0 1.6 3.2 4.8
SCALE IN KM
N
(VEL. m/s)
0325 Z

Figure 4.5

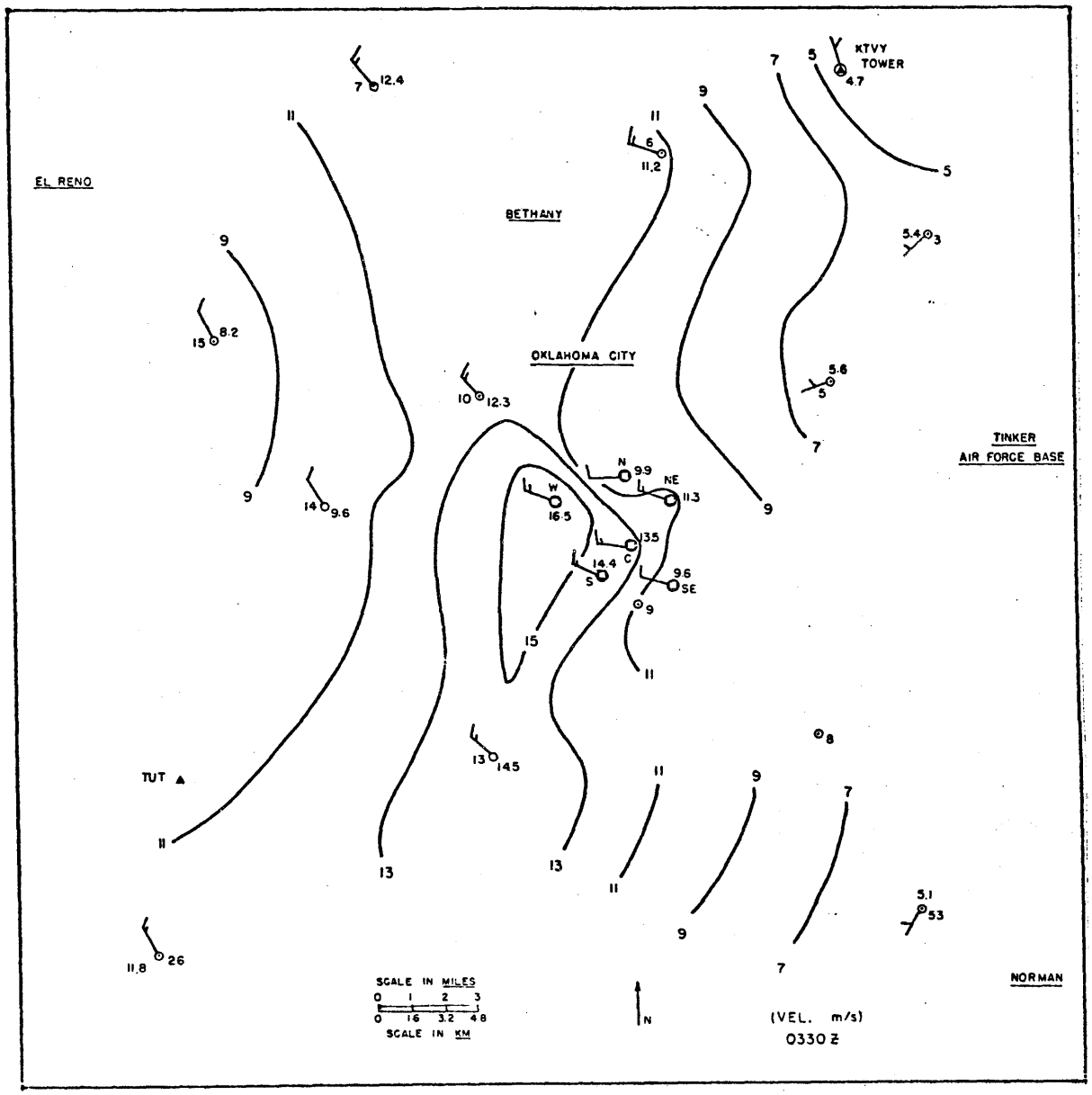
EL RENO
BETHANY
OKLAHOMA CITY
TINKER
AIR FORCE BASE
NORMAN
TUT
KTVY
TOWER
SCALE IN MILES
0 1 2 3
0 1.6 3.2 4.8
SCALE IN KM
N
(VEL. m/s)
0330 Z

Figure 4.6

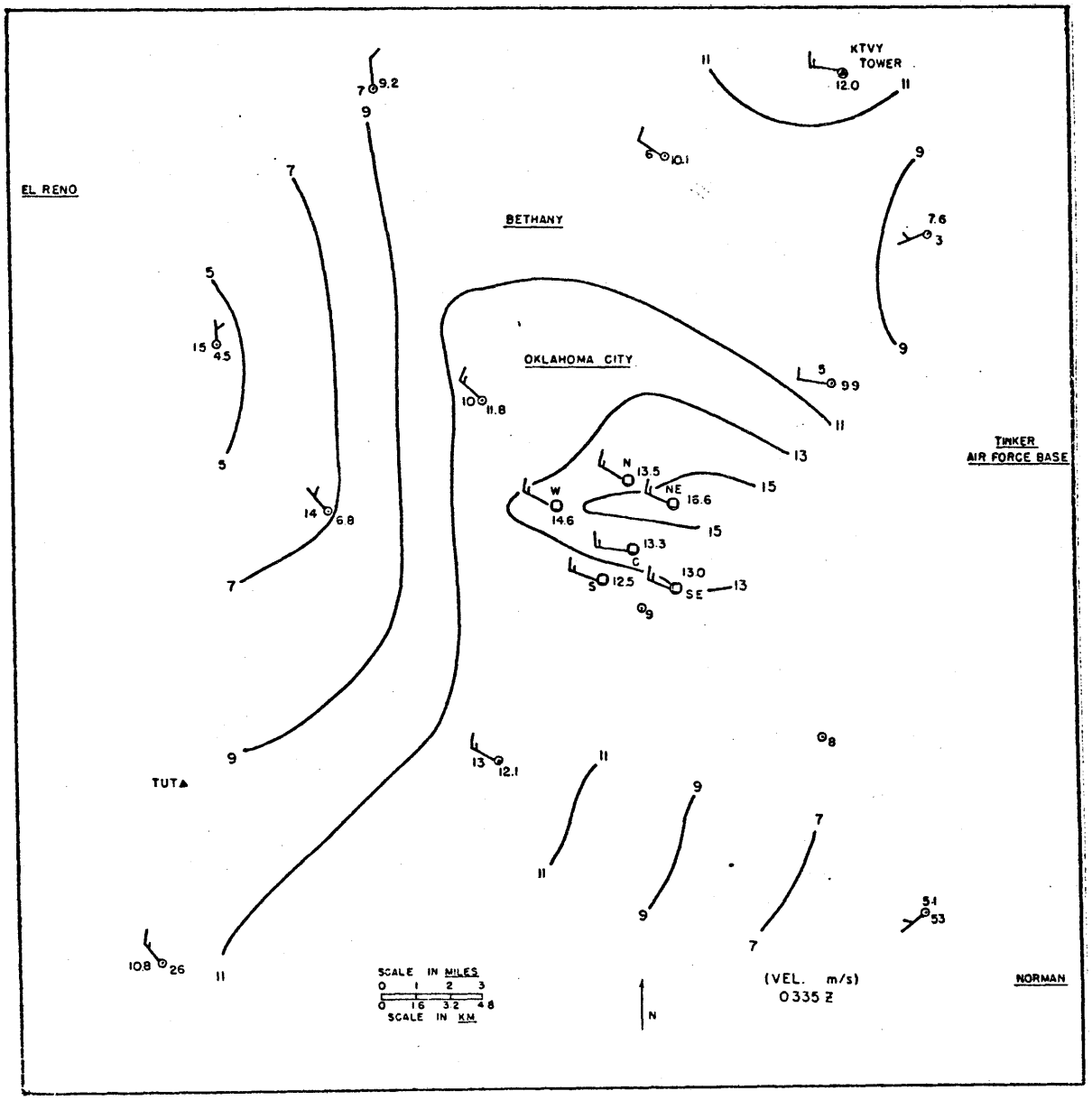
KTVY
TOWER
12.0
EL RENO
BETHANY
OKLAHOMA CITY
TINKER
AIR FORCE BASE
TUT
NORMAN
9.2
10.1
7.6
4.5
9.9
11.8
6.8
13.5
14.6
15.6
13.3
12.5
13.0
12.1
10.8
26
5.1
SCALE IN MILES
0 1 2 3
SCALE IN KM
(VEL. m/s)
0335 Z
N

Figure 4.7

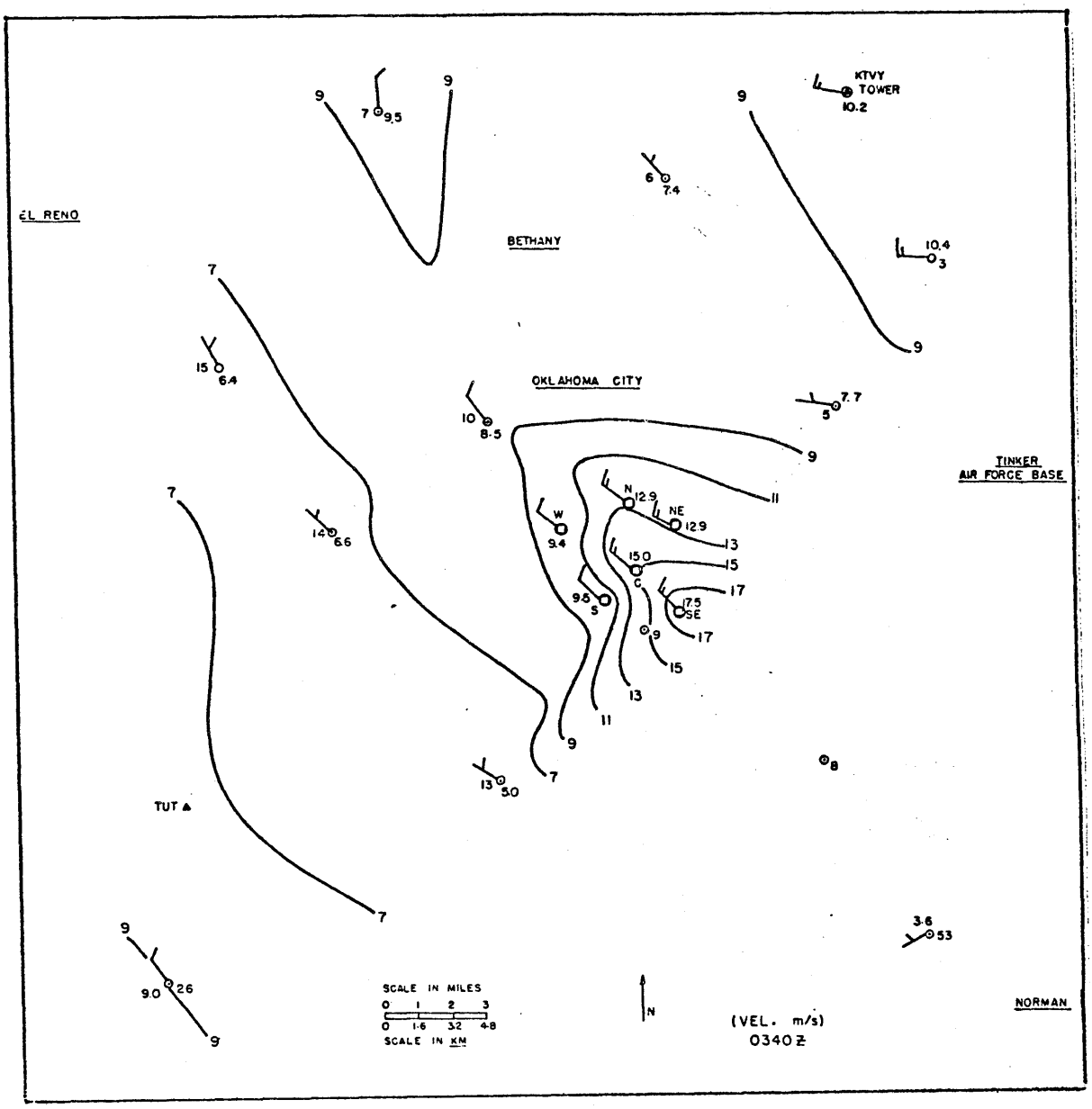
KTVY
TOWER
10.2
EL RENO
BETHANY
OKLAHOMA CITY
TINKER
AIR FORCE BASE
NORMAN
TUT
SCALE IN MILES
0 1 2 3
0 1.6 3.2 4.8
SCALE IN KM
N
(VEL. m/s)
0340Z

Figure 4.8

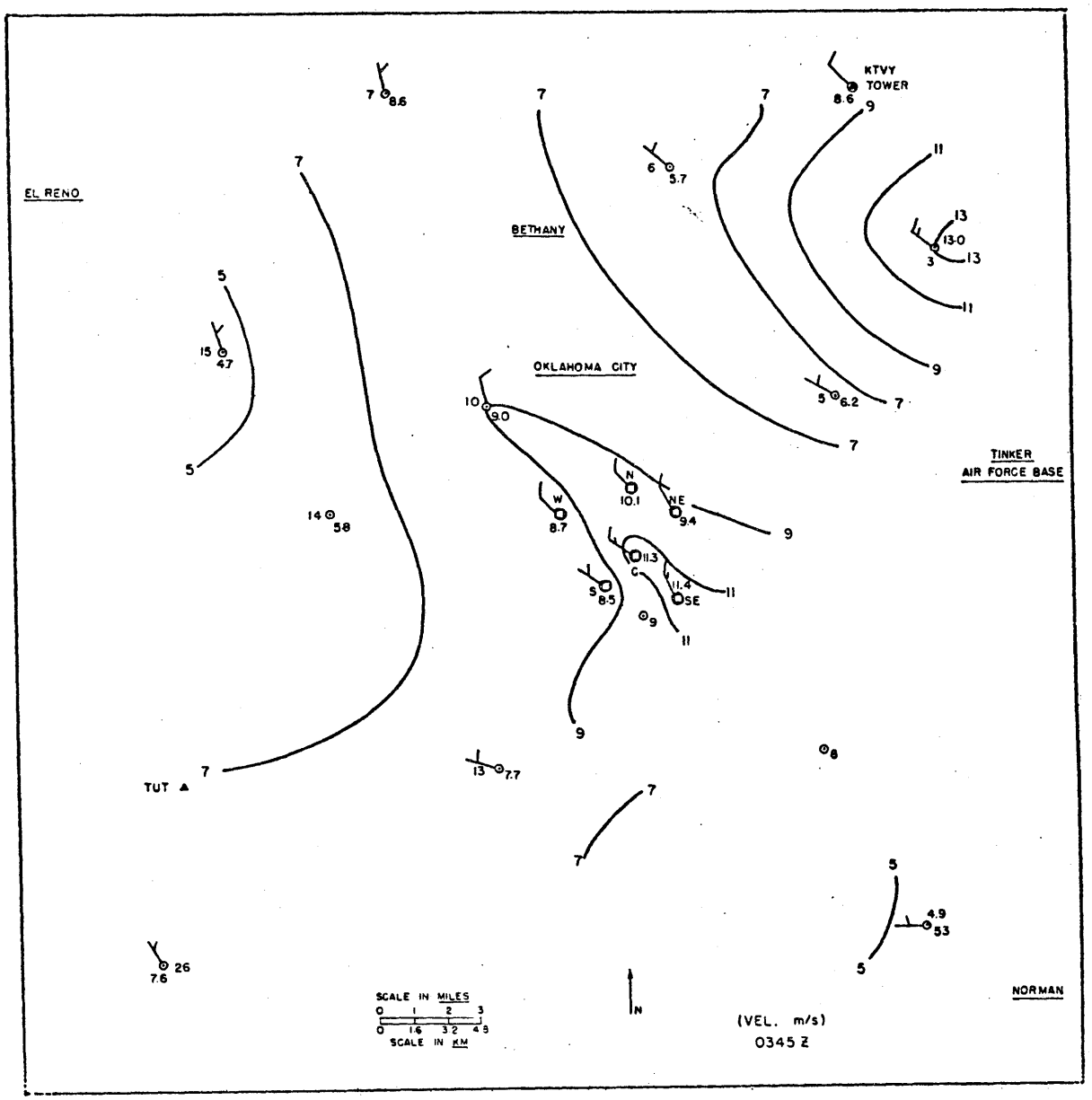
EL RENO
BETHANY
OKLAHOMA CITY
KTVY TOWER
TINKER AIR FORCE BASE
NORMAN
TUT
SCALE IN MILES
SCALE IN KM
(VEL. m/s)
0345 Z

Figure 4.9

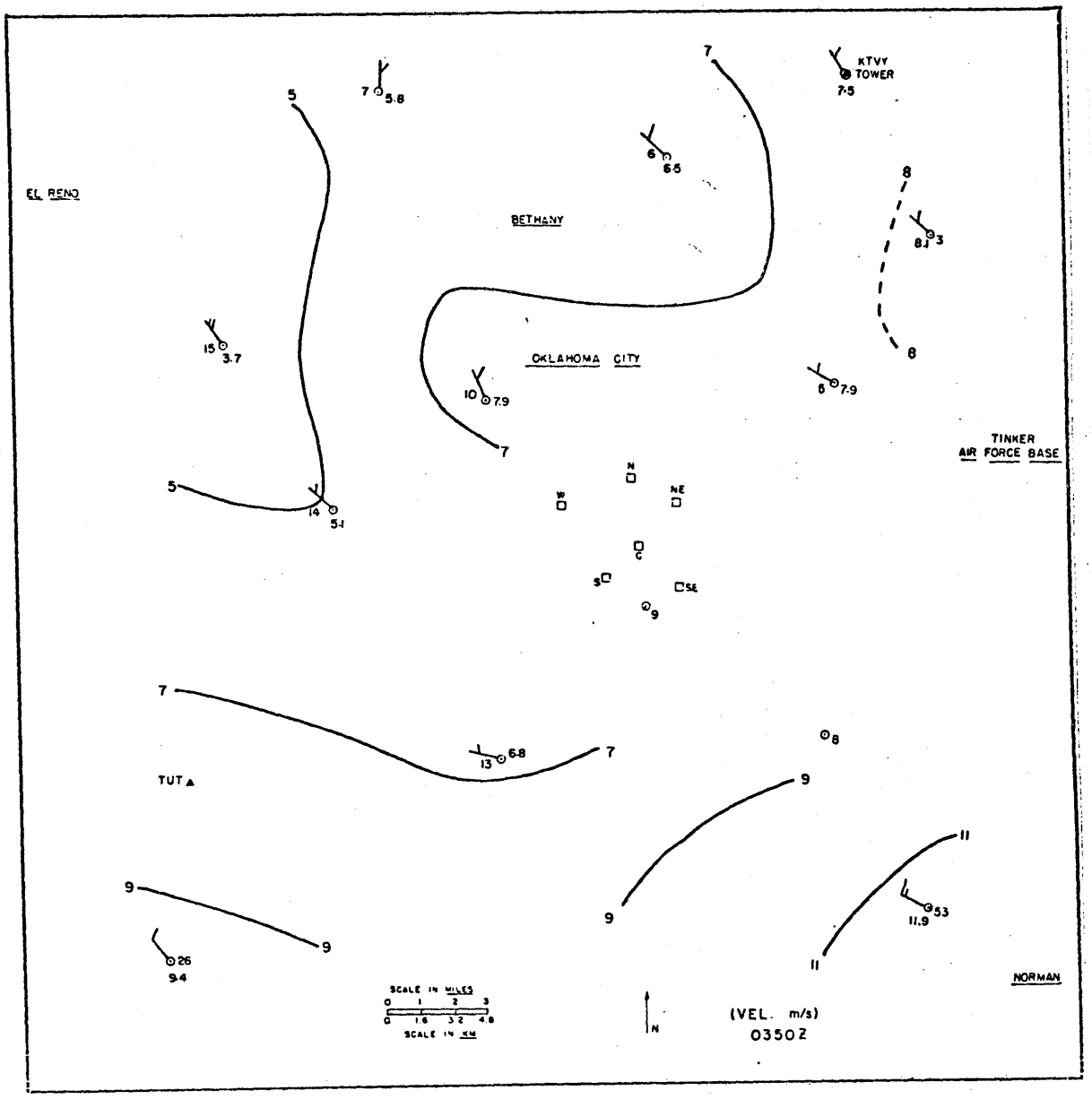
EL RENO
BETHANY
OKLAHOMA CITY
TINKER AIR FORCE BASE
NORMAN
TUT
KTVY TOWER
7.5
7
5.8
6
6.5
8
8.3
15
3.7
10
7.9
8
7.9
5
14
5.1
7
13
6.8
9
9.4
11
11.9
5.3
N
NE
W
C
S
SE
SCALE IN MILES
0 1 2 3
0 1.6 3.2 4.8
SCALE IN KM
(VEL. m/s)
0350Z

Figure 4.10

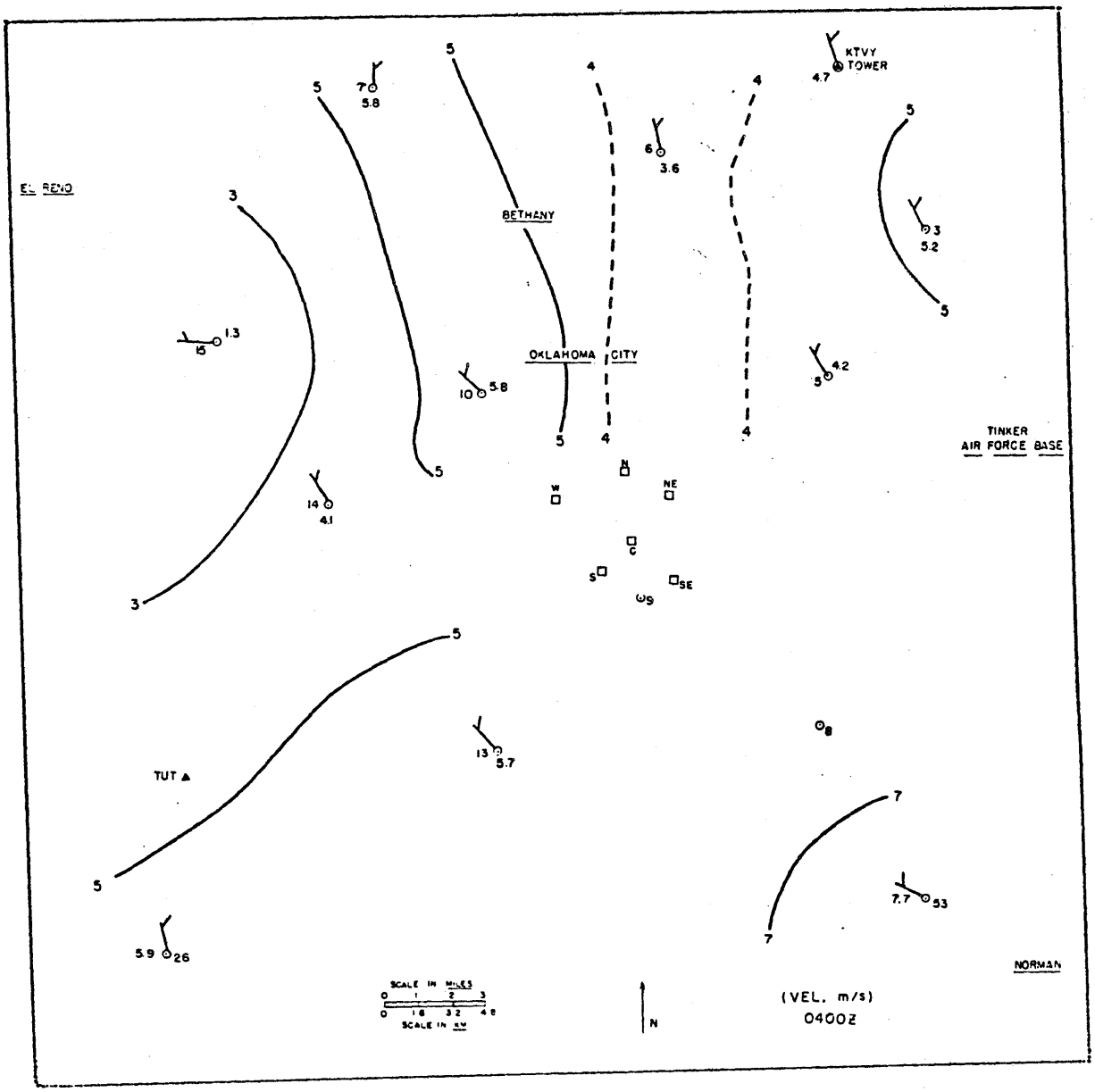
EL RENO
BETHANY
OKLAHOMA CITY
KTVY TOWER
TINKER AIR FORCE BASE
NORMAN
TUT
N
NE
W
C
S
SE
SCALE IN MILES
SCALE IN KM
(VEL. m/s)
0400Z

Figure 4.11

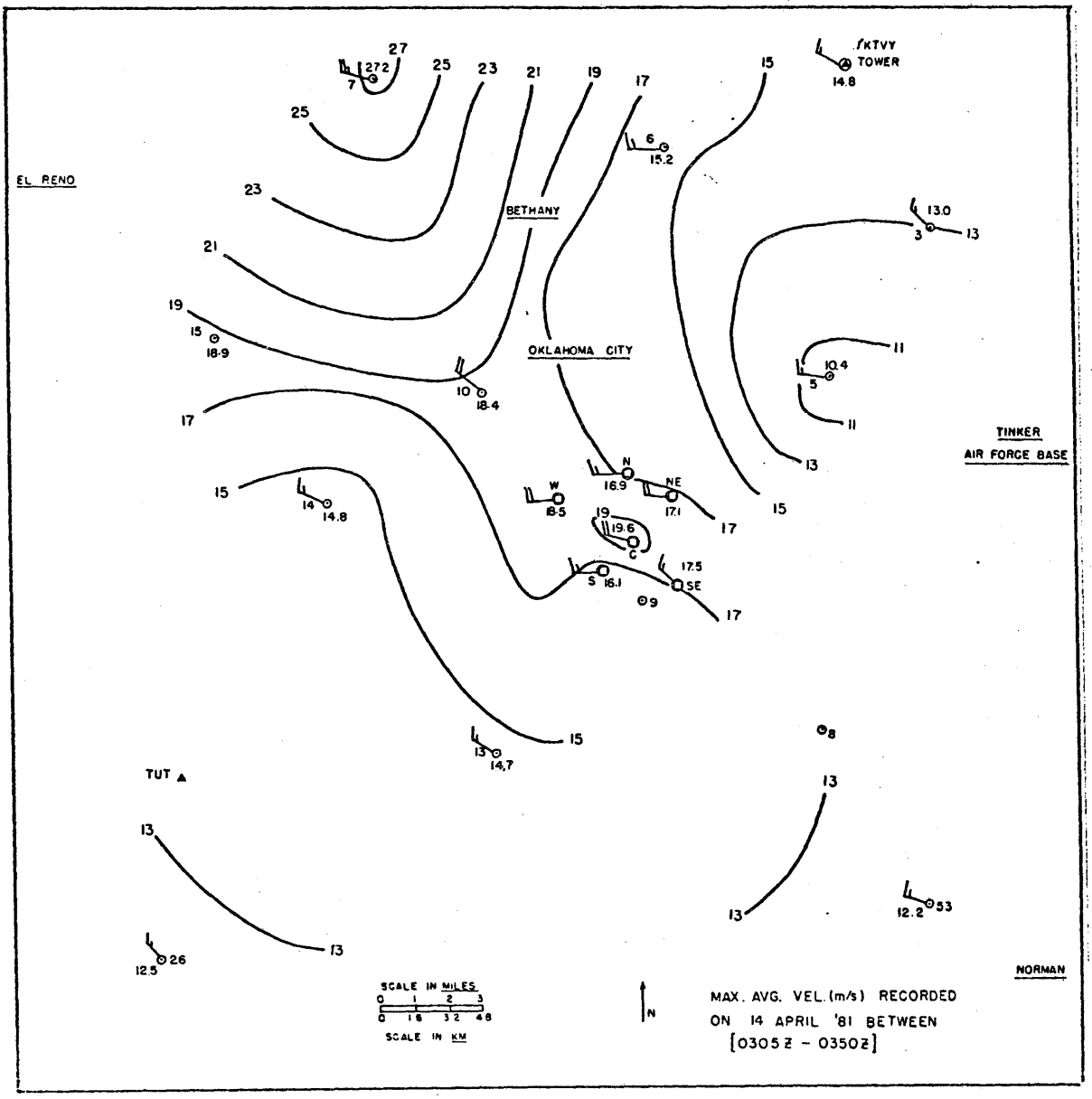
EL RENO
BETHANY
OKLAHOMA CITY
TINKER
AIR FORCE BASE
NORMAN
TUT
KTVY
TOWER
14.8
27
25
23
21
19
17
15
13
11
7
6
15.2
13.0
3
10.4
5
18.9
18.4
10
14
14.8
N
16.9
NE
17.1
W
18.5
19
19.6
C
S
16.1
17.5
SE
9
13
14.7
8
12.2
53
12.5
26
SCALE IN MILES
0 1 2 3
0 1.6 3.2 4.8
SCALE IN KM
N
MAX. AVG. VEL.(m/s) RECORDED
ON 14 APRIL '81 BETWEEN
[0305Z - 0350Z]

Figure 4.12

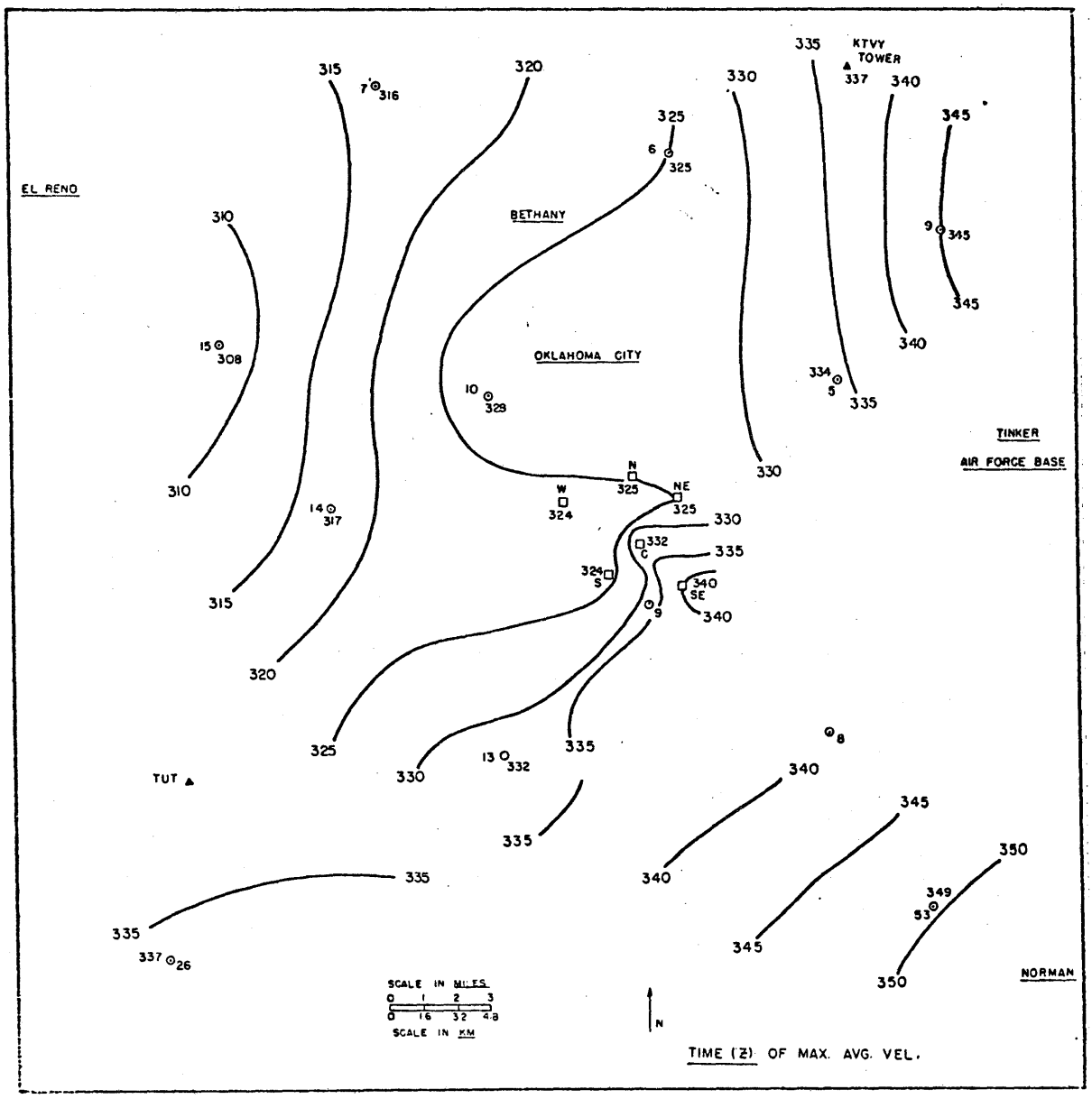
EL RENO
BETHANY
OKLAHOMA CITY
TINKER
AIR FORCE BASE
NORMAN
KTVY
TOWER
TUT
315
316
320
325
330
335
337
340
345
350
310
308
328
324
332
317
326
SCALE IN MILES
0 1 2 3
0 1.6 3.2 4.8
SCALE IN KM
N
TIME (Z) OF MAX. AVG. VEL.

Figure 4.13

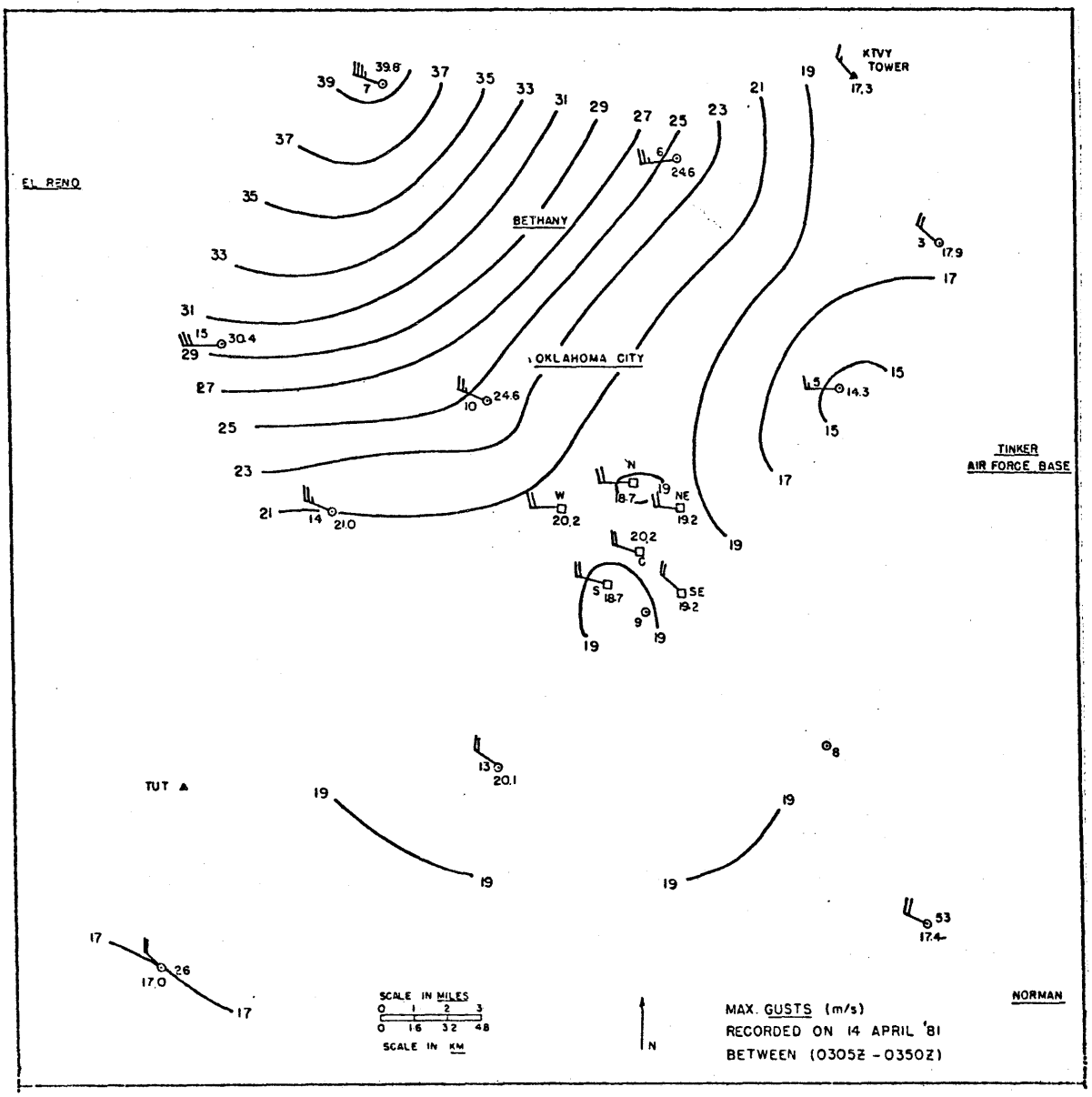
EL RENO
BETHANY
OKLAHOMA CITY
KTVY TOWER
17.3
TINKER AIR FORCE BASE
NORMAN
TUT
39.8
7
39
37
35
33
31
29
27
25
23
21
19
6
24.6
3
17.9
15
30.4
10
24.6
5
14.3
14
21.0
W
20.2
N
18.7
19
NE
19.2
20.2
C
S
18.7
9
SE
19.2
13
20.1
8
17
26
17.0
53
17.4
SCALE IN MILES
0 1 2 3
0 1.6 3.2 4.8
SCALE IN KM
N
MAX. GUSTS (m/s)
RECORDED ON 14 APRIL '81
BETWEEN (0305Z - 0350Z)

Figure 4.14

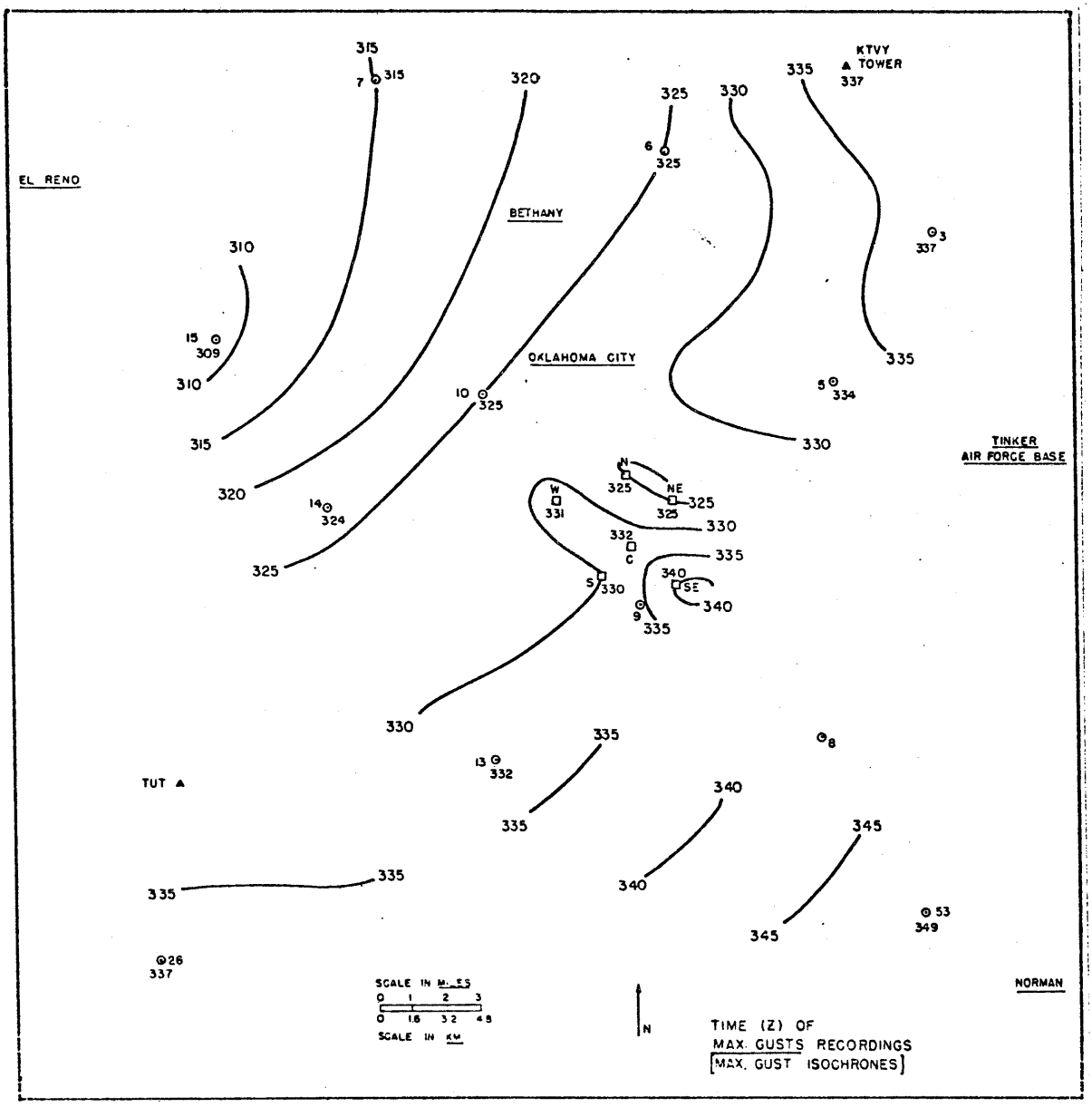
EL RENO
BETHANY
OKLAHOMA CITY
KTVY
TOWER
TINKER
AIR FORCE BASE
TUT
NORMAN
315
320
325
330
335
340
345
310
SCALE IN MILES
0 1 2 3
SCALE IN KM
0 1.6 3.2 4.8
N
TIME (Z) OF
MAX. GUSTS RECORDINGS
MAX. GUST ISOCHRONES

Figure 4.15

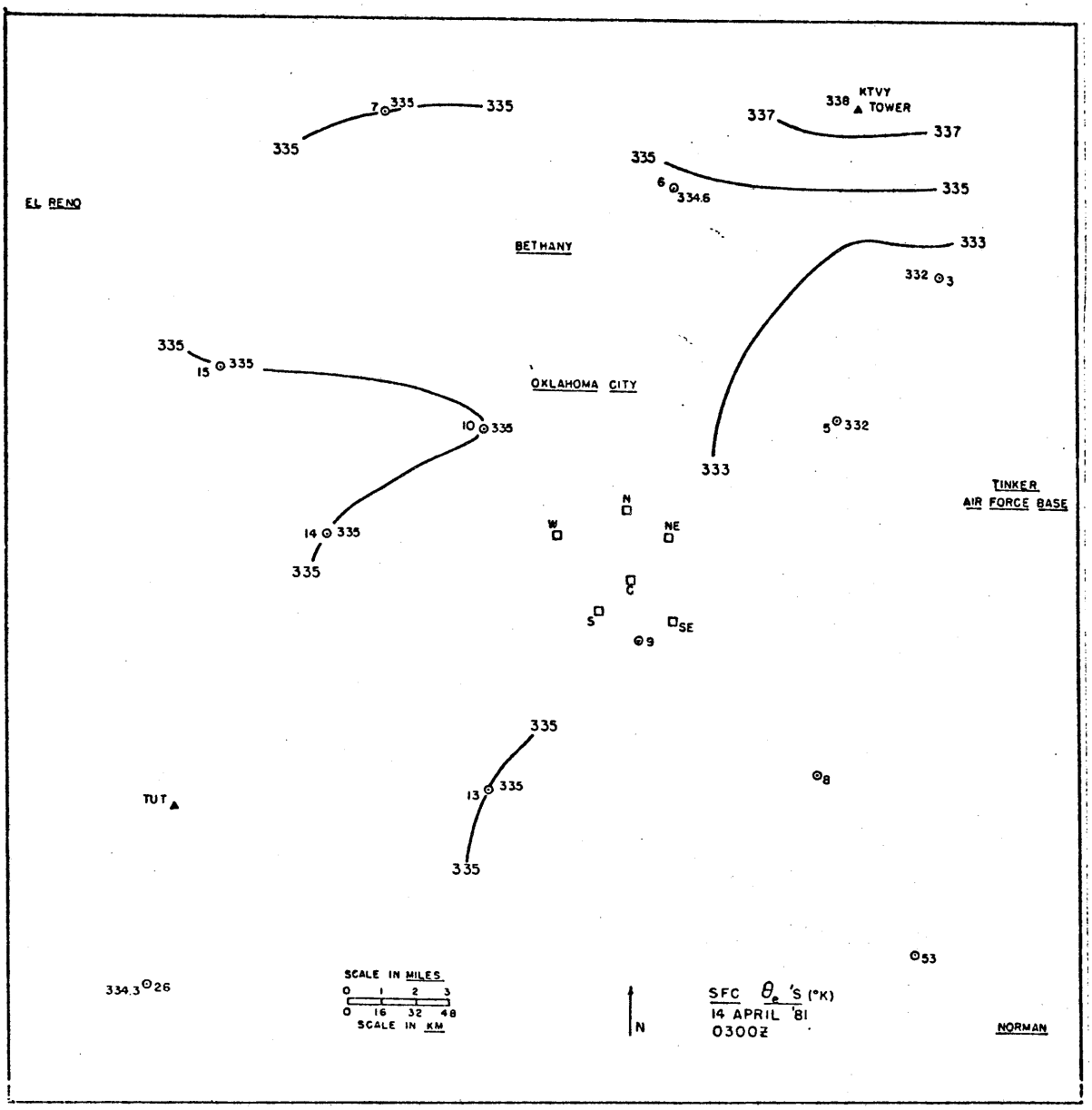
EL RENO
BETHANY
OKLAHOMA CITY
TINKER
AIR FORCE BASE
NORMAN
TUT
KTVY
TOWER
338
337
337
335
335
335
335
335
335
335
335
335
335
333
333
332
332
334.6
334.3
26
53
8
9
5
3
15
14
13
10
7
6
N
NE
W
SE
S
SCALE IN MILES
0 1 2 3
0 16 32 48
SCALE IN KM
N
SFC θ_e's (°K)
14 APRIL '81
0300Z

Figure 4.16

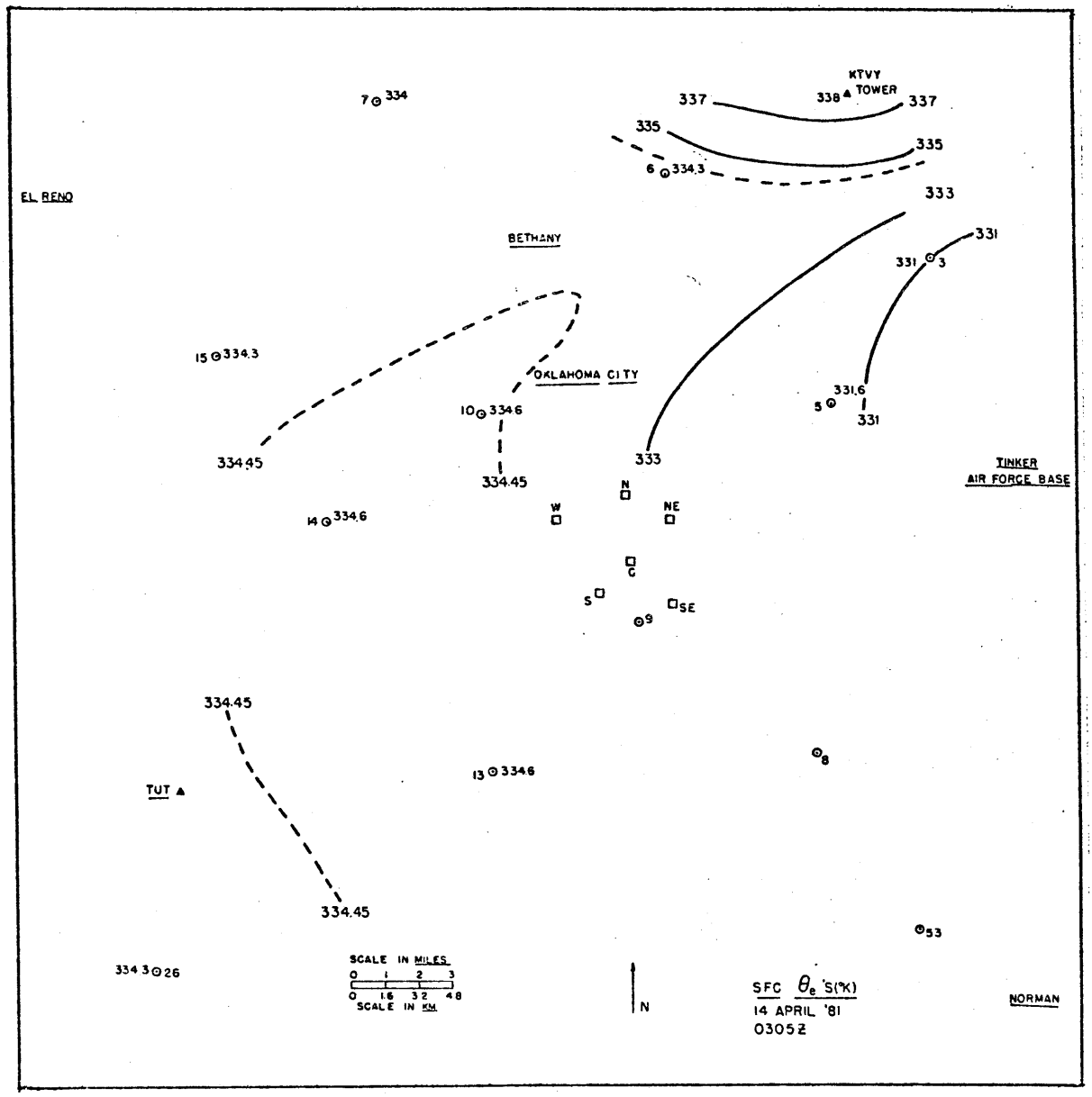
KTVY TOWER
337
338
337
335
335
6 334.3
333
331
331
3
7 334
EL RENO
BETHANY
15 334.3
OKLAHOMA CITY
10 334.6
334.45
334.45
333
331.6
5
331
TINKER AIR FORCE BASE
14 334.6
N
W
NE
C
S
SE
9
334.45
TUT
13 334.6
8
334.45
53
334.3 26
SCALE IN MILES
0 1 2 3
0 1.6 3.2 4.8
SCALE IN KM
N
SFC θ_e'S(°K)
14 APRIL '81
0305Z
NORMAN

Figure 4.17

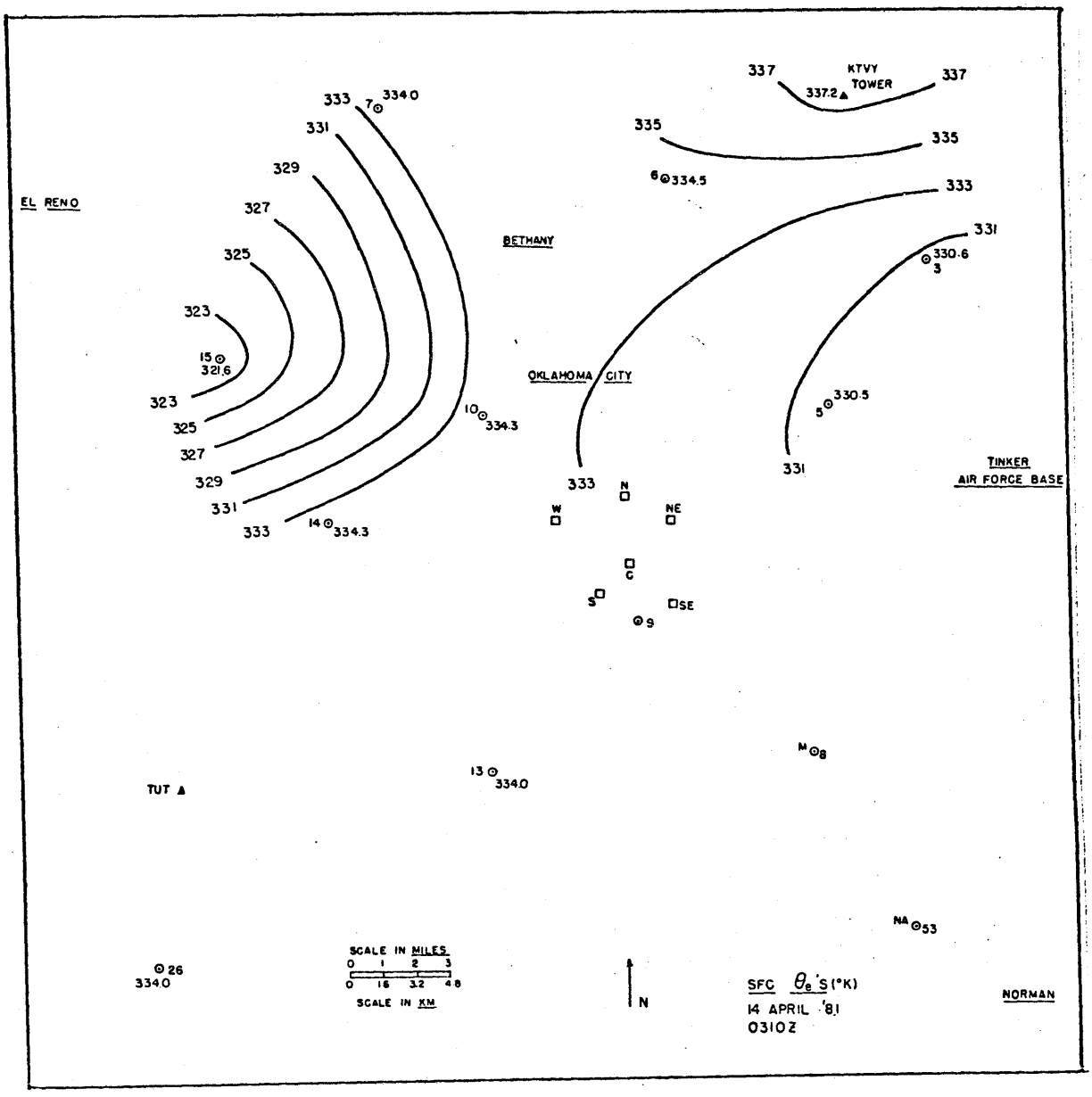
EL RENO
BETHANY
OKLAHOMA CITY
TINKER AIR FORCE BASE
NORMAN
TUT
KTVY TOWER
337.2
337
335
333
331
329
327
325
323
334.0
334.5
330.6
330.5
321.6
334.3
SCALE IN MILES
0 1 2 3
0 1.6 3.2 4.8
SCALE IN KM
N
SFC θ_e'S (°K)
14 APRIL '81
0310Z

Figure 4.18

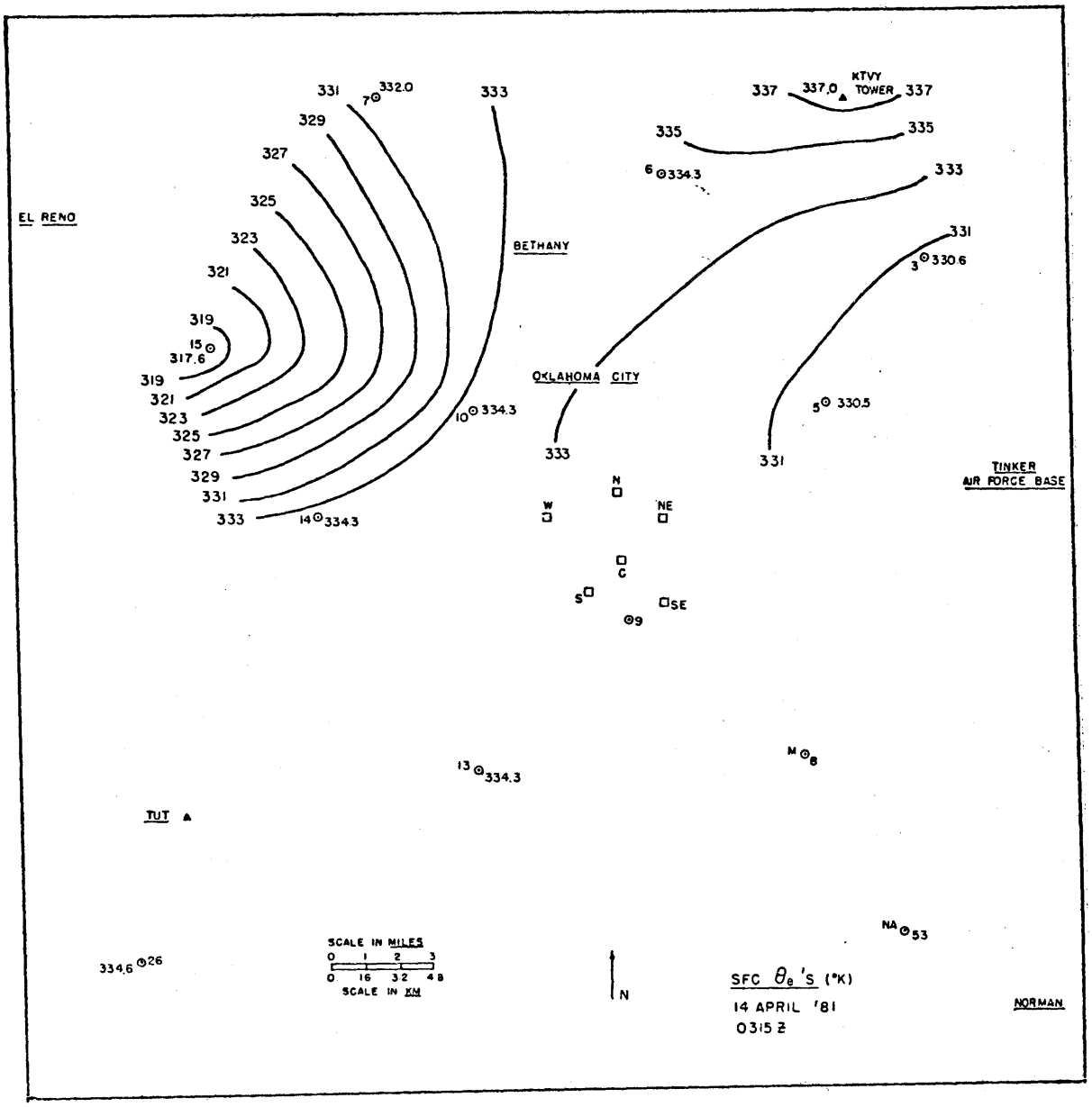
EL RENO
BETHANY
OKLAHOMA CITY
TINKER AIR FORCE BASE
NORMAN
TUT
KTVY TOWER
331
7 332.0
333
329
327
325
323
321
319
15 317.6
319
321
323
325
327
329
331
333
14 334.3
10 334.3
337
337.0
337
335
335
6 334.3
333
331
3 330.6
333
331
5 330.5
N
W
NE
C
S
SE
9
13 334.3
M 8
NA 53
334.6 26
SCALE IN MILES
0 1 2 3
0 1.6 3.2 4.8
SCALE IN KM
N
SFC θe 's (°K)
14 APRIL '81
0315 Z

Figure 4.19

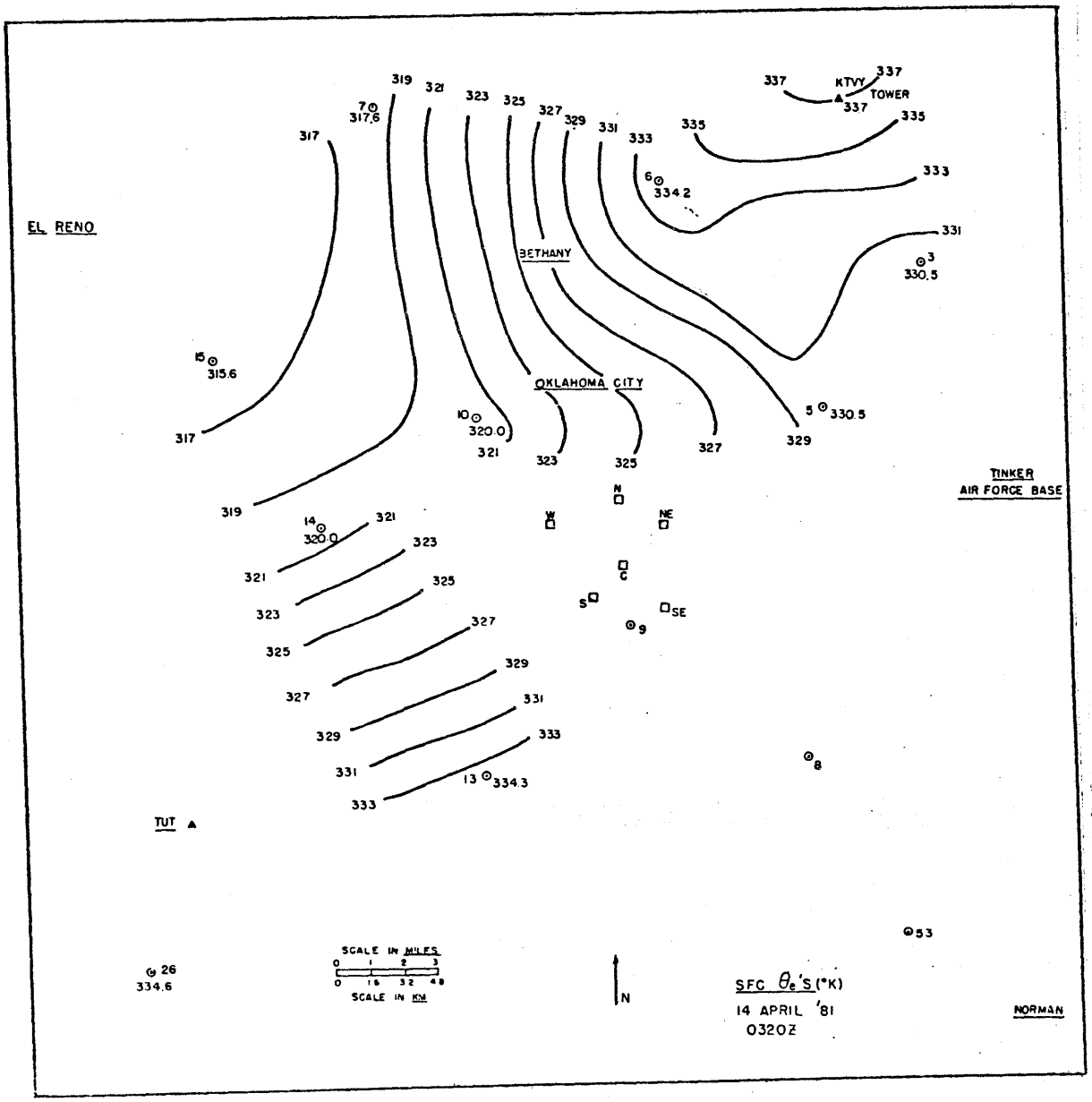
EL RENO
BETHANY
OKLAHOMA CITY
TINKER AIR FORCE BASE
NORMAN
TUT
KTVY TOWER
SCALE IN MILES
SCALE IN KM
N
SFC θe's (°K)
14 APRIL '81
0320Z

Figure 4.20

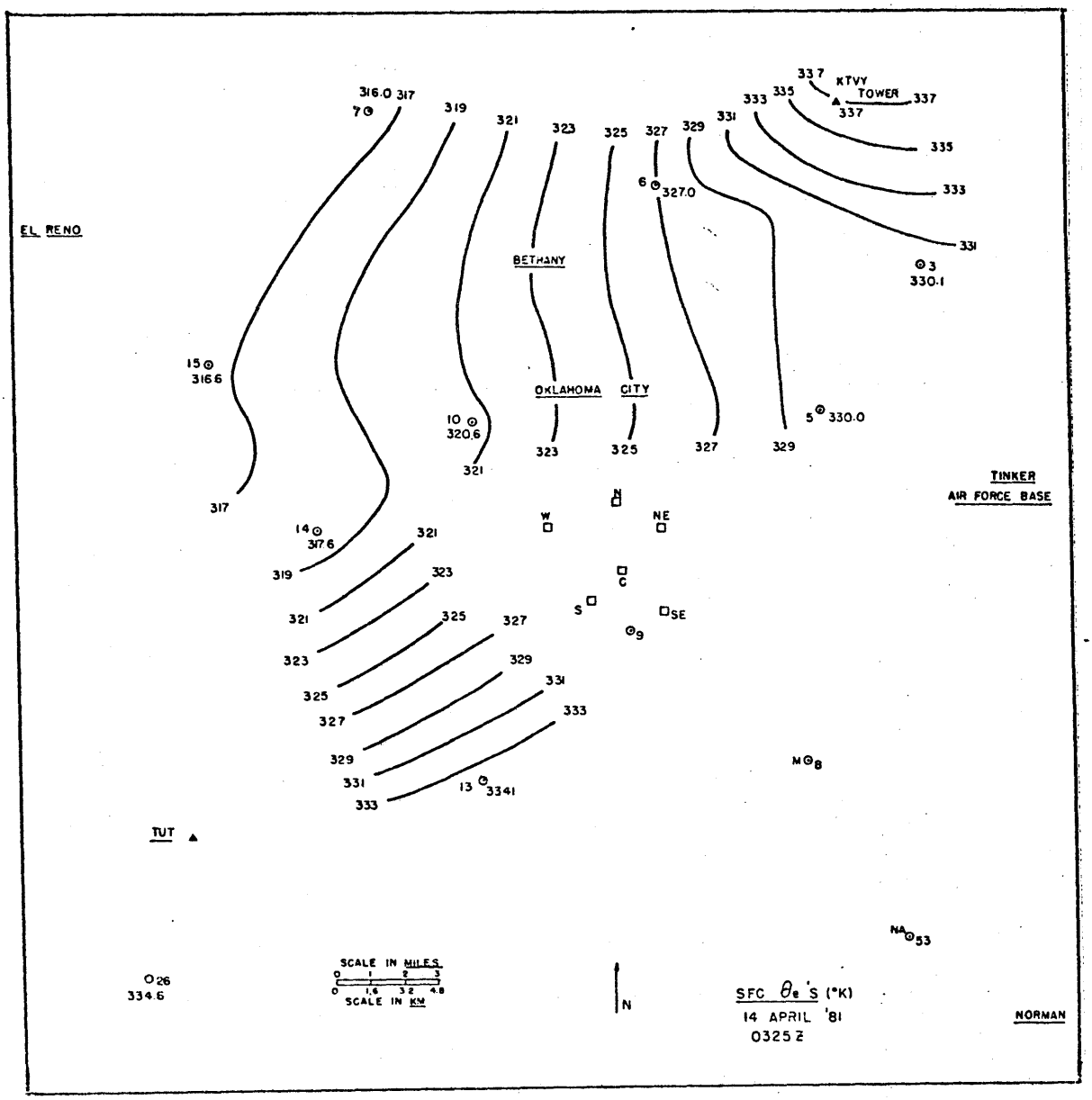
EL RENO
BETHANY
OKLAHOMA CITY
TINKER AIR FORCE BASE
NORMAN
TUT
KTVY TOWER
316.0
317
319
321
323
325
327
329
331
333
335
337
327.0
330.1
330.0
316.6
320.6
317.6
334.1
SCALE IN MILES
SCALE IN KM
N
NE
W
C
S
SE
SFC θe's (°K)
14 APRIL '81
0325 Z

Figure 4.21

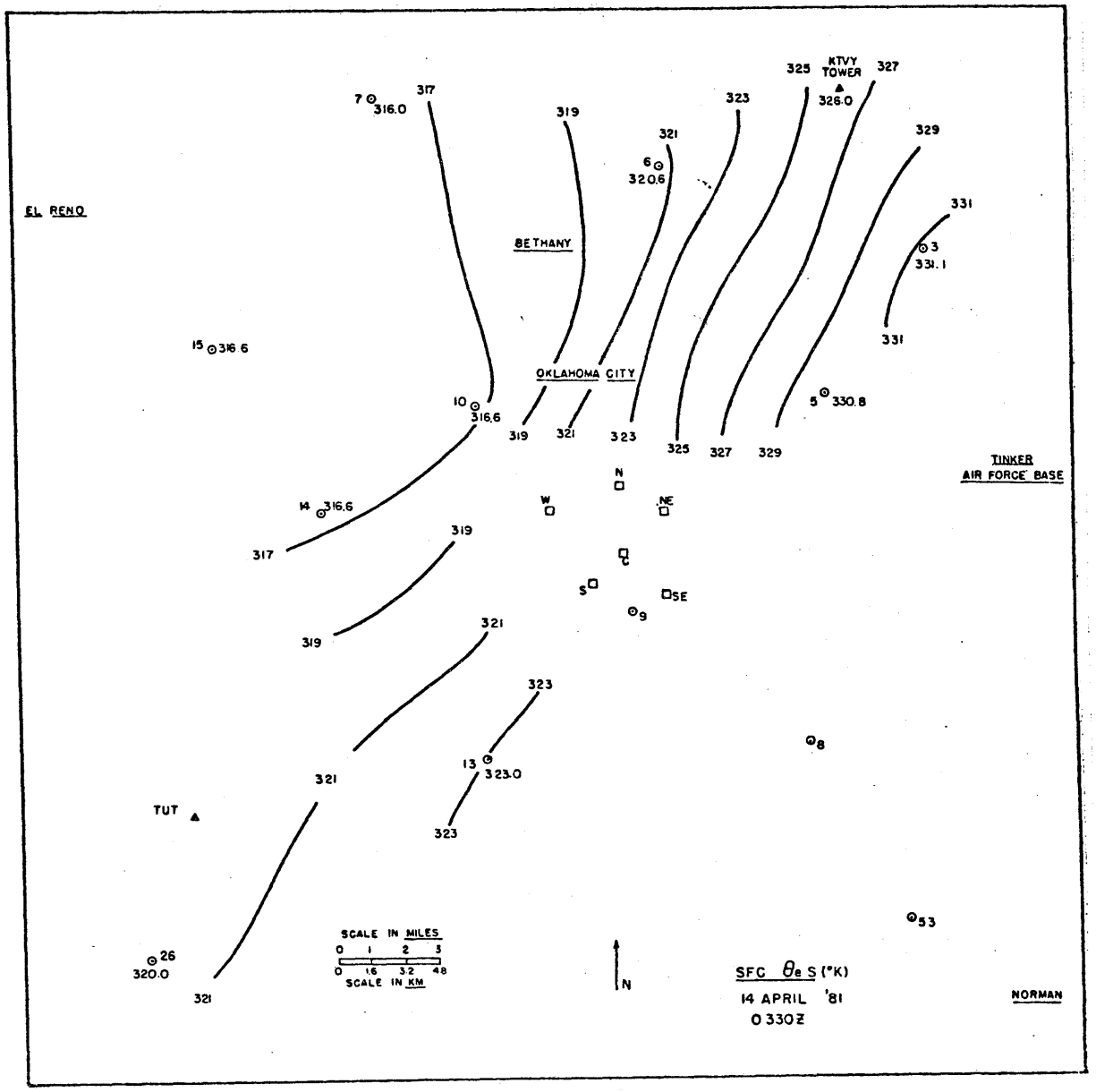
EL RENO
BETHANY
OKLAHOMA CITY
KTVY TOWER
326.0
TINKER AIR FORCE BASE
NORMAN
TUT
7 316.0
6 320.6
3 331.1
15 316.6
10 316.6
14 316.6
13 323.0
5 330.8
9
8
53
26 320.0
317
319
321
323
325
327
329
331
N
W
NE
SE
S
SCALE IN MILES
0 1 2 3
0 1.6 3.2 4.8
SCALE IN KM
SFC θe S (°K)
14 APRIL '81
0330Z

Figure 4.22

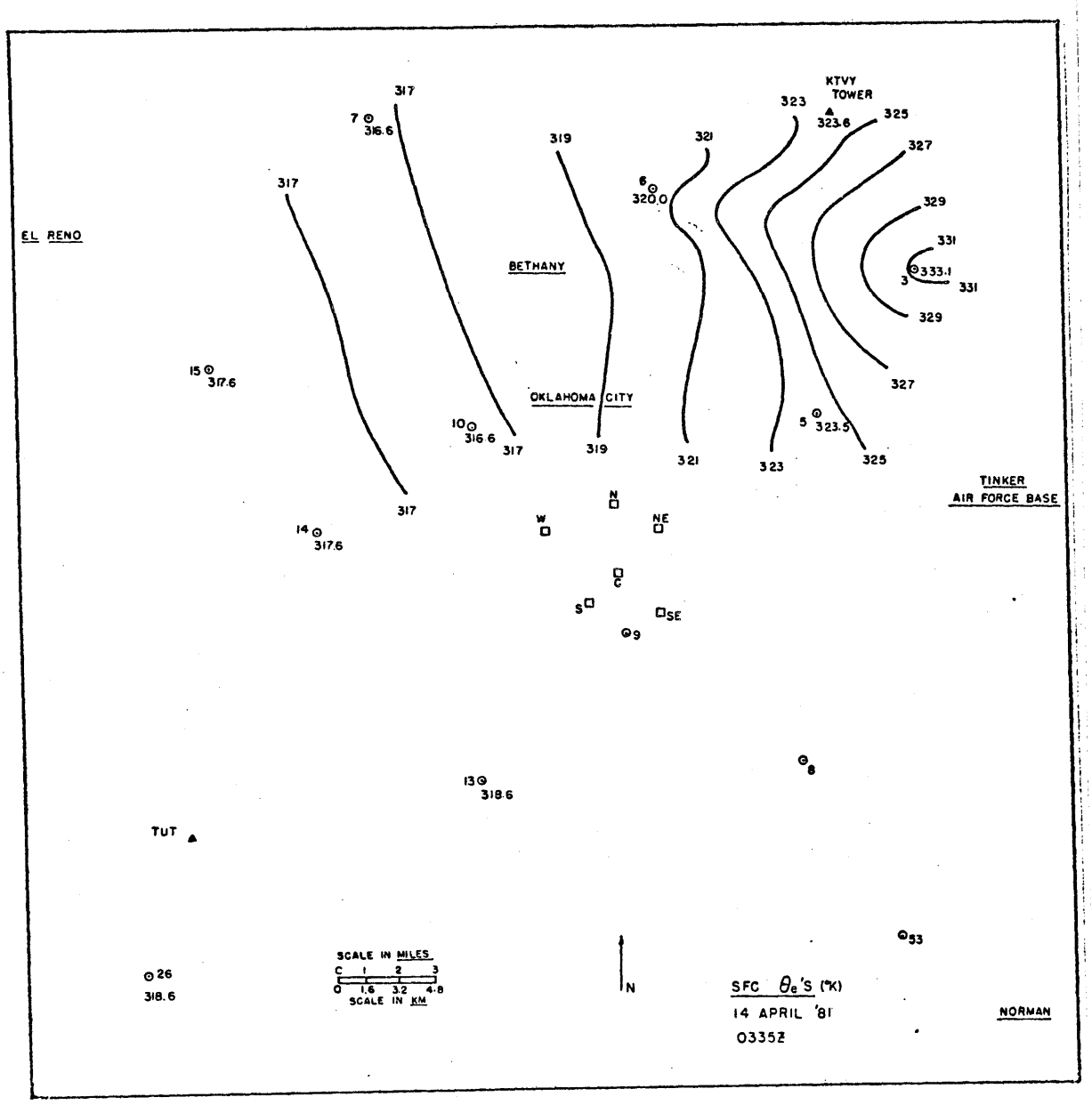
KTVY
TOWER
323.6
EL RENO
BETHANY
OKLAHOMA CITY
TINKER
AIR FORCE BASE
NORMAN
TUT
317
316.6
319
321
320.0
323
325
327
329
331
333.1
317.6
316.6
323.5
N
NE
W
C
S
SE
9
8
13
318.6
14
317.6
15
317.6
10
316.6
6
320.0
5
323.5
3
333.1
7
316.6
26
318.6
53
SCALE IN MILES
0 1 2 3
0 1.6 3.2 4.8
SCALE IN KM
N
SFC θe's (°K)
14 APRIL '81
0335Z

Figure 4.23

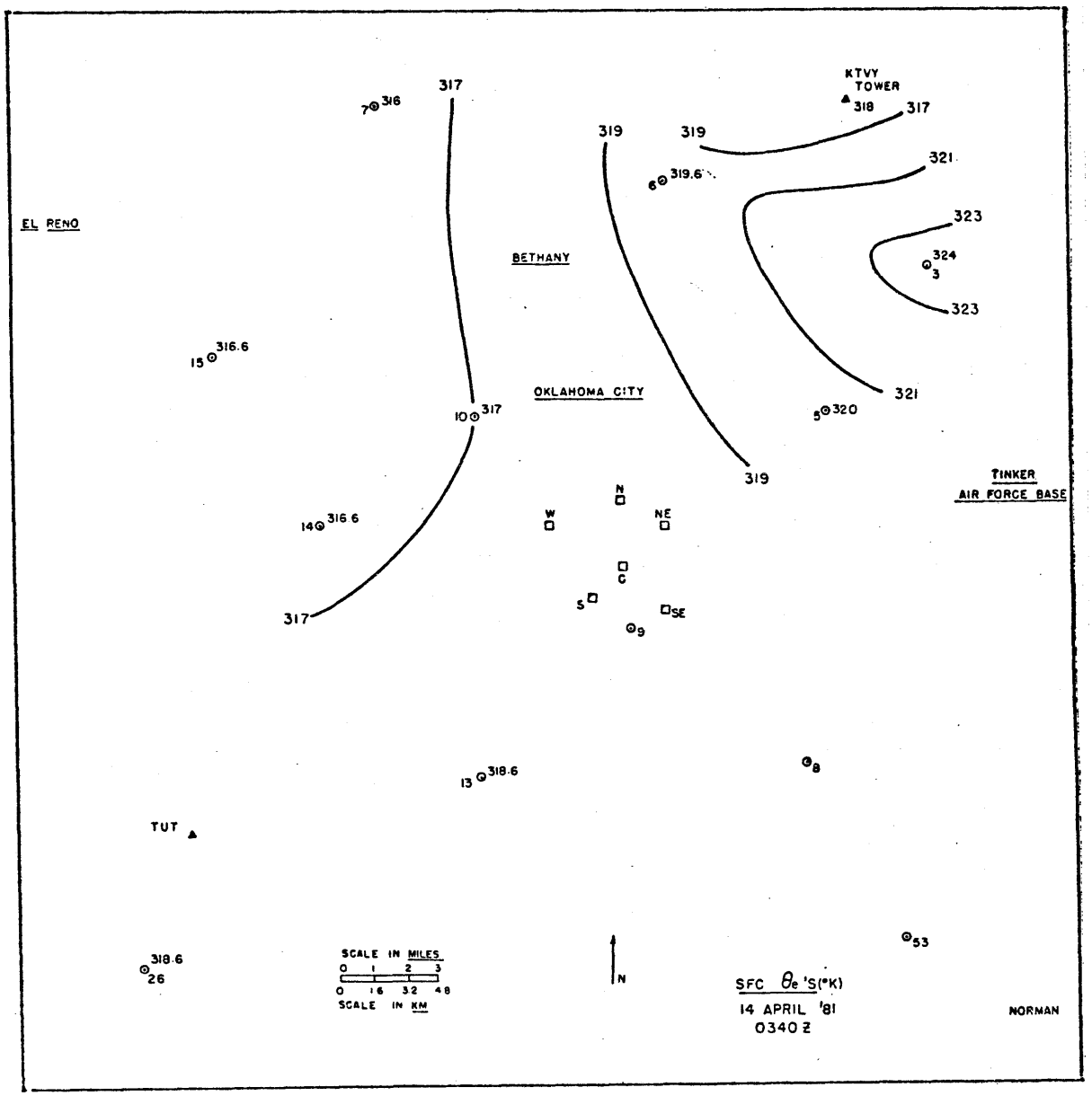
KTVY
TOWER
318
317
319
319
321
323
324
323
321
317
316
316.6
317
319.6
319
320
316.6
317
318.6
318.6
26
53
8
9
EL RENO
BETHANY
OKLAHOMA CITY
TINKER
AIR FORCE BASE
TUT
NORMAN
N
W
NE
C
S
SE
SCALE IN MILES
0 1 2 3
0 1.6 3.2 4.8
SCALE IN KM
N
SFC θe 'S(°K)
14 APRIL '81
0340 Z

Figure 4.24

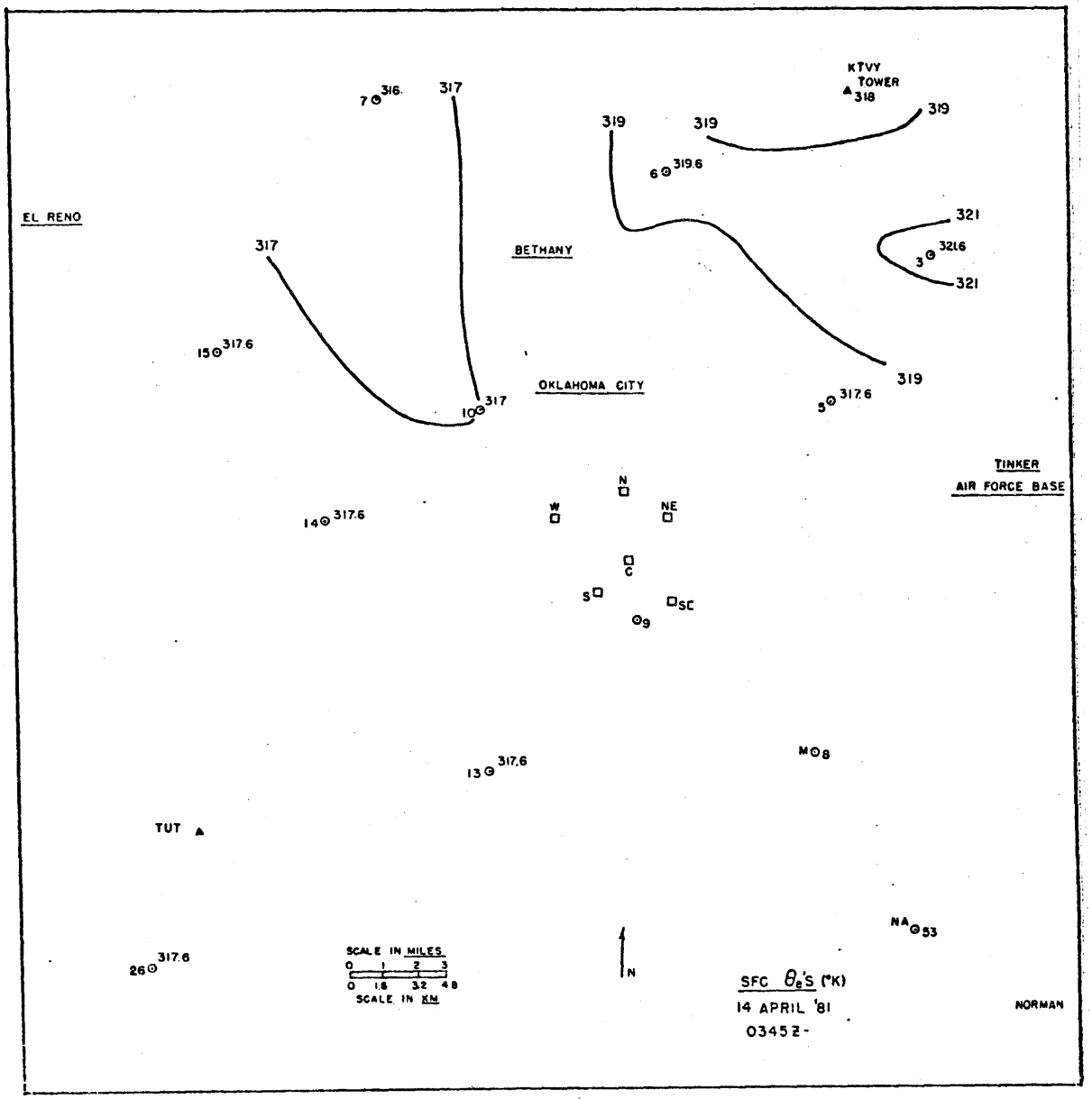
EL RENO
BETHANY
OKLAHOMA CITY
TINKER
AIR FORCE BASE
NORMAN
KTVY
TOWER
318
316
317
317
319
319
319
319.6
321
321.6
321
317.6
317
317.6
317.6
317.6
317.6
317.6
TUT
N
W
NE
C
S
SC
SCALE IN MILES
0 1 2 3
0 1.6 3.2 4.8
SCALE IN KM
N
SFC θe's (°K)
14 APRIL '81
0345Z-

Figure 4.25

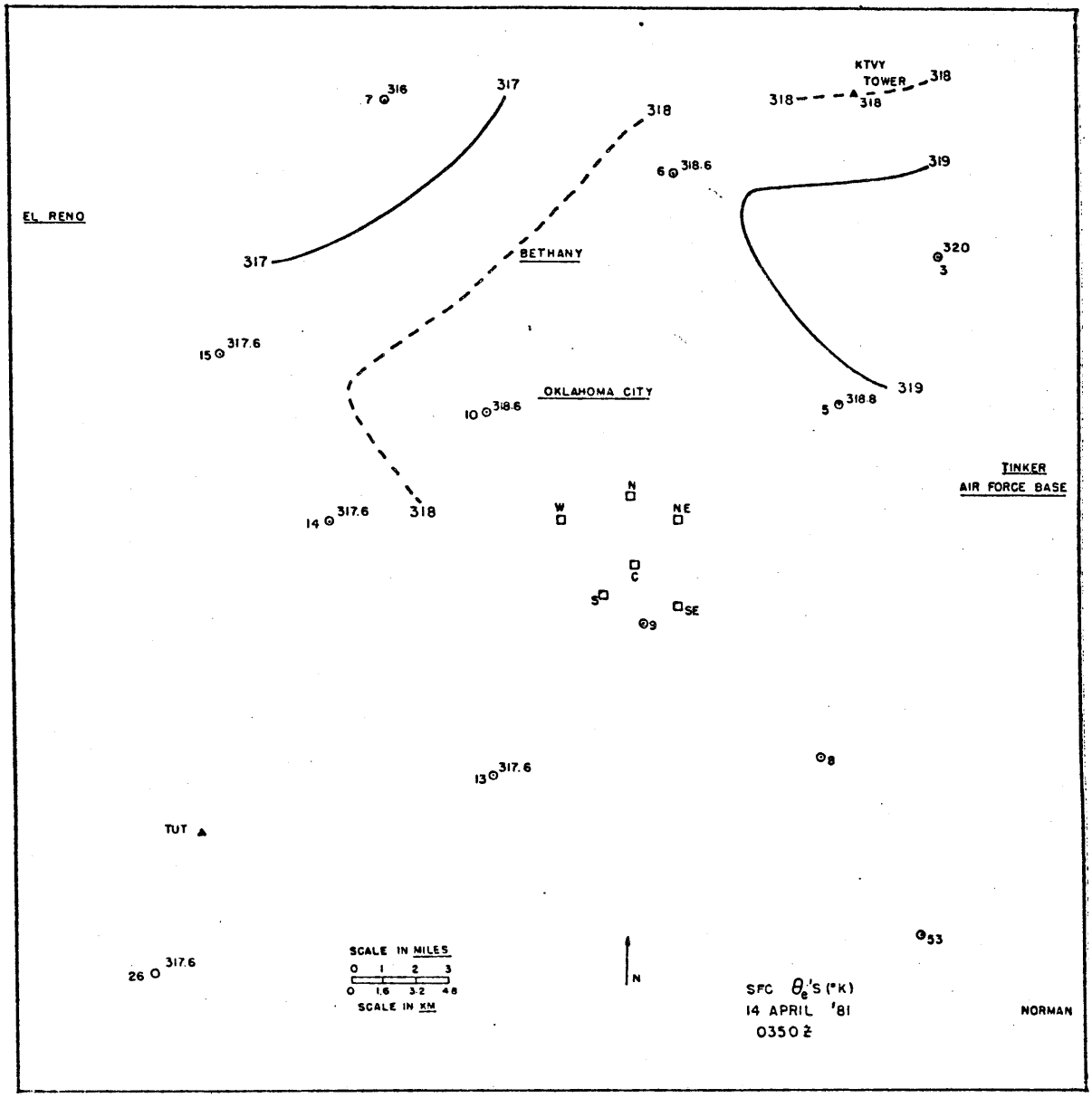
EL RENO
BETHANY
OKLAHOMA CITY
TINKER
AIR FORCE BASE
NORMAN
KTVY
TOWER
TUT
317
318
319
320
316
317.6
318.6
318.8
SCALE IN MILES
0 1 2 3
0 1.6 3.2 4.8
SCALE IN KM
N
NE
W
C
S
SE
SFC θ_e'S (°K)
14 APRIL '81
0350 Z

Figure 4.26

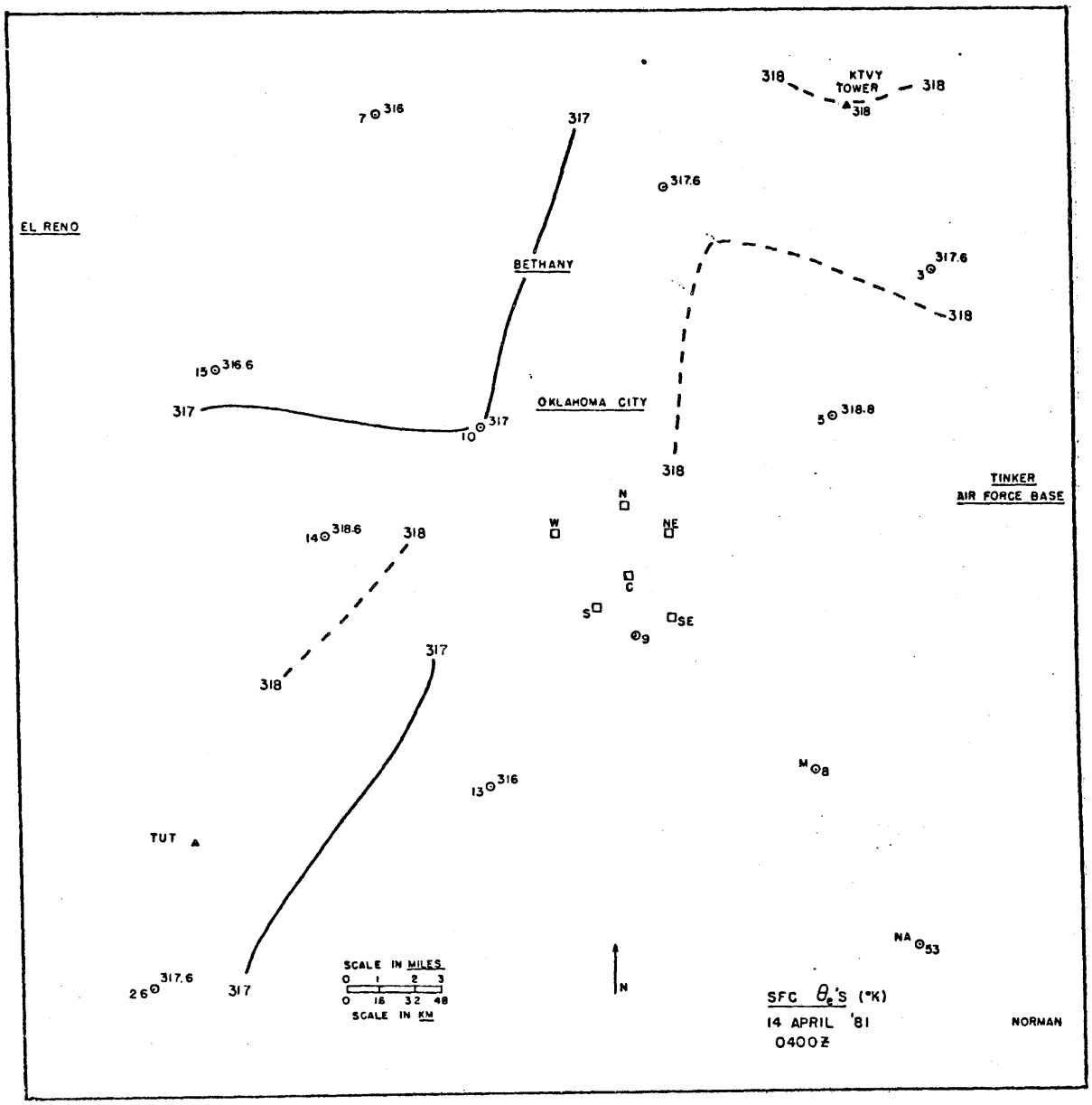
KTVY TOWER
318
318
318
7 316
317
317.6
EL RENO
BETHANY
317.6
3
318
15 316.6
317
OKLAHOMA CITY
10 317
5 318.8
318
TINKER AIR FORCE BASE
N
W
NE
14 318.6
318
C
S
SE
9
317
318
M 8
13 316
TUT
NA 53
SCALE IN MILES
0 1 2 3
0 16 32 48
SCALE IN KM
N
SFC θe'S (°K)
14 APRIL '81
0400Z
NORMAN
26 317.6
317

Figure 4.27

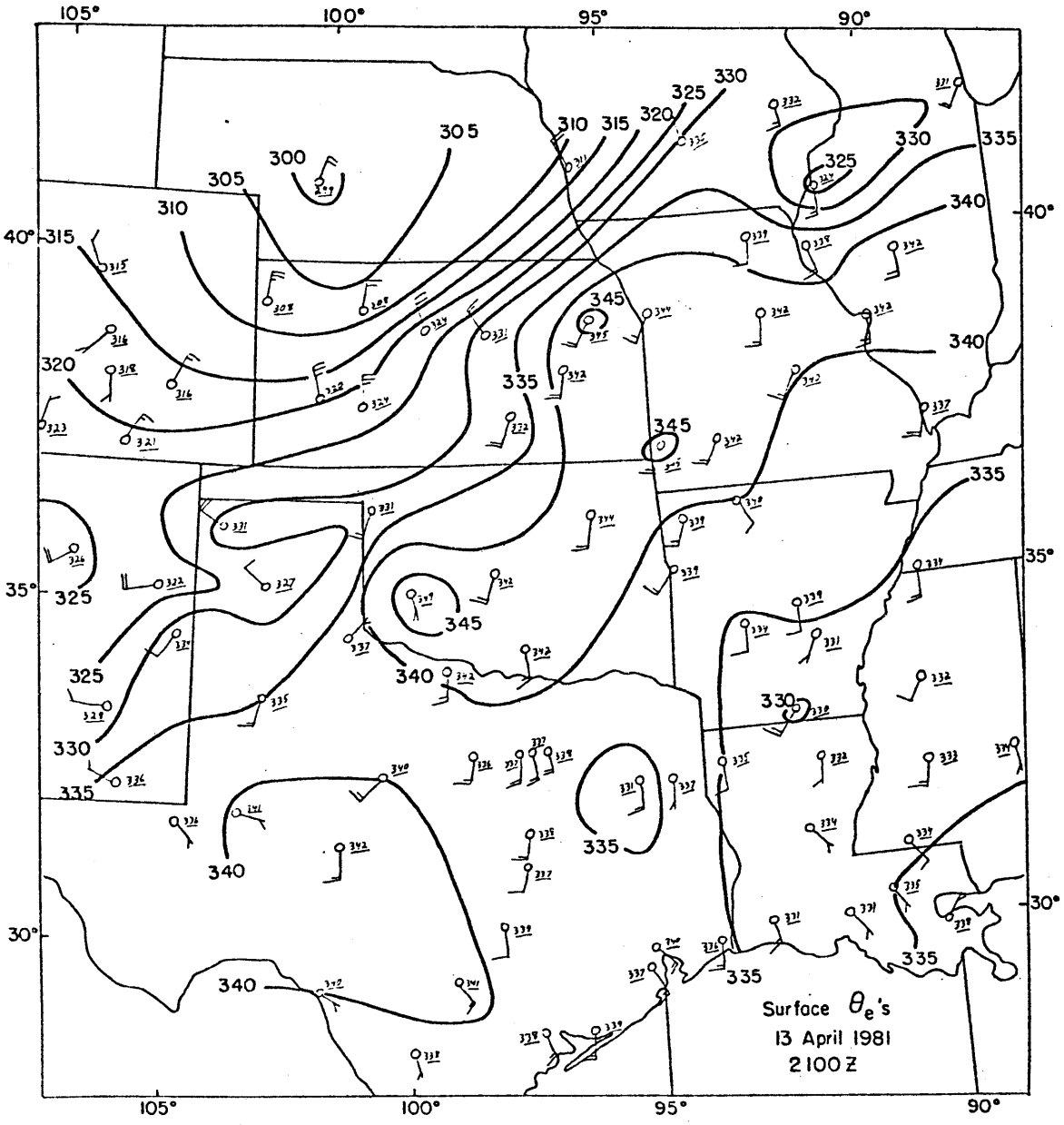

Figure 4.28

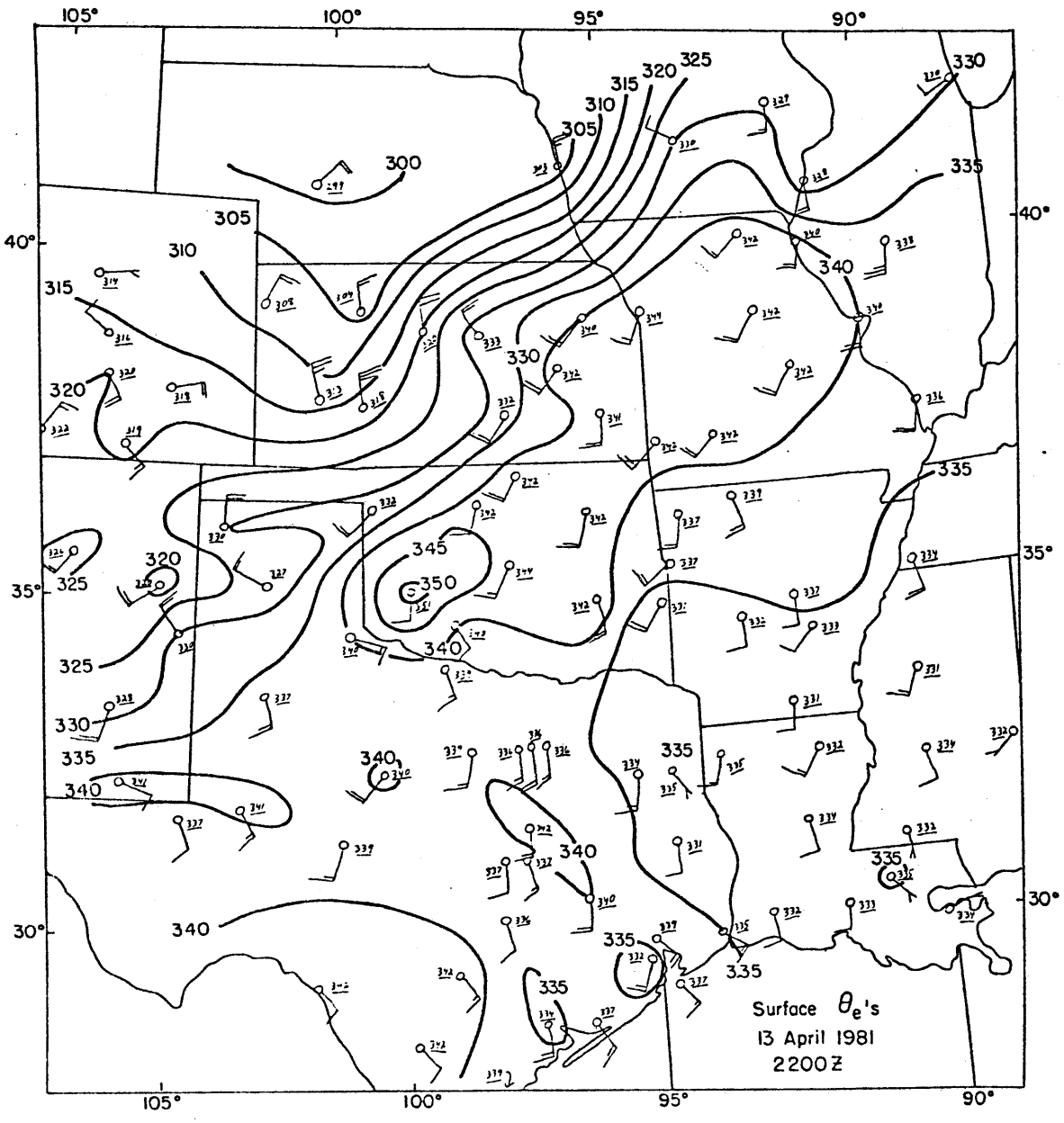

Figure 4.29

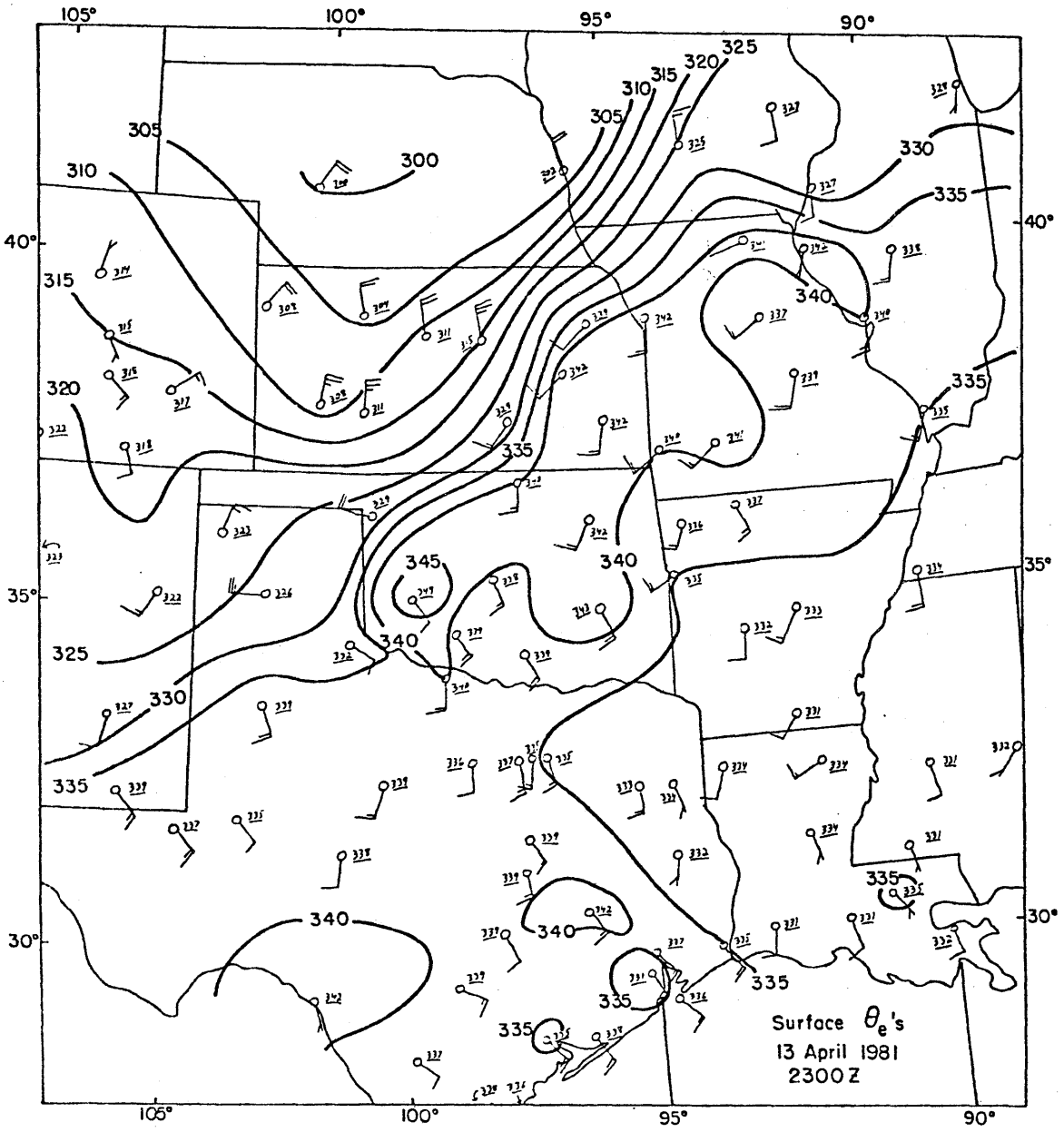

Figure 4.30

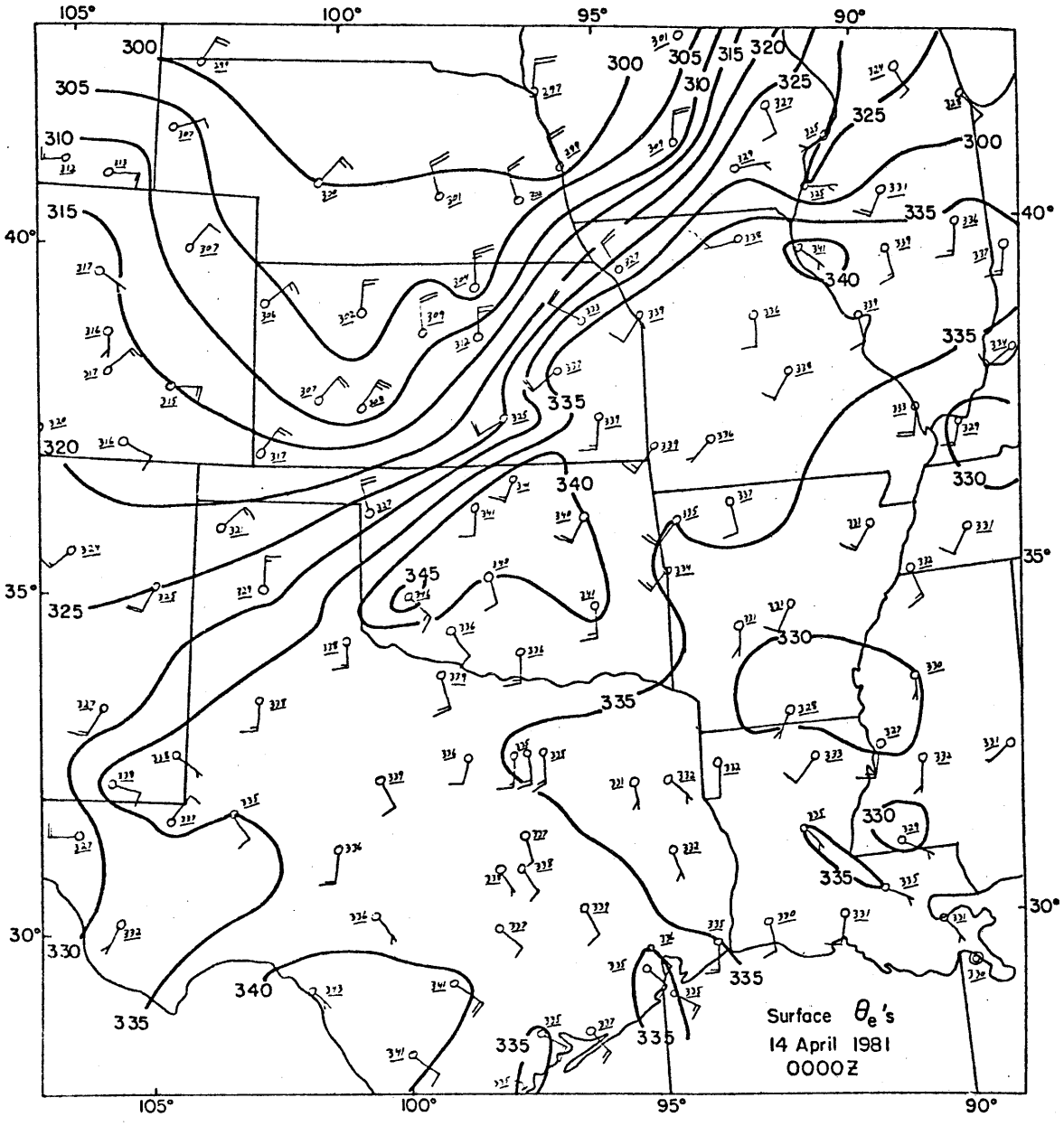

Figure 4.31

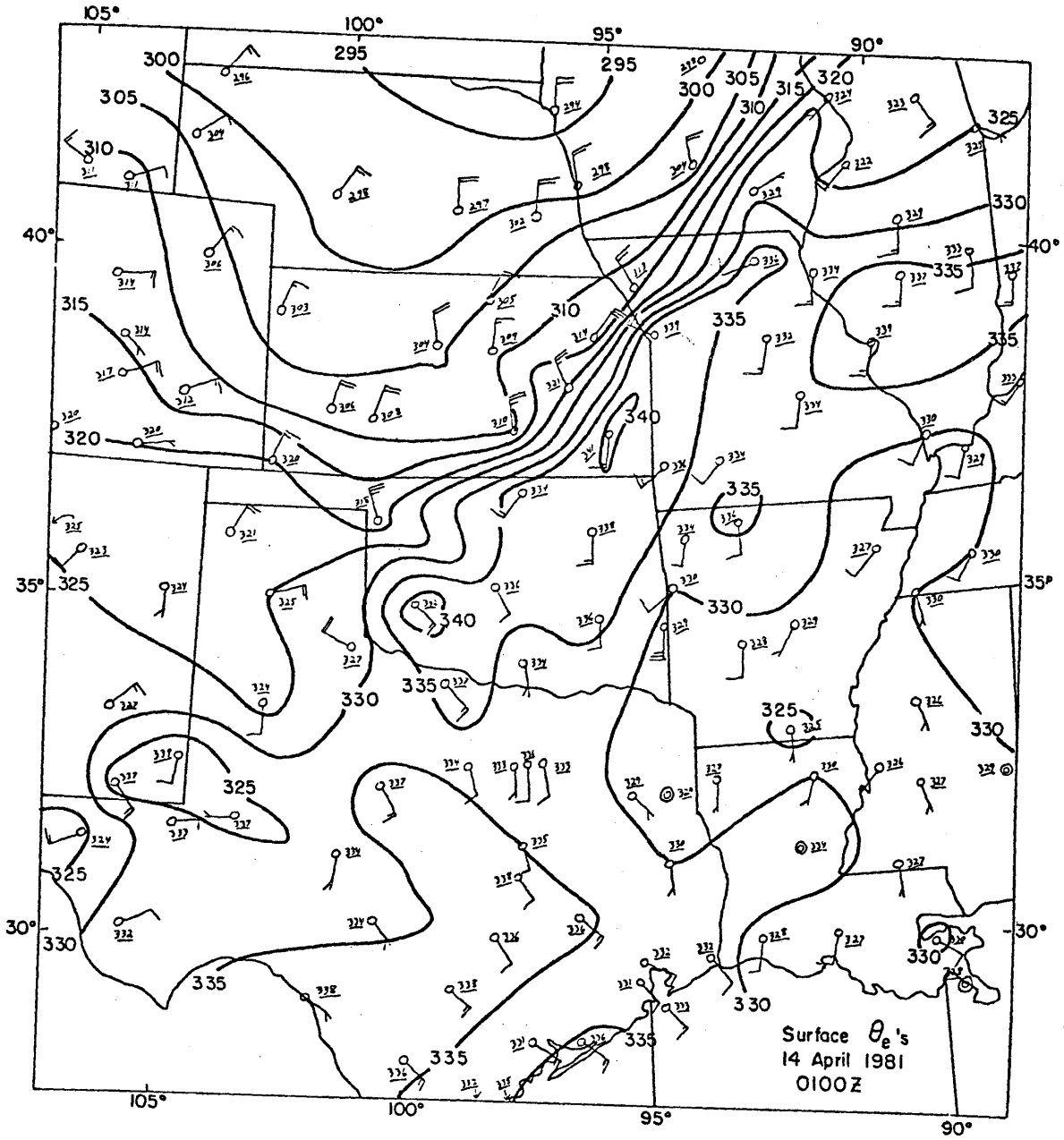

Figure 4.32

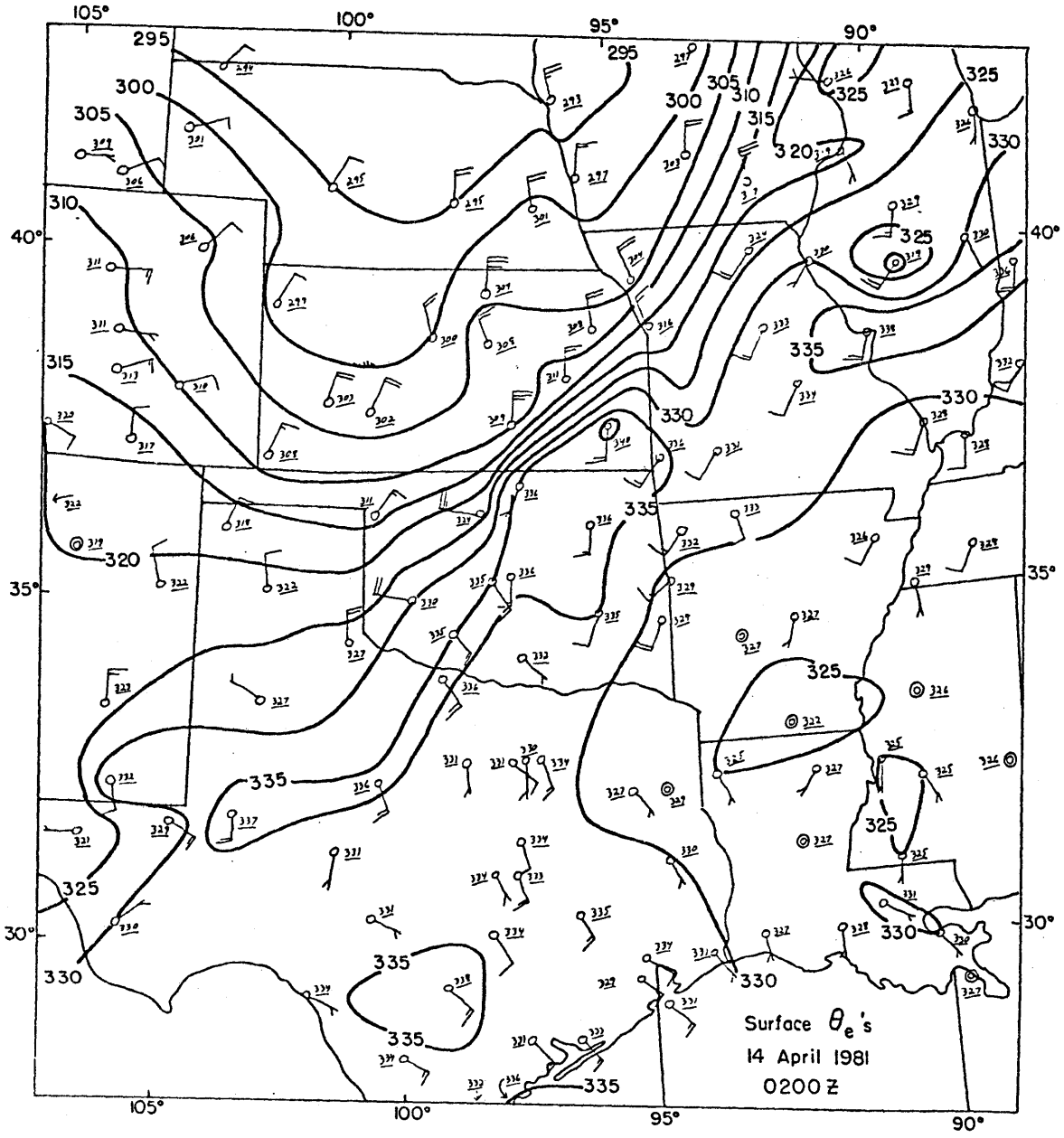

Figure 4.33

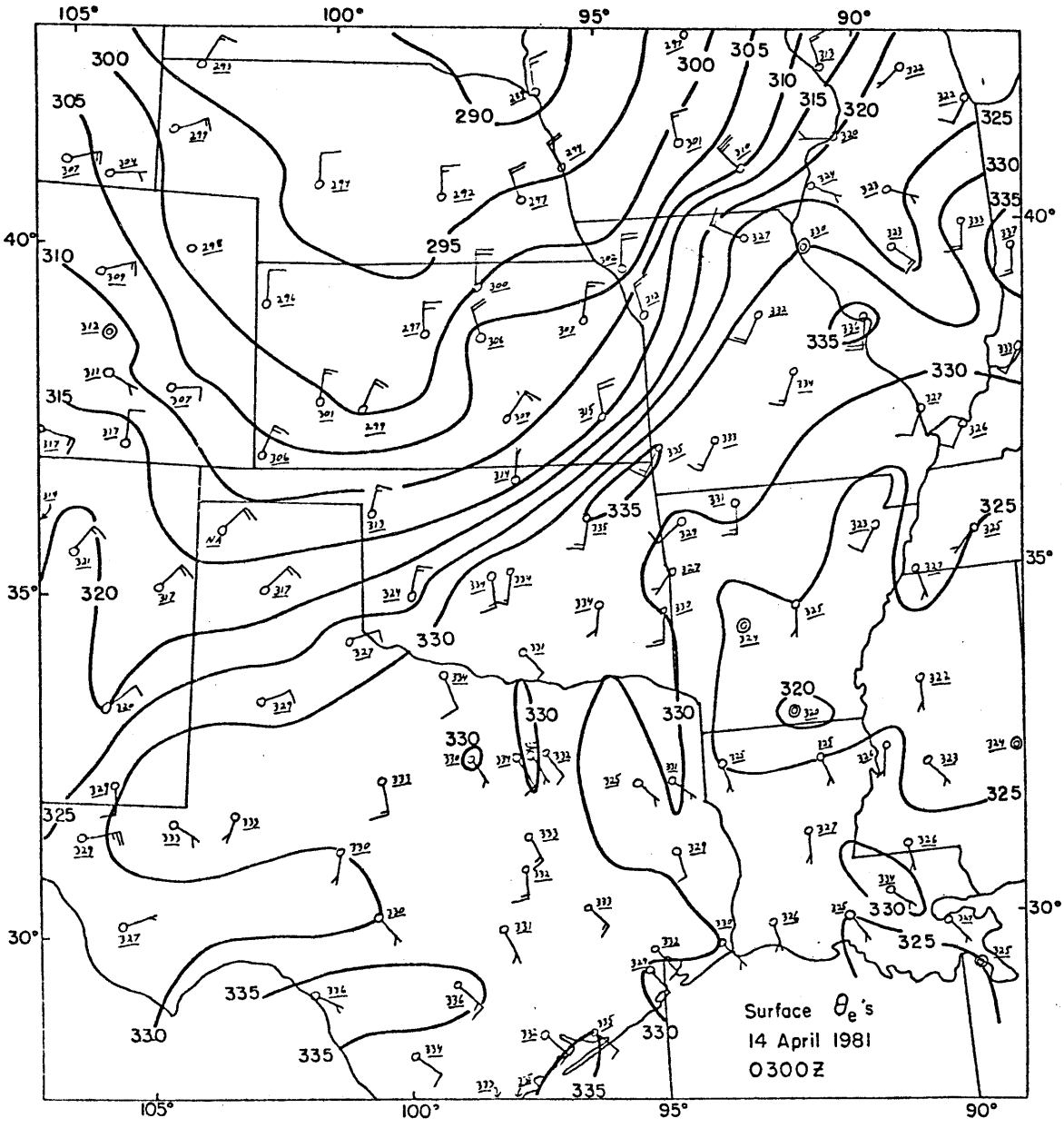

Figure 4.34

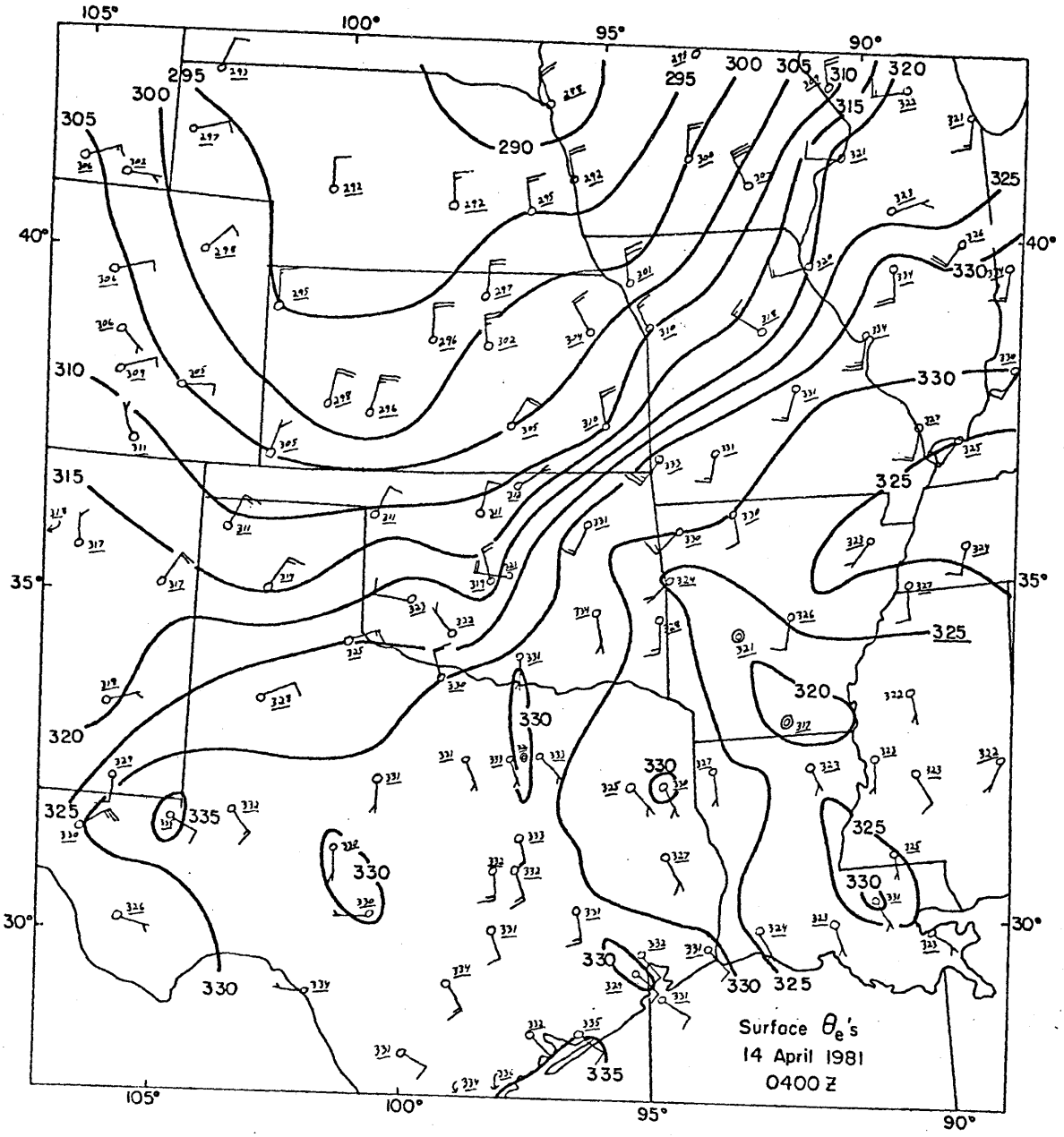

Figure 4.35

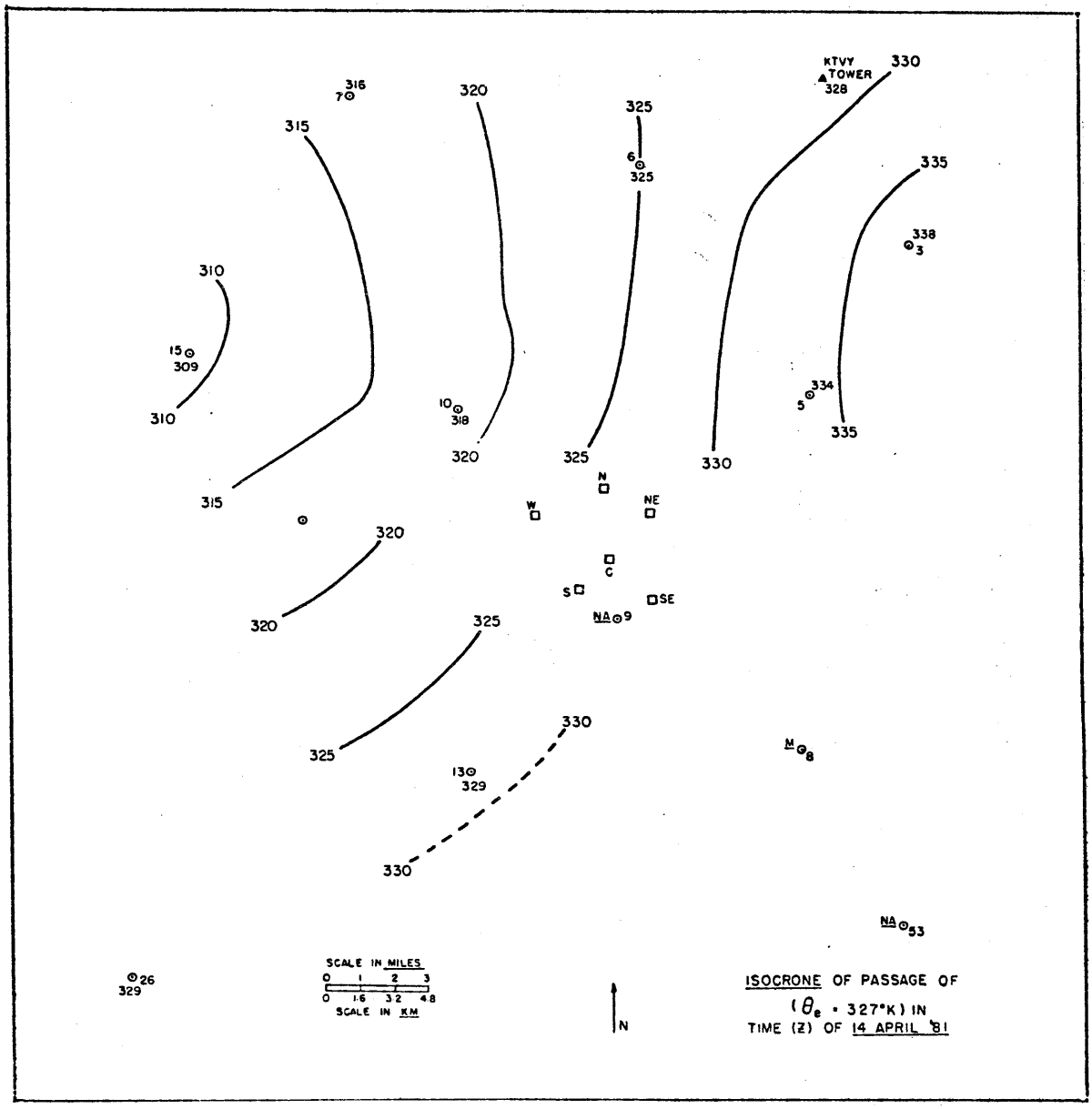
KTVY TOWER 328
330
316
7
320
315
325
6
325
335
338
3
310
15
309
310
10
318
320
325
330
334
5
335
315
N
W
NE
C
S
SE
NA 9
320
320
325
325
330
13
329
330
M 8
NA 53
26
329
SCALE IN MILES
0 1 2 3
0 1.6 3.2 4.8
SCALE IN KM
N
ISOCRONE OF PASSAGE OF
(θe = 327°K) IN
TIME (Z) OF 14 APRIL '81

Figure 4.36

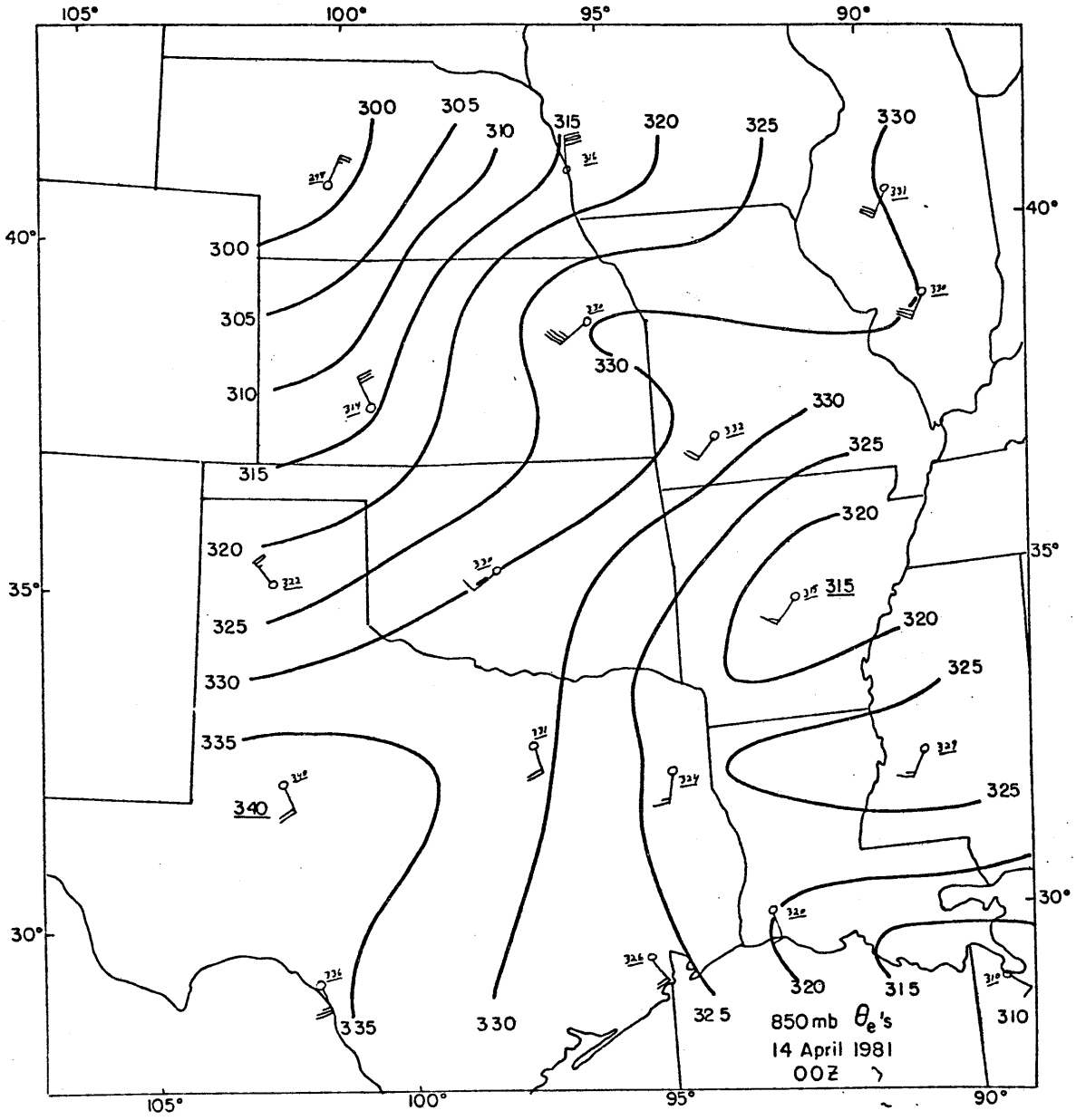
105°
100°
95°
90°
40°
35°
30°
300
305
310
315
320
325
330
335
340
850mb θe's
14 April 1981
00Z

Figure 4.37

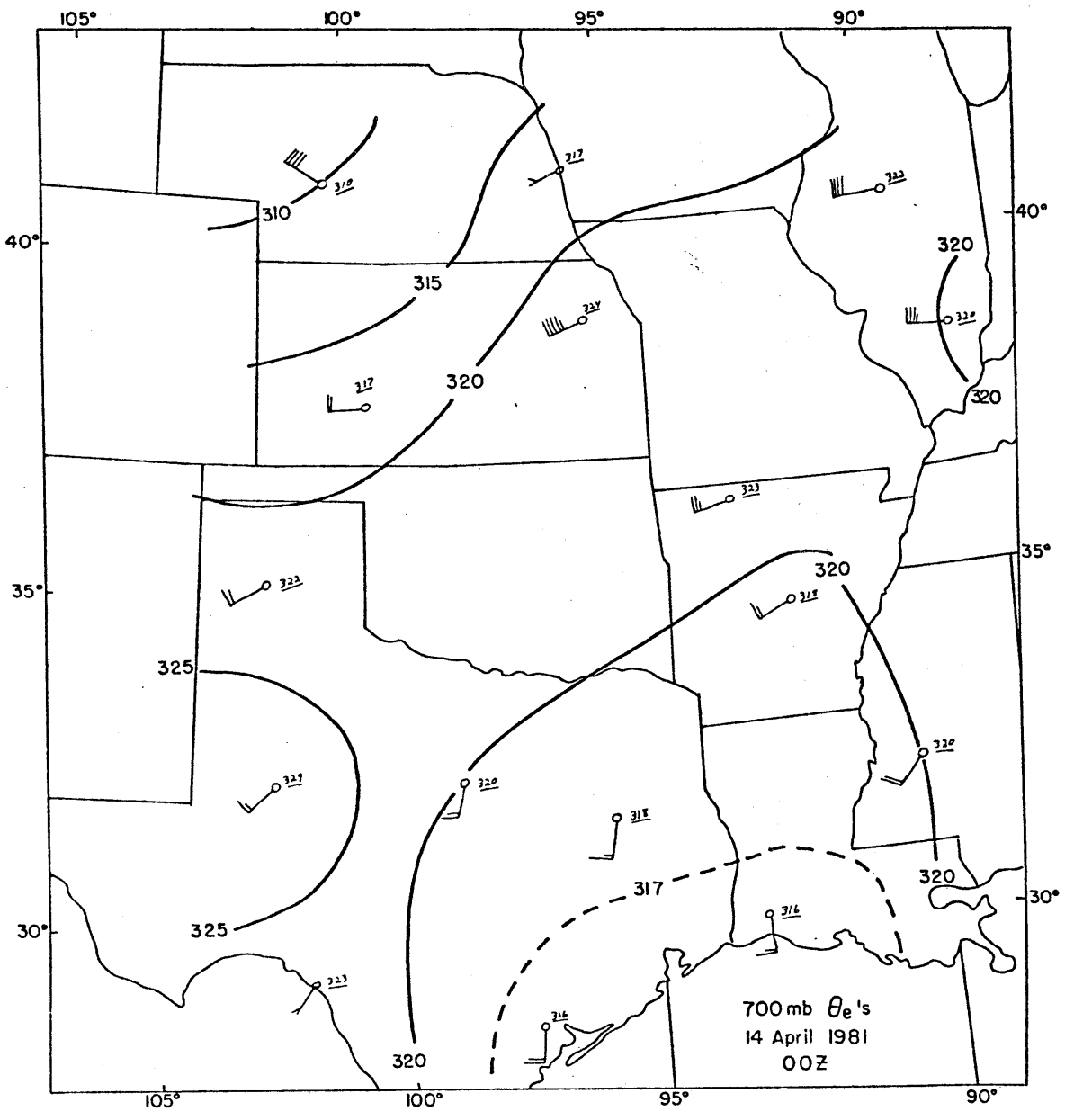
105°
100°
95°
90°
40°
35°
30°
310
315
320
325
317
700 mb θe's
14 April 1981
00Z

Figure 4.38

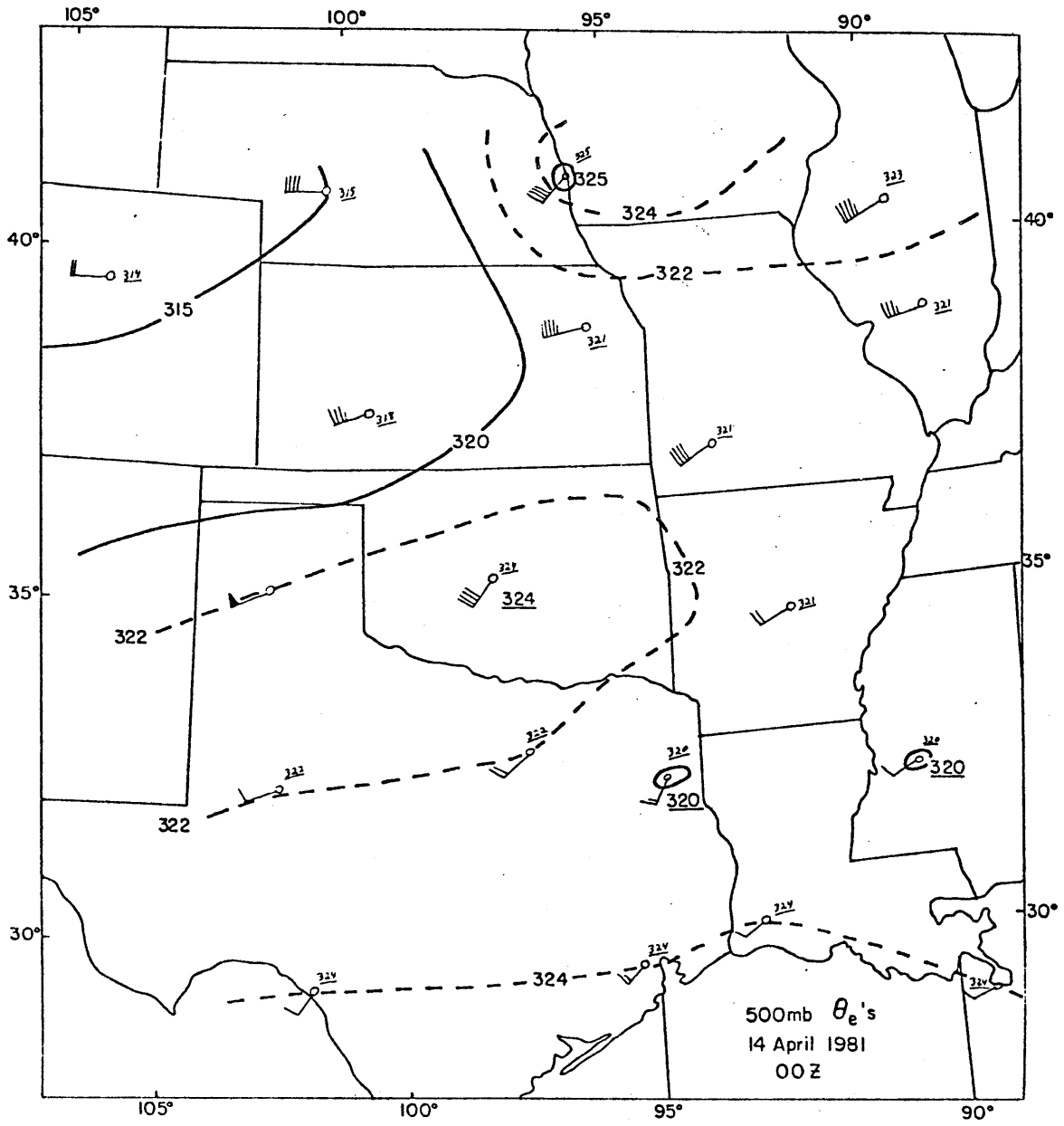
105°
100°
95°
90°
40°
35°
30°
315
320
322
324
325
500mb θ_e's
14 April 1981
00Z

Figure 4.39

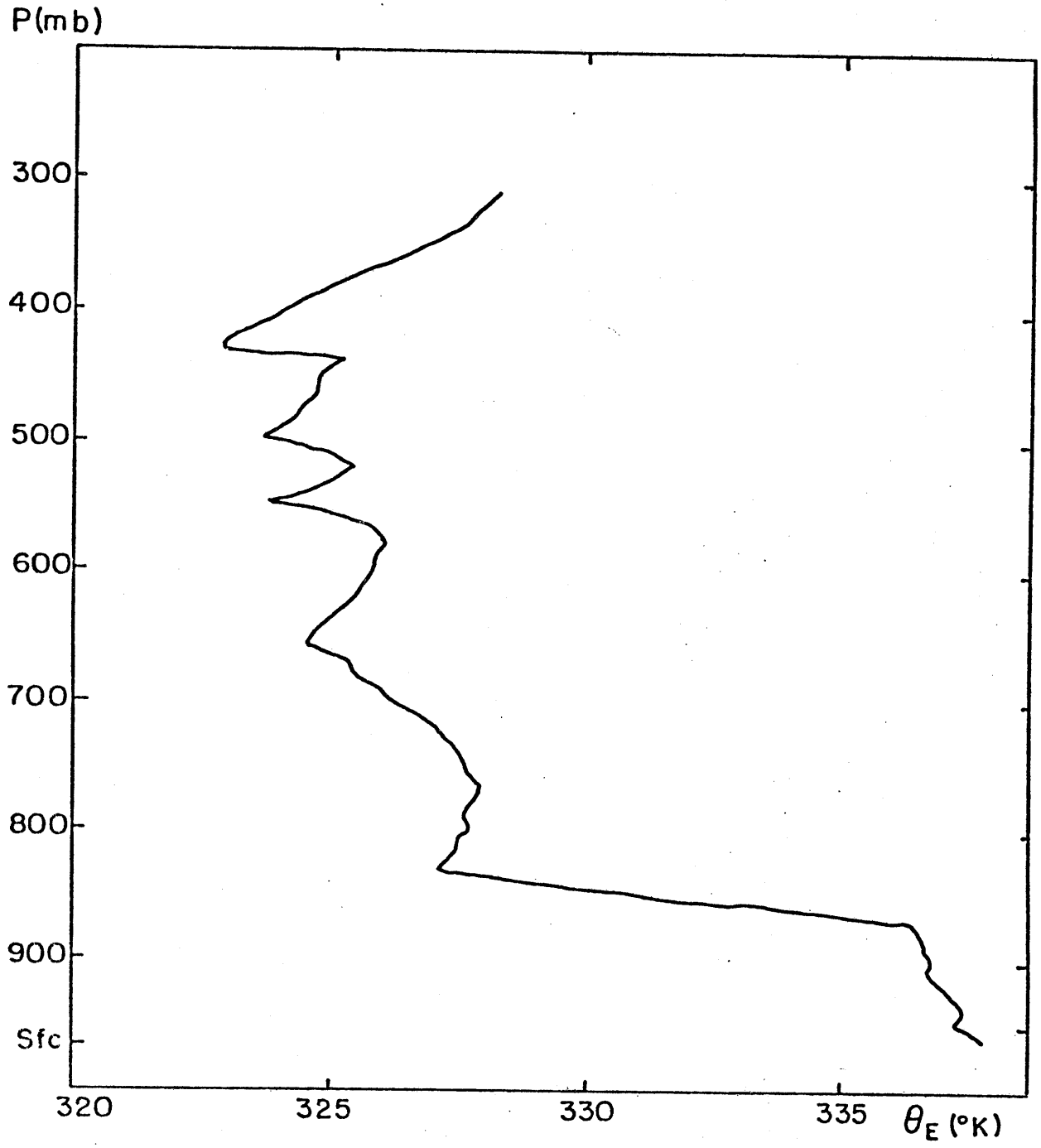

Figure 4.40

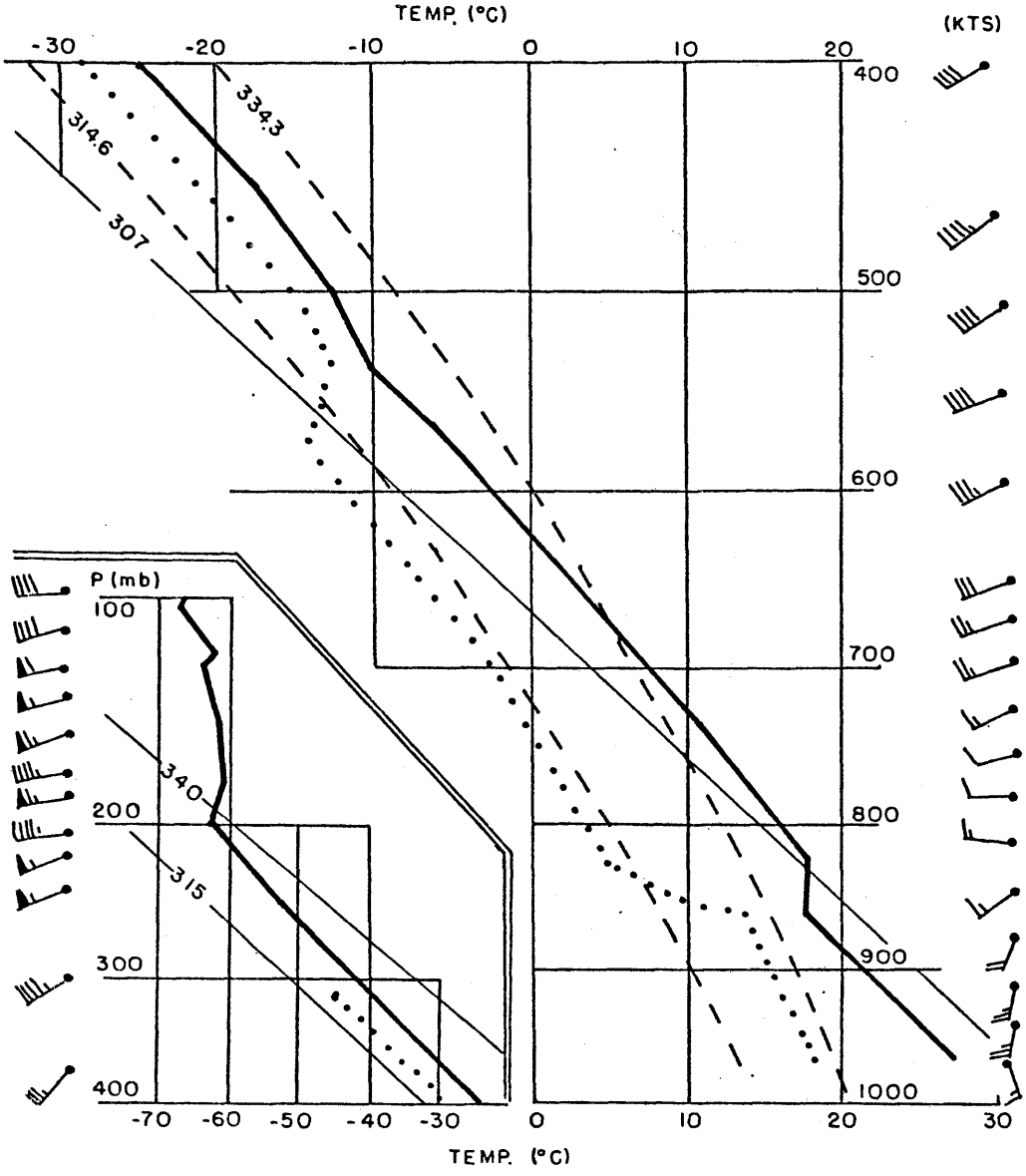
TEMP. (°C)
-30
-20
-10
0
10
20
(KTS)
400
500
600
700
800
900
1000
3343
3146
307
P (mb)
100
200
300
400
340
315
-70
-60
-50
-40
-30
0
10
20
30
TEMP. (°C)

Figure 4.41

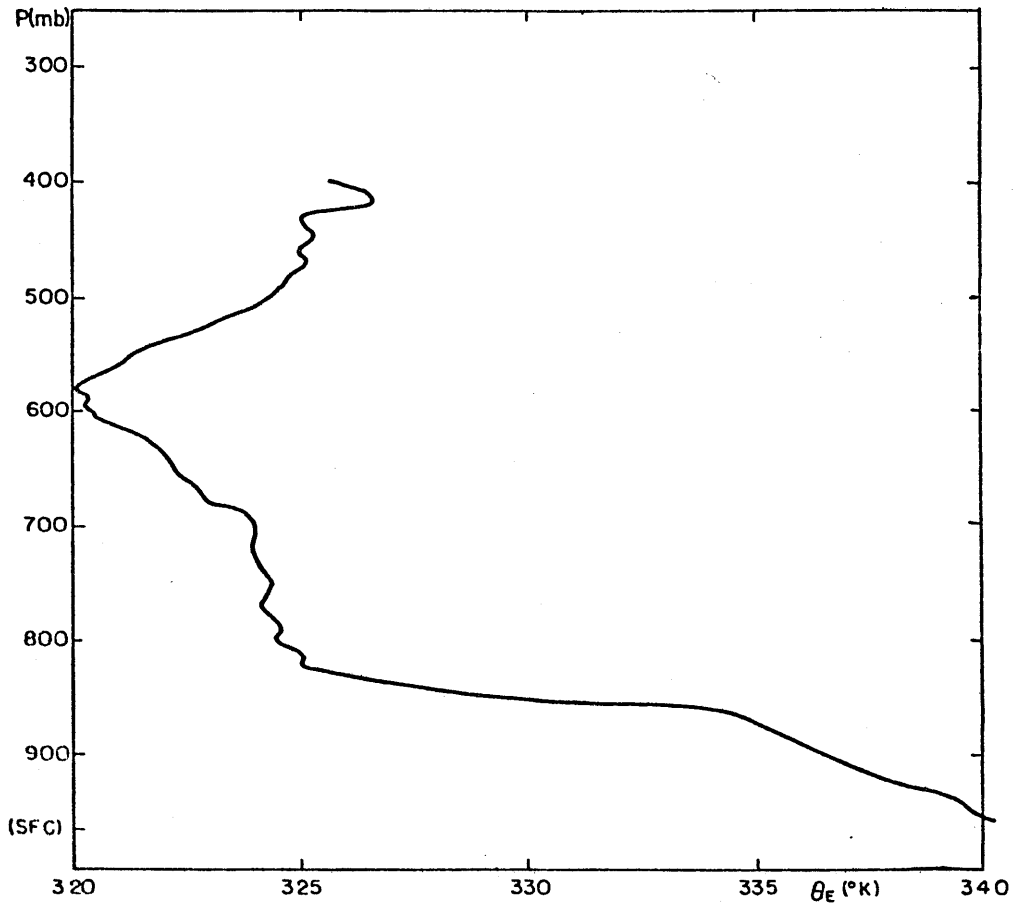

Figure 4.42

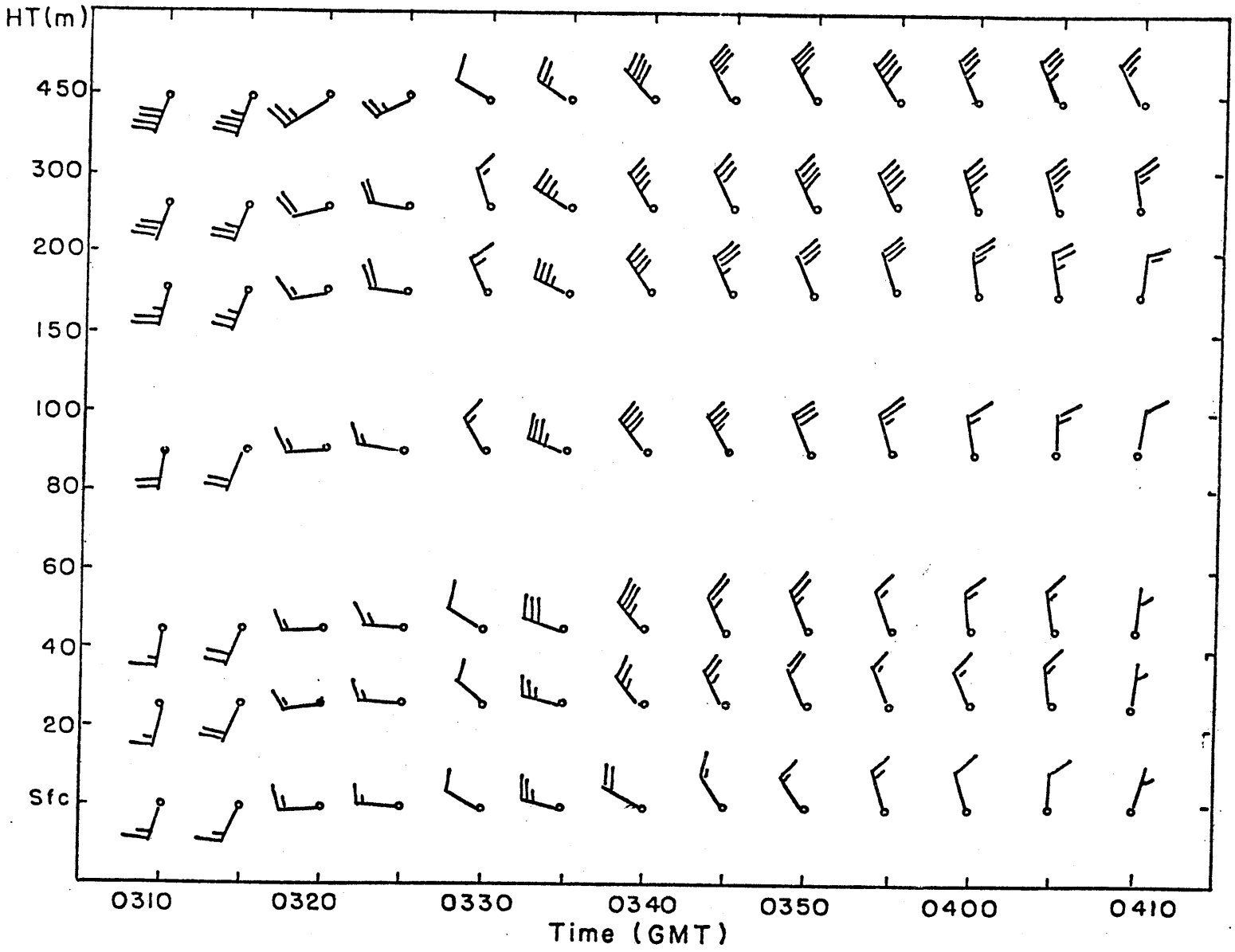
HT(m)
450
300
200
150
100
80
60
40
20
Sfc
0310
0320
0330
0340
0350
0400
0410
Time (GMT)

Figure 4.43

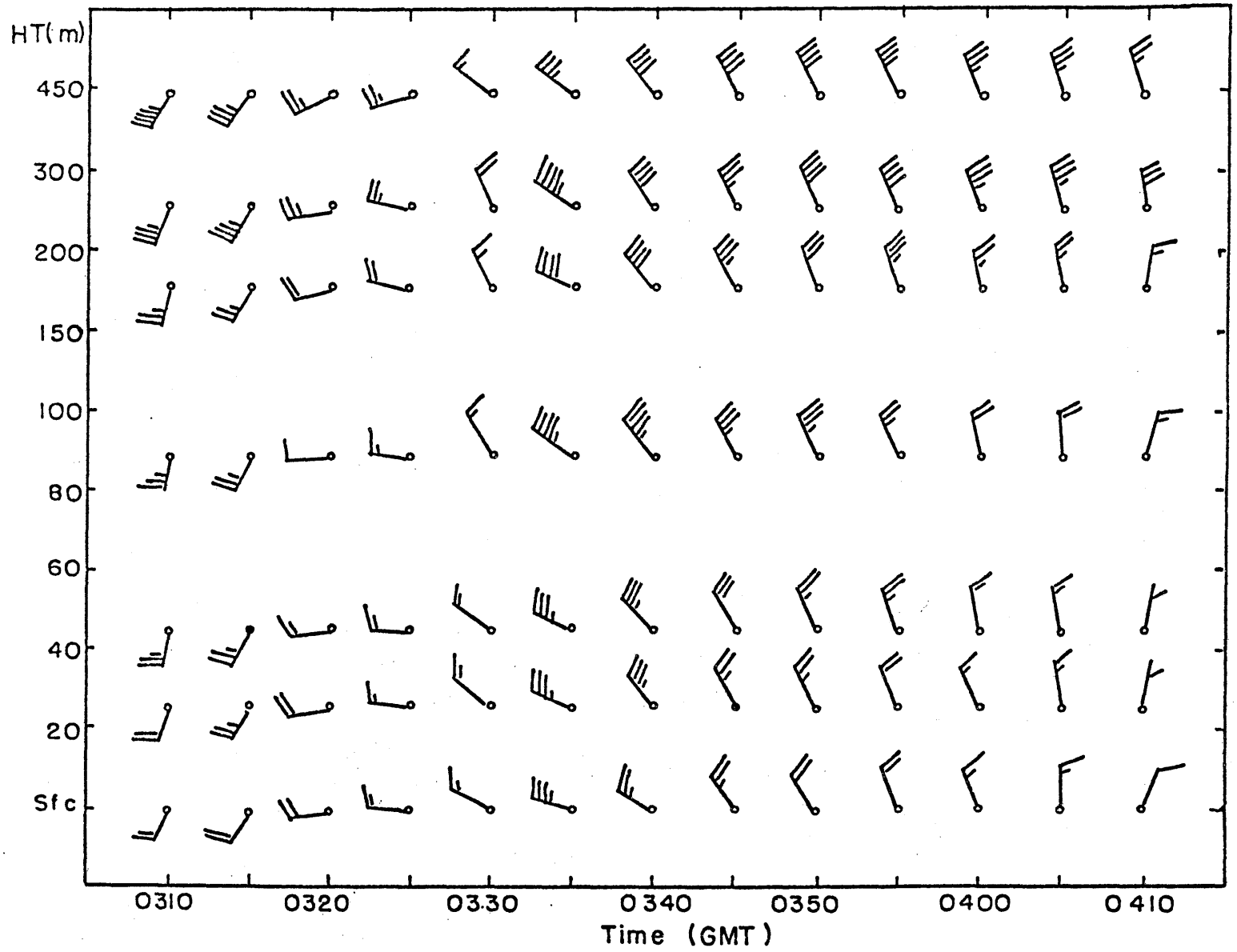
HT(m)
450
300
200
150
100
80
60
40
20
Sfc
0310
0320
0330
0340
0350
0400
0410
Time (GMT)

Figure 4.44

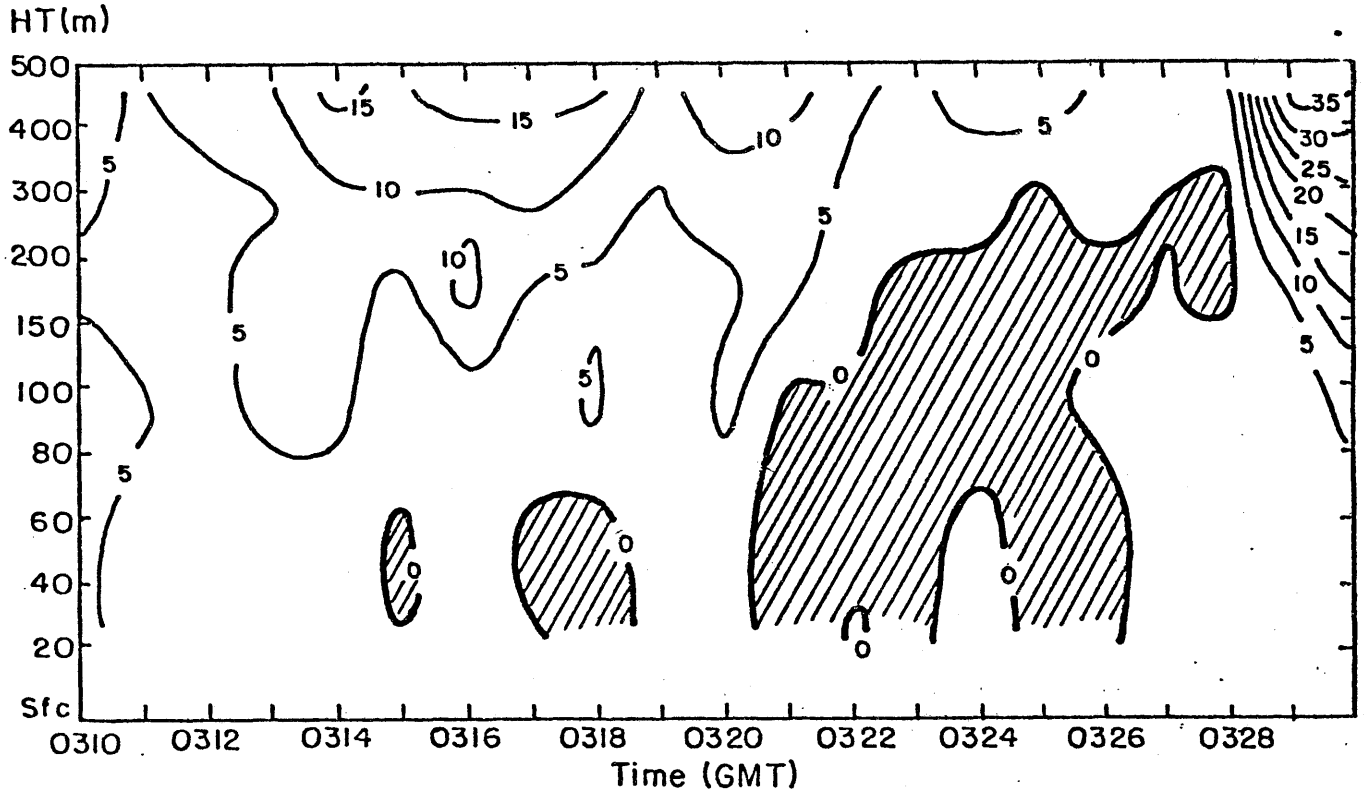

Figure 4.45

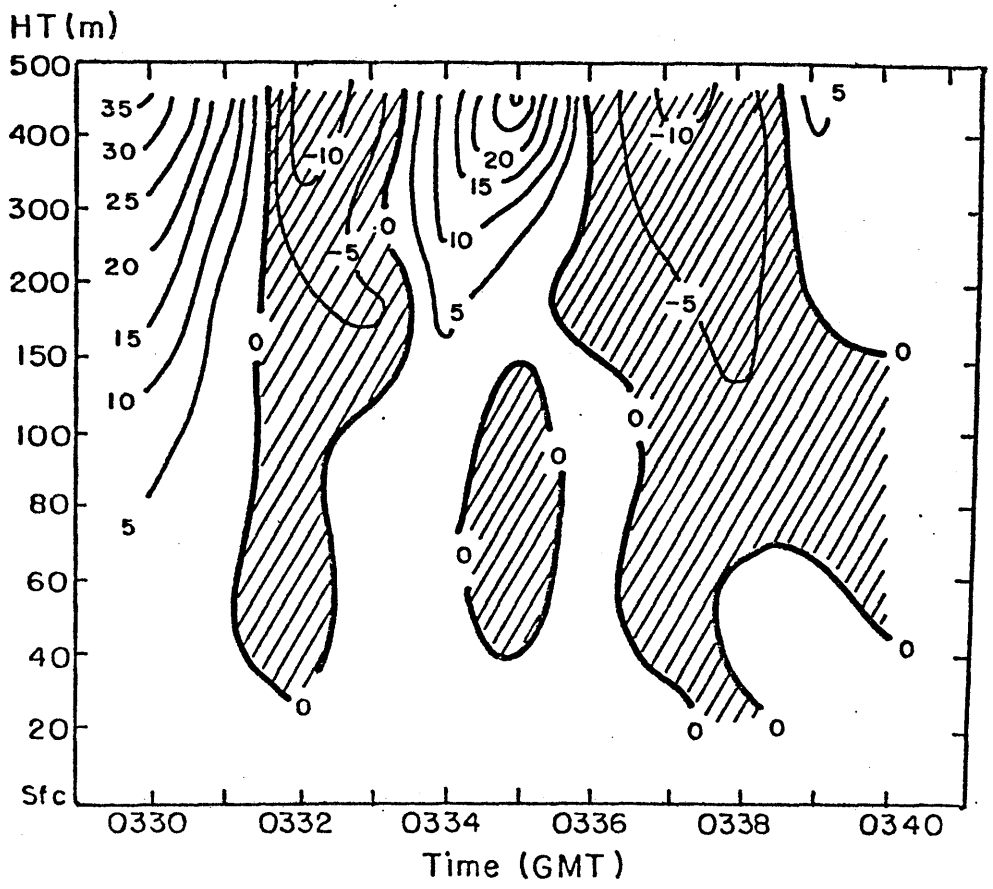

Figure 4.46

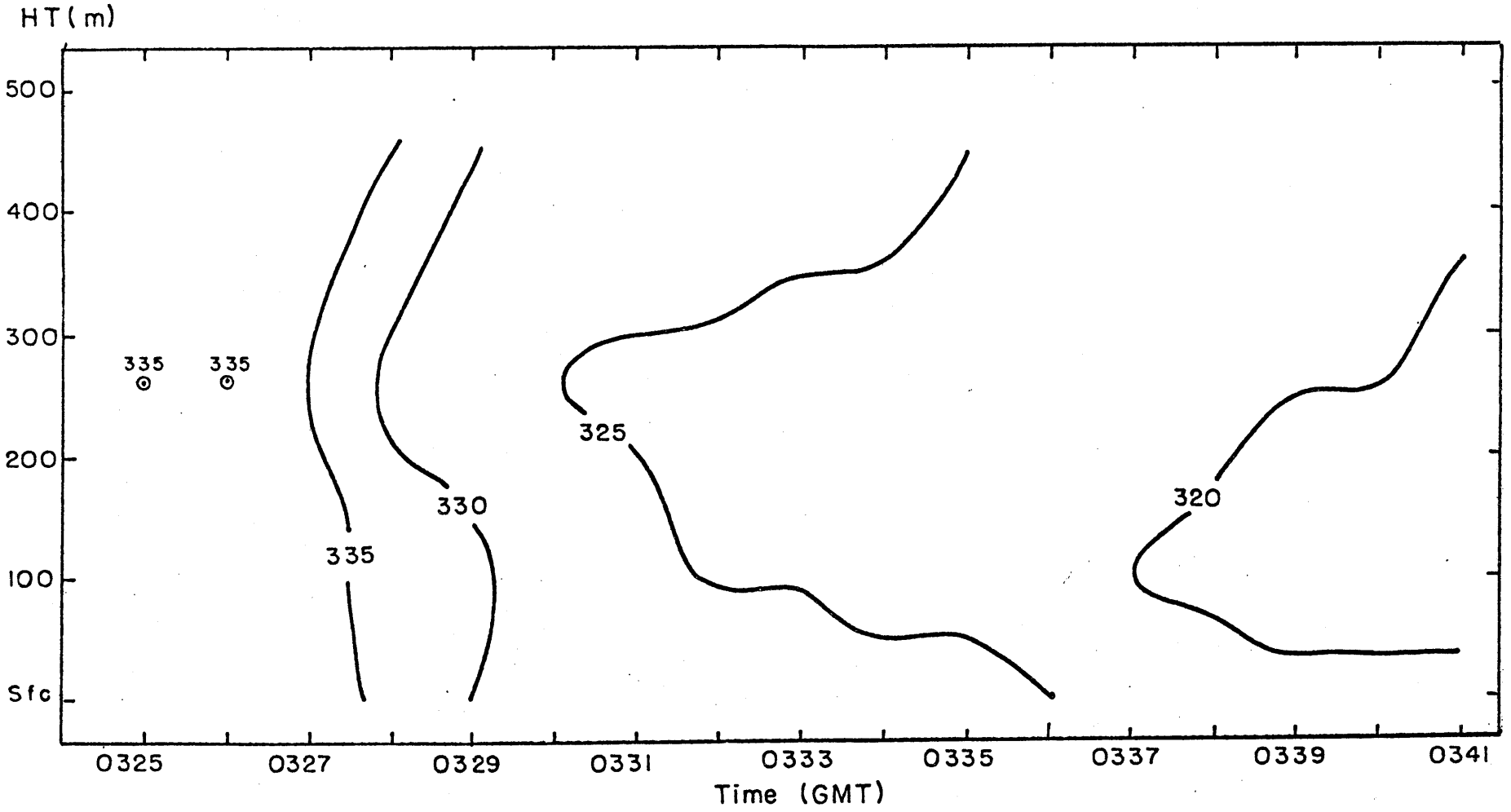
HT (m)
500
400
300
200
100
Sfc
335
335
335
330
325
320
0325
0327
0329
0331
0333
0335
0337
0339
0341
Time (GMT)

Figure 4.47

5. SIMILARITY MODEL

a. Description

To investigate the notion that the downburst may be a penetrative downdraft, a model was constructed using the conservation equations for penetrative thermals, developed by Emanuel (1981). These conservation equations, for mass, momentum, heat and water deficit were modified in order to incorporate distributed sources and analytically integrated to give the values for the thermals. These may be expressed as follows:

RADIUS:

$$R = R_o - \alpha Z \qquad (1)$$

BUOYANCY:

$$B = F/R^3 \qquad (2)$$

where

$$F = (N^2/4\alpha)(R^4-R_o^4)-M(((az+b)R^3-bR_o^3)+(a/4\alpha)(R^4-R_o^4))+F_o \qquad (3)$$

VERTICAL VELOCITY:

$$W^2 = -(1/16)N^2\alpha^{-2}R^2(1-(R^{-8}/R_o^{-8}))+(1/8)N^2\alpha^{-2}R_o^4R^{-2}(1-(R^{-4}/R_o^{-4}))$$
$$-(1/2)MbR_o^3\alpha^{-1}R^{-2}(1-(R^{-4}/R_o^{-4}))+(1/16)Ma\alpha^{-2}R^2(1-(R^{-8}/R_o^{-8}))$$
$$-(1/8)MaR_o^4\alpha^{-2}R^{-2}(1-(R^{-4}/R_o^{-4}))-(1/2)F_o\alpha^{-1}R^{-2}(1-(R^{-4}/R_o^{-4}))$$
$$+(2/7)M\alpha^{-1}R(aR_o\alpha^{-1}+b)(1-(R^{-7}/R_o^{-7}))$$
$$-(2/7)g\alpha^{-1}R(aR_o\alpha^{-1}+b)(1-(R^{-7}/R_o^{-7}))$$
$$-(1/4)a\alpha^{-2}R^2(M-g)(1-(R^{-8}/R_o^{-8}))+K_o(R^{-6}/R_o^{-6}) \qquad (4)$$

MIXING RATIO:

$$q = (Q/R^3) + L_c \qquad (5)$$

where

$$Q = (1/4\alpha)(c+a)(R^4-R_o^4) + Q_o \qquad (6)$$

In the above equations, M equals $L_vg/C_p\bar{T}_v$, where L_v is the latent heat of vaporization, g the acceleration of gravity, C_p the heat capacity for dry air at constant pressure and $\bar{T}_v$ represents a constant reference virtual temperature; N is a Brunt-Vaisala frequency defined $N^2 = (g/\theta^*)(d\theta^*/dz)$, where θ^* corresponds to the virtual potential temperature; L_c is the total water of the cloud which takes into account the vapor mixing ratio and liquid water content. The entrainment constant α is set equal to 0.285, which is

the value determined by Morton, Taylor, and Turner (1956) for dry thermals.

The main purpose of the model is to test the notion that environmental air with observed EPT can descend to the surface after mixing with cloudy air. Figure 4.40, shown previously, depicts the vertical profile of EPT over Tuttle for 0205 GMT (approximately one hour before the occurrance of the downburst). The air at the level at which the EPT was a minimum (430 mb) was chosen as the initial sample used in the integration. The Tuttle sounding (Figure 3.17) for 0205 GMT was assumed to best represent the vertical profile of the atmosphere over the mesonet at the time of the downburst. The surface air represented in this sounding was lifted reversibly to produce the cloudy environment of the thermal. From this, estimates of the cloud liquid water, total water content, temperature, virtual temperature and mixing ratios were available for input into the model.

The model consists of two layers. The top layer begins at the level of entrainment and extends down to the lifting condensation level. The second layer extends from this point to the surface. Vertical variations of the potential temperature, liquid water content and vapor mixing ratio of the cloud produced from the Tuttle sounding were fitted to straight lines in each layer as shown in Figures 5.1, 5.2, and 5.3 respectively. The vertical distributions of liquid water content and vapor mixing ratio are described by az+b

and cz+d. These variables show up in equations (3), (4), and (6). The thermals' initial buoyancy and water vapor content were specified at the top of the first layer from the Tuttle sounding. An arbitrary initial radius (R_o) was specified as well as values of F_o and Q_o which were calculated from equations (2) and (5), respectively. Also, an arbitrary initial vertical velocity was specified. At the top of the second layer, the integration was restarted, keeping all the thermal properties constant. This was necessary because of the different profiles of the potential temperature and the vapor mixing ratio in the boundary layer.

For each case, values of the variables used in the model were calculated at the corresponding depth. Thickness values were calculated from the Tuttle sounding using hydrostatics. The virtual temperature, liquid water content, vapor mixing ratio and total cloud water were all calculated since these variables were necessary in order to estimate the buoyancy and saturation deficit of the thermal. The thermals' radius, buoyancy, vertical velocity and vapor mixing ratio were first calculated using equation (1) - (6). The virtual temperature of the thermal is then given by $((B \cdot \overline{T}_v)/g)+T_{vc}$, where T_{vc} is the virtual temperature of the cloud. Given the virtual temperature of the thermal, the thermals' temperature is calculated. The saturation vapor mixing ratio of the thermal was computed using the Clausius-Clapeyron equation. The condensation temperature for the thermal was needed for the calculation of its equivalent

potential temperature. This condensation temperature was determined through an iterative scheme to a desired small difference in entropy from the thermals' initial state to its condensation level.

Once started, the model was run until the thermal saturated, its vertical velocity became equal to zero, or it reached the surface.

b. Entrainment of Environmental Air of Low EPT

As mentioned earlier, the environmental air at the 430 mb level, over Tuttle, was initially entrained into the cloud that was developed using the data from the Tuttle sounding from 0205 GMT. This environmental air represented the state of the initial thermal at this level. Some of the thermals' initial properties included a buoyancy of approximately -0.210 ms-2; temperature of 253.15 degrees K; relative humidity of 8%; equivalent potential temperature of 322.8 degrees K, and an initial vertical velocity (W_o) of 0.0 ms^{-1}.

Several choices were made for the cloud distribution of liquid water. The first case considered was one in which the liquid water results from pseudo-adiabatic ascent, with no fall-out permitted. As a second experiment, the pseudo-adiabatic liquid water content of the cloud was redistributed evenly between the level of entrainment and the surface, yielding a value of 4.59 gm kg^{-1}. In order to take into account depletion of cloud water by precipitation, the effects of different constant cloud liquid water content were also tested. The model was run with liquid water contents of 4.0, 3.0, 2.0 and 1.0 gm

kg^{-1}. Values for liquid water content and total water content at the point of the thermals' initial release are listed in Table 5-1 for various distributions of cloud liquid water.

Cloud Distribution of Liquid Water	Liquid Water Content	Total Water Content
Pseudo-Adiabatic	10.80	13.60
4.59 C	4.59	7.39
4.00 C	4.00	6.80
3.00 C	3.00	5.80
2.00 C	2.00	4.80
1.00 C	1.00	3.80

Table 5-1. Values of liquid water content and total water content at level of entrainment. 'C' refers to constant. Values are in gm kg^{-1}.

Figure 5.4 shows the maximum fall depth of the unsaturated thermals for several cloud liquid water distributions. The 'X''s in the figure refer to the 'critical' values of R_o, below which the thermal became saturated somewhere in its fall. The maximum fall depth attained, approximately 4800 m, was by the thermal of critical radius, R_c, released into the pseudo-adiabatic cloud. When the cloud liquid water content was distributed evenly through the cloud, the maximum fall depth, when compared with that of the pseudo-adiabatic

cloud, decreased. Further decreases in maximum fall depth occurred when the cloud water content was reduced. The fall depth decreased with increasing initial radius, except when the constant cloud liquid water content was less than about 1.5 gm kg-1. Figure 5.5 shows the buoyancy as a function of height for the thermals of initial radius R_c for various cloud liquid water distributions. For the curves corresponding to constant cloud liquid water content, there is an increase in the rate at which the buoyancy increases, as the constant cloud liquid water is decreased. The rate of increasing buoyancy is reflected in the decrease of the maximum fall depth of the thermals of initial radius R_c. The greater amount of negative buoyancy depicted by the curve corresponding to the psuedo-adiabatic cloud is due to the rapid entrainment, and evaporation of the high liquid water content of the cloud. When the constant cloud liquid water content was less than 1.5 gm kg-1, the rate at which the buoyancy increased, for increasing R_o, decreased.

The maximum vertical velocities attained for unsaturated thermals and their associated cloud liquid water distributions are shown in Figure 5.6. The 'X''s again correspond to R_c. The maximum vertical velocity (-17.0 ms^{-1}) attained was for the thermal of initial radius R_c released into the pseuod-adiabatic cloud. With decreasing cloud liquid water content, maximum vertical velocities also decreased, in accord with the smaller negative buoyancies.

The profiles of the vertical velocity as a function of height for the thermals of initial radius Rc for several cloud liquid water contents are shown in Figure 5.7. The tendency for decreasing vertical velocity with decreasing cloud liquid water distributions is most evident. The velocities fall off from their maxima at substantial rates, due to the rapid increase in buoyancy below their peak velocity level.

Figure 5.8 shows the results of increasing the initial vertical velocity of the thermal while holding its initial radius constant. This was done for the thermal of initial radius Rc released into the pseudo-adiabatic cloud. The thermals' critical radius, R_c, is independent of the initial vertical velocity. Also shown is a plot of the maximum fall depth. There is only a slight increase in both the fall depth and maximum vertical velocity with increasing initial velocity. None of the other parameters are affected by the change in the initial vertical velocity. Regardless of the changes experienced by the thermal, these large initial vertical velocities are rather unrealistic.

The thermals' EPT is plotted as a function of height in Figure 5.9 in which the traces correspond to the thermals of initial radius R_c and for various cloud liquid water distributions. The rate at which the EPT increased with decreasing cloud liquid water content was due in part to the fact that the R_c of the thermals decreased with decreasing cloud liquid water. For all cases, the EPT of the

thermal showed a rise through its descent, which indicated that the thermal was being diluted, as it must in this model of turbulent convection.

c. Thermal Re-Initialized by New Environmental Parameters

It is obvious from the previous section that in no case did the thermal reach the surface. The thermal was initialized using environmental air, represented by the Tuttle sounding, that was entrained into the cloud. This entrained air had an EPT of approximately 322 degrees K, several degrees warmer than the minimum EPT which was actually recorded over the mesonet. For this reason we feel that the Tuttle sounding was not entirely representative of the environment in which the downburst formed. In order to account for the potentially colder air that was probably present aloft, we reinitialized the thermal with an EPT of 315 degrees K. Other initial conditions given to the thermal were: a buoyancy of -0.406 ms^{-2}; a vapor mixing ratio of 0.05 gm kg^{-1}; a saturation vapor mixing ratio of 1.12 gm kg^{-1}; a relative humidity of approximatelyl 5% (3% lower than the relative humidity of the initial thermal in the first case where the actual environmental air was entrained) and an initial vertical velocity of 0.0 ms^{-1}. 0.05 gm kg^{-1} was chosen as the value of the vapor mixing ratio because this low value was observed from the Tuttle sounding close to the entrainment level of 430 mb.

The same cloud properties that were used for the set of runs undertaken in the previous section were used here with the new initial conditions.

The runs which were made for the thermal with an initial EPT of 315.4 degrees K yielded qualitatively the same results as those of the previous section. There were, however, quantitative differences. Figure 5.10 shows the maximum fall depth of the unsaturated thermals for various cloud liquid water distributions. When compared with Figure 5.4, it is evident that the maximum fall depth attained by the re-initialized thermal is much greater. The thermal of initial radius R_c released into the pseudo-adiabatic cloud attained a fall depth of within 250 m of the surface. This is approximately 1500 m more than its counterpart in Figure 5.4. The maximum vertical velocity of unsaturated thermals and their corresponding cloud liquid water distributions are plotted in Figure 5.11. The velocities are approximately twice as large as those which are shown in Figure 5.6. The maximum vertical velocity attained in these runs is -28.5 ms-1, achieved by the thermal of initial radius R_c in the pseudo-adiabatic liquid water distribution. Figure 5.12 shows the results of increasing the initial vertical velocity of the thermal while continuing to hold its radius constant. This was run for the thermal of initial radius R_c = 6286 m and the pseudo-adiabatic cloud liquid water distribution. Only when the initial vertical velocity was -20.0 ms-1 did the thermal manage to

reach the surface, but as mentioned previously, these large initial vertical velocities are questionable. Figures 5.13 and 5.14 show plots of buoyancy and vertical velocity respectively as functions of height for the thermals of initial radius R_c for various cloud liquid water distributions. When compared with Figures 5.5 and 5.7, the only qualitative discrepancy which appears is the decrease in the buoyancy below a depth of -5900 m for the cloud with a pseudo-adiabatic liquid water distribution. This is due to the assumed neutral stratification of the boundary layer. Figure 5.15 shows EPT as a function of height for the thermals of initial radius Rc.

d. Splitting of the Thermal

The results so far show that the magnitude of the negative buoyancy decreases and actually changes sign as the thermal expands during its descent. This is due to the decrease of the surface area to volume ratio, and thus to the rate of entrainment of liquid water, as the thermal descends. Emanuel (1981) pointed that this would lead to reversed momentum generation near the thermals' unsaturated core and this in turn would lead to the break up of the thermal into smaller entities. This idea is incorporated in the model by allowing the thermal to split at the level at which the buoyancy becomes positive. At this level, the volume of the thermal is split and the thermals' new radius, R_o*, takes the value of R_o. Also, Fo and Qo are given new values which incorporate R_o*, the current buoyancy and

vapor mixing ratio and total cloud water content at that level. K_o is replaced by the current value of W^2 at that level. The temperatures and vertical velocity, as well as the vapor mixing ratios of the thermal are unchanged through the splitting process. The linear equations representing the liquid water content and vapor mixing ratio of the cloud are altered to fit the re-initialization.

The splitting principal is incorporated by splitting the volume of the thermal once in half at the level of neutral buoyancy. It was found that for the thermal with the initially lower EPT, greater fall depths were attained. For this reason, we use this initial thermal. A set of runs are then made in which the volume of the thermal is split in thirds (again, only one split is allowed). It was observed that the thrice split thermal fell somewhat further than did the thermal which was split in half. For both sets of runs, the buoyancy of the split thermal continued to increase through its descent.

We decided to follow thermals of various arbitrary sizes formed from the splitting process. The new initial radii of these thermals are denoted by R_o*. Figure 5.16 shows the results of this experiment. It is found that the thermals of R_o* between 960 m and 1080 m, within the cloud in which the liquid water distributions was kept constant at 4.59 gm kg^{-1}, were able to reach the surface. The large amount of cloud liquid water available to the descending thermal in the boundary layer aided the evaporation which enabled the thermal to attain this depth. The vertical velocities upon impact

with the ground were less than or equal to 3.0 ms-1. The diameter of the thermals at this point varied between 3200 m and 3400 m. As the cloud liquid water distribution is decreased, the thermals fall depth also decreases. For the cloud in which the liquid water distribution is pseudo-adiabatic, the fall depth decreases as R_o* decreases. These runs were made for the thermals in which the initial radius was R_c, represented by the 'X''s in Figure 5.10.

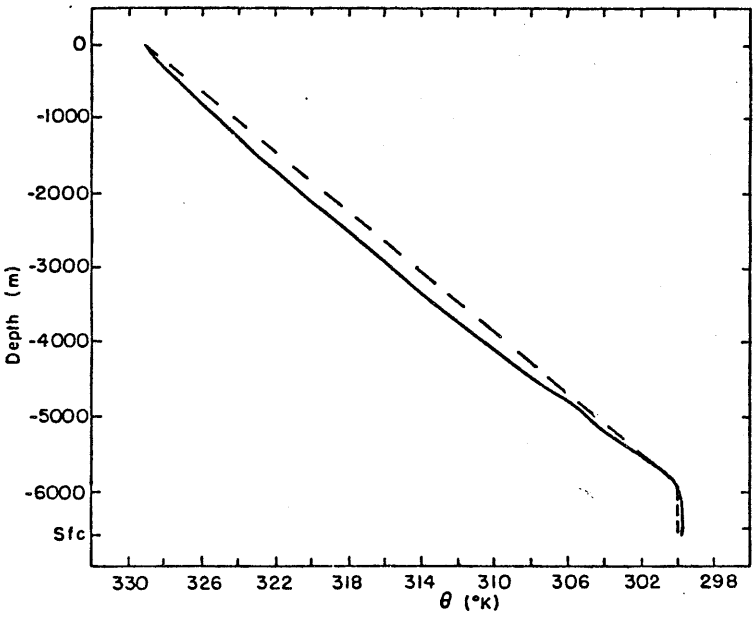

Figure 5.1

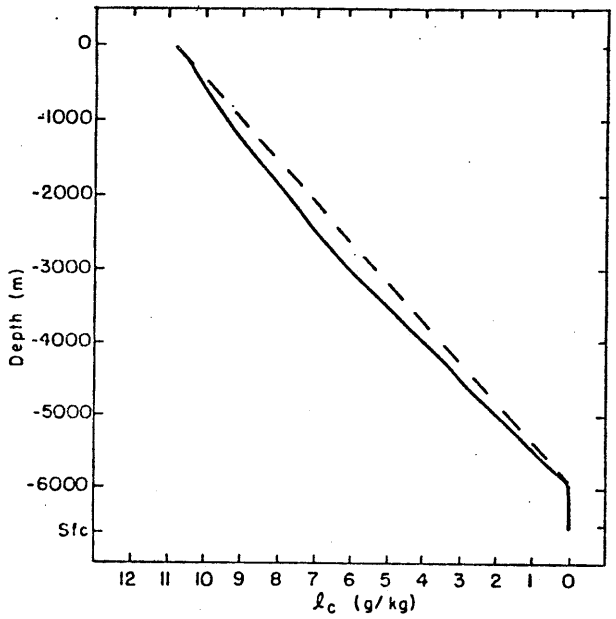

Figure 5.2

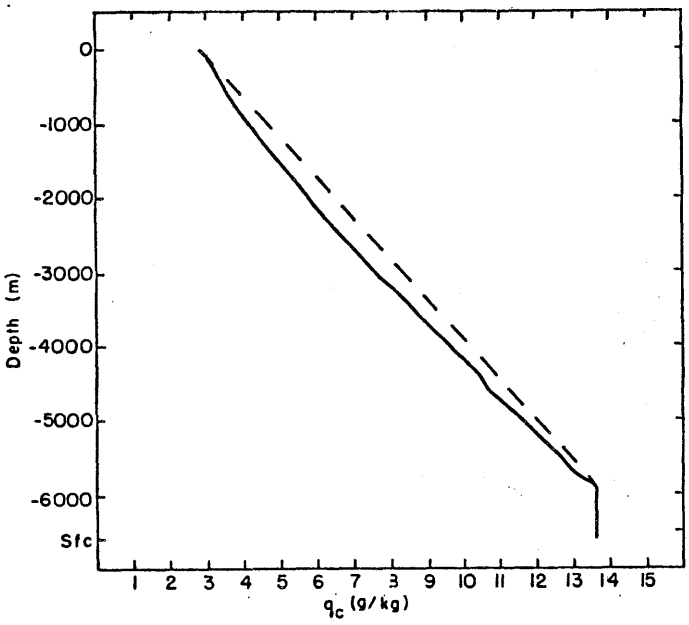

Figure 5.3

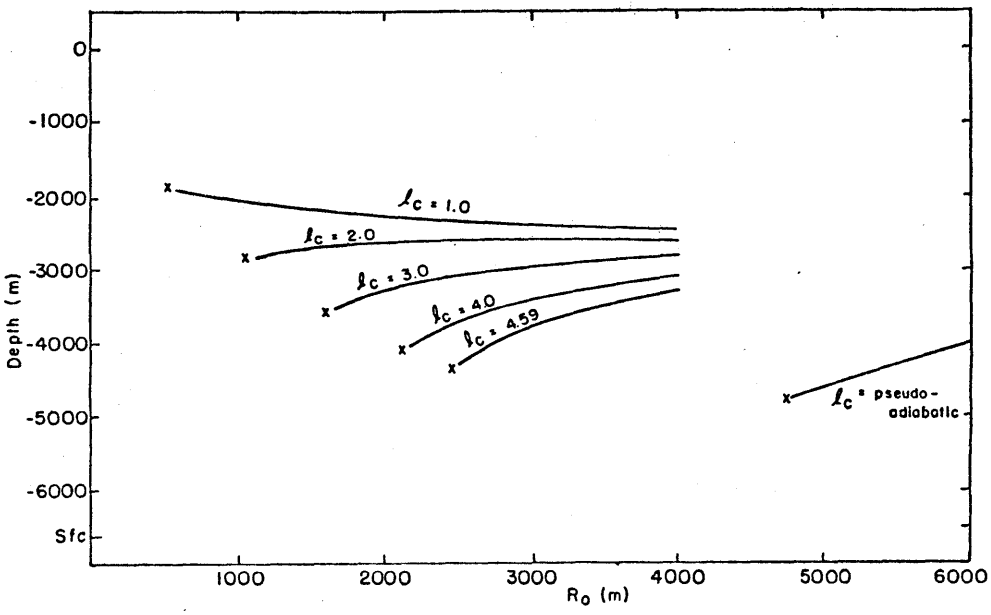

Figure 5.4

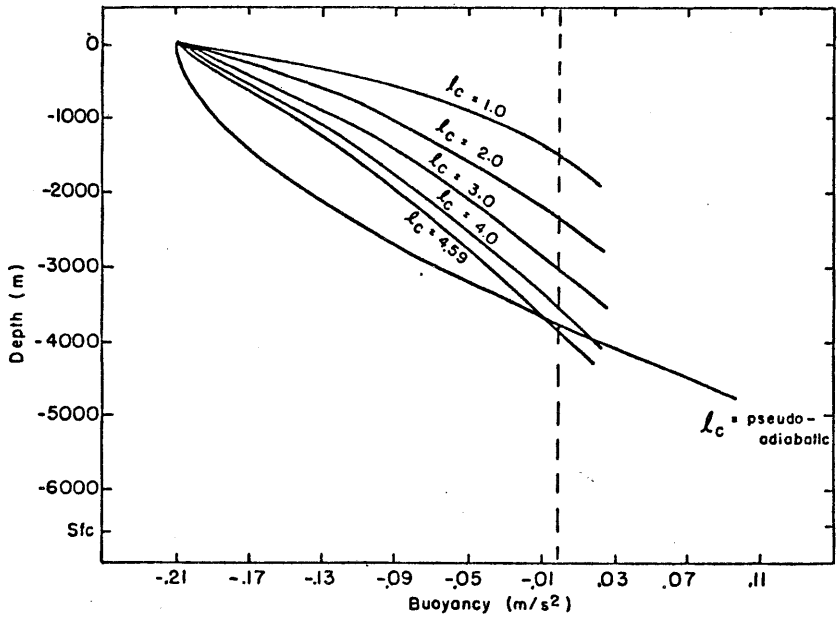

Figure 5.5

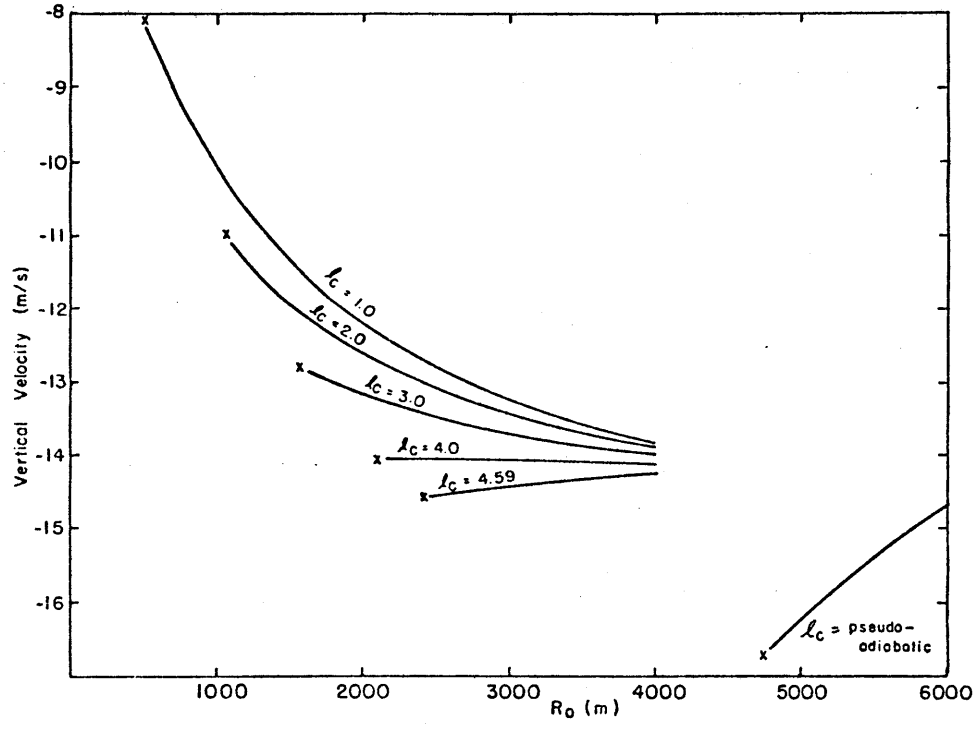

Figure 5.6

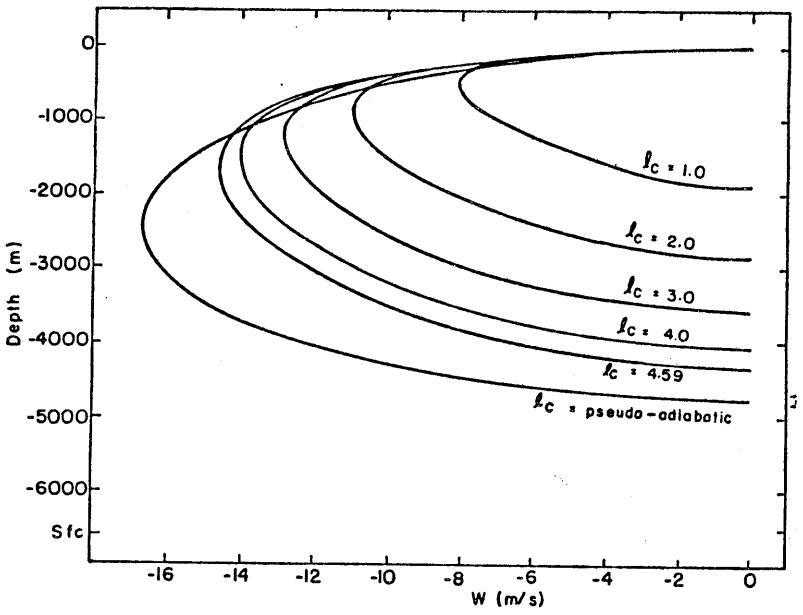

Figure 5.7

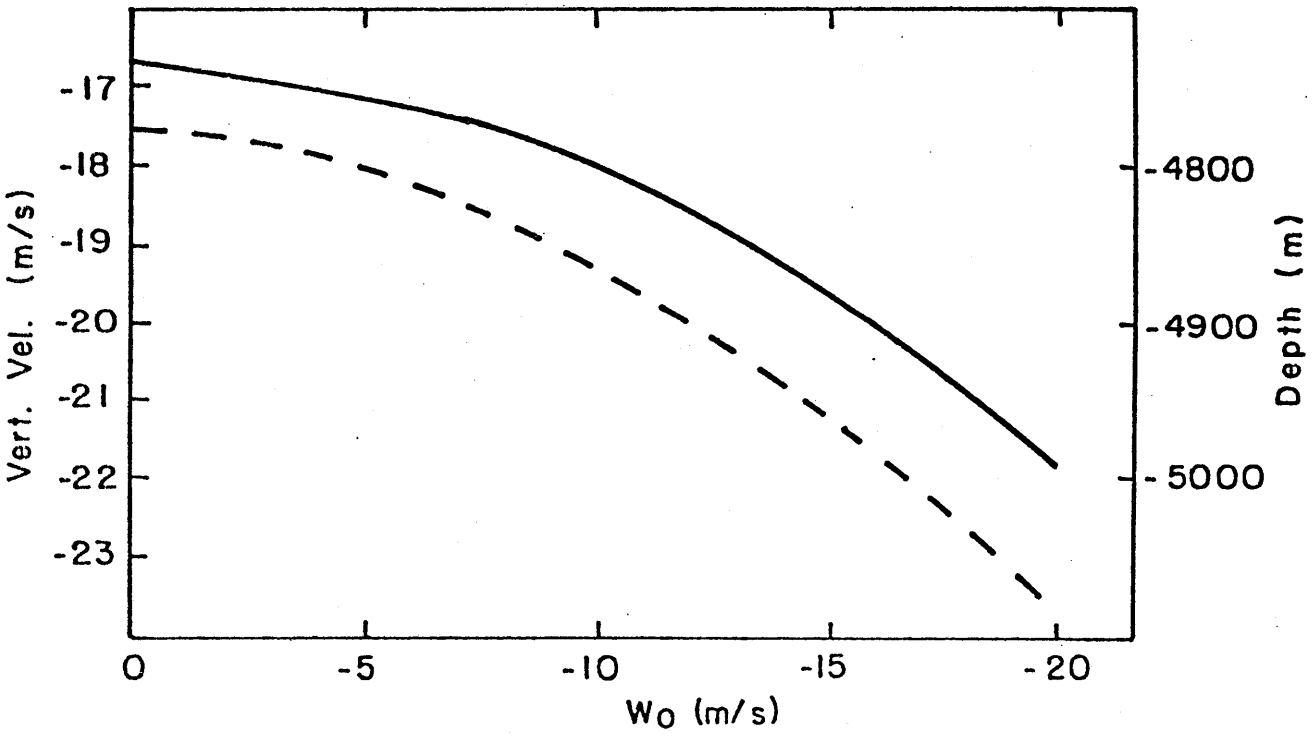

Figure 5.8

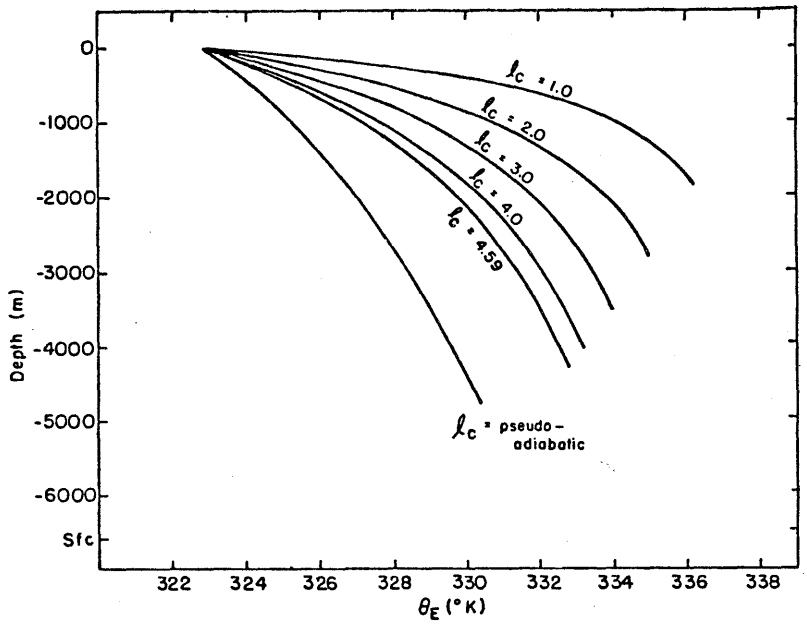

Figure 5.9

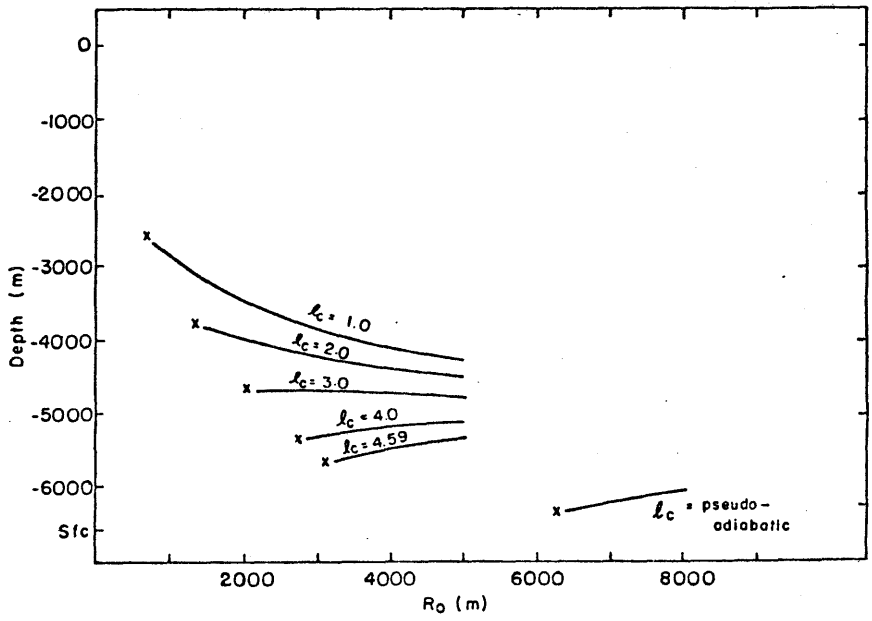

Figure 5.10

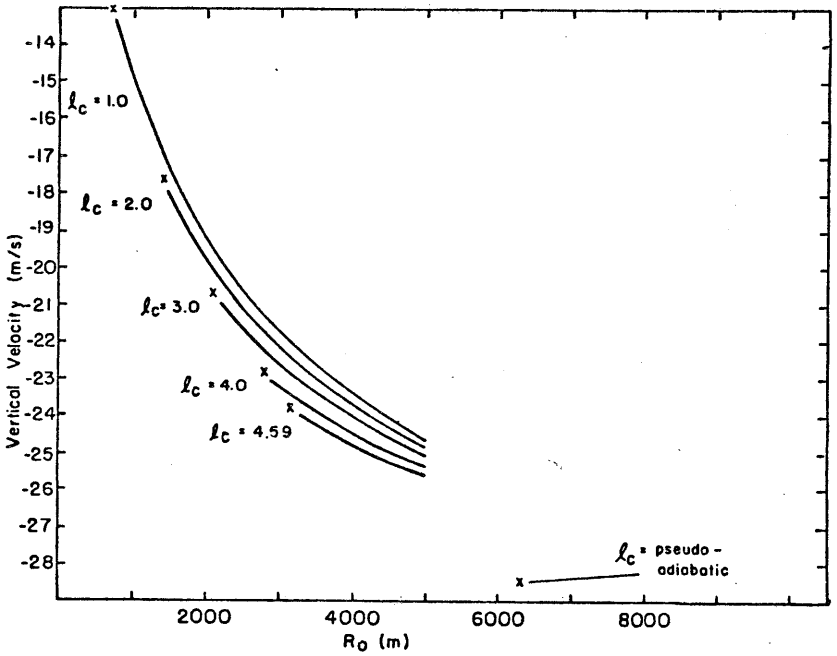

Figure 5.11

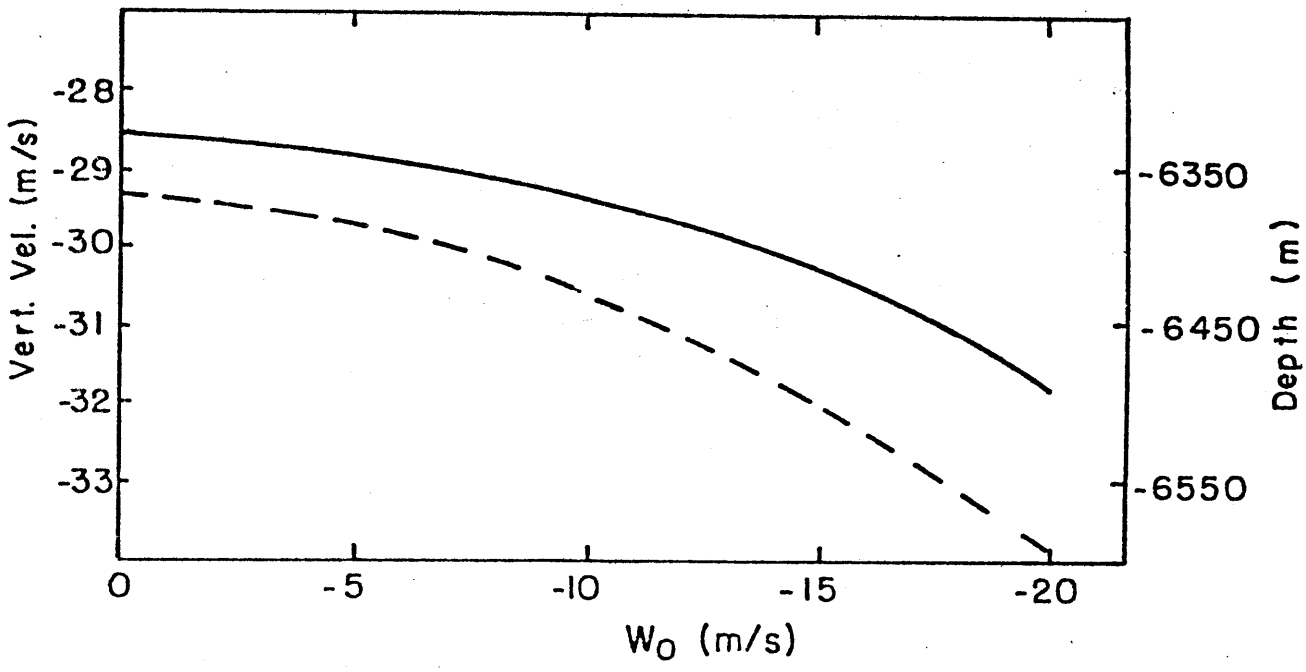

Figure 5.12

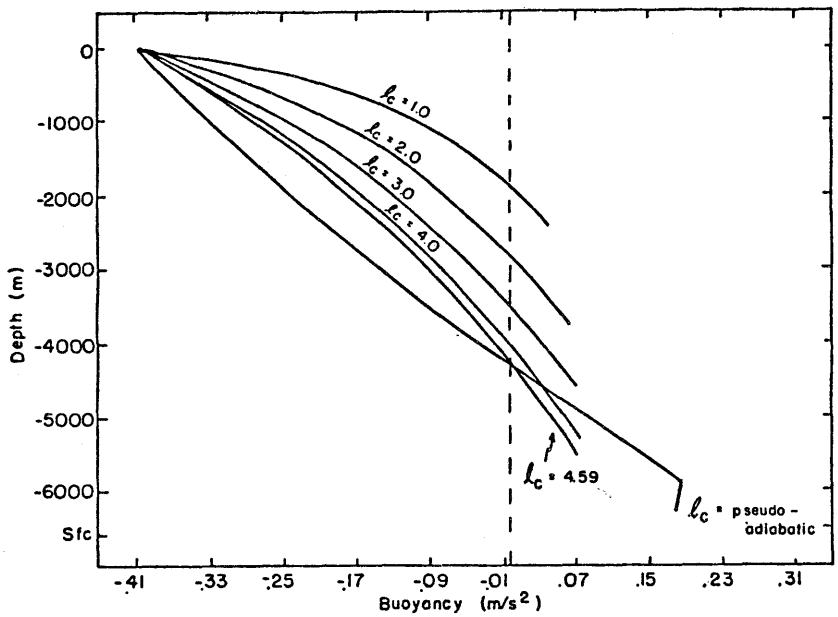

Figure 5.13

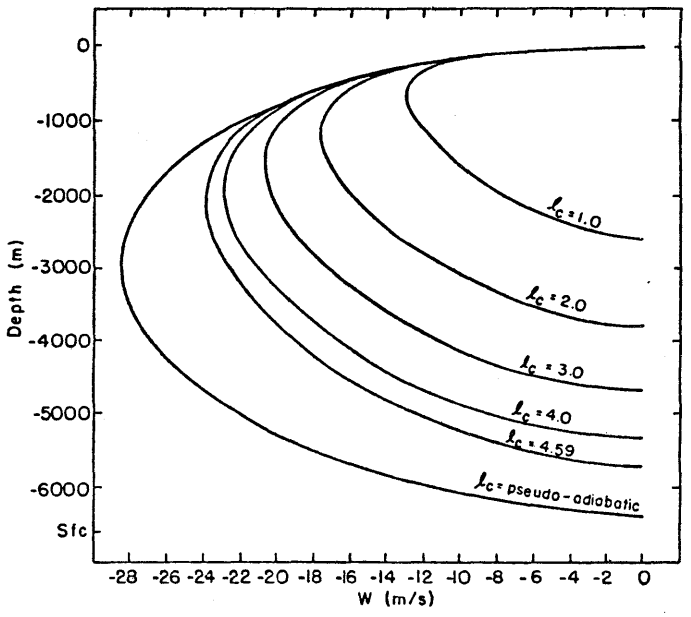

Figure 5.14

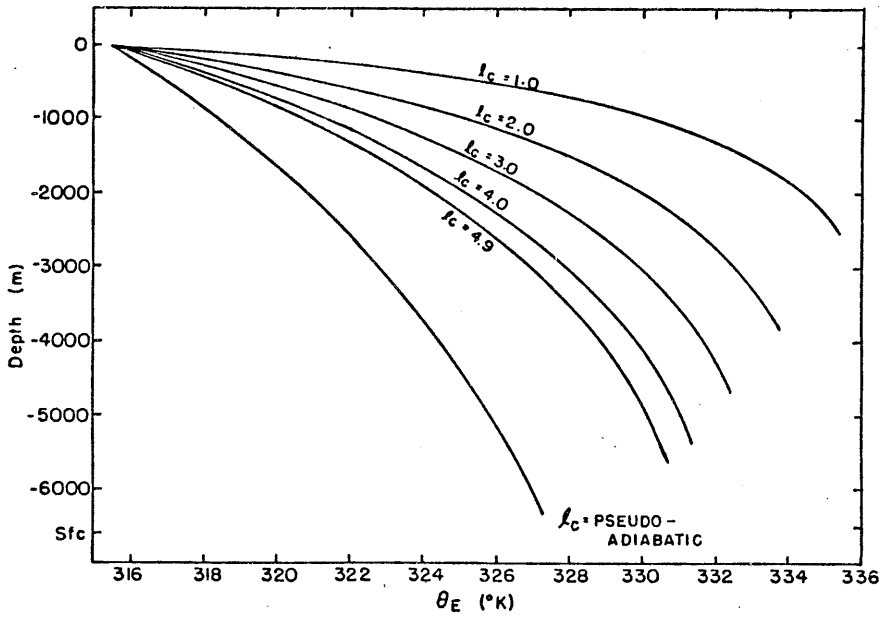

Figure 5.15

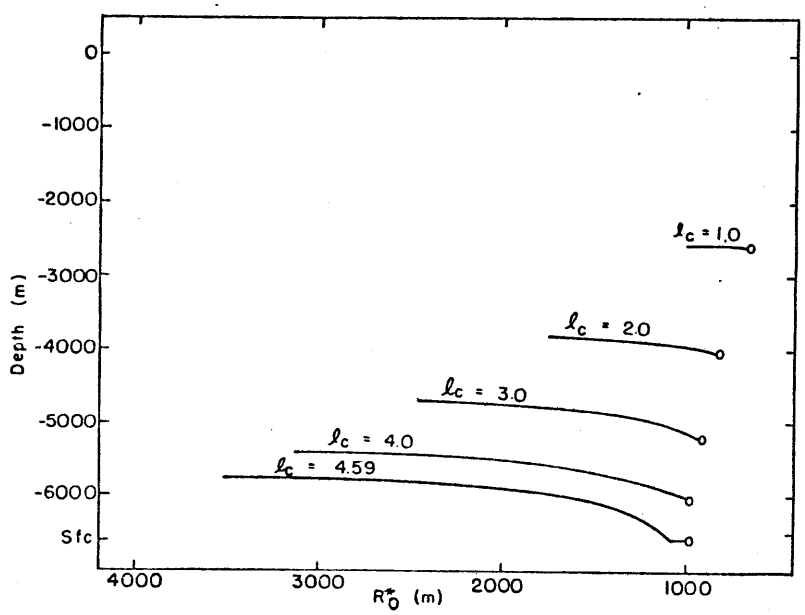

Figure 5.16

6. SUMMARY

The analysis of this case shows that at least one downburst occurred within the mesonet which surrounded Oklahoma City on April 1981. The overall synoptic situation seemed conducive to the well organized convective activity which developed and moved into the Oklahoma City area at about 0300 GMT on the 14th.

The observations over the mesonet were instrumental in detecting the small scale thermodynamic and kinematic perterbations associated with the downburst. The major velocity and EPT perterbations appeared to move radially into the mesonet and lasted for only a matter of minutes. The KTVY-Tower analysis showed rather clearly that a series of possible gust fronts and a cold front passed through. Strictly by definition, it is possible to state that a downburst did not exist near the tower, but major distortions, including high winds in the analyzed fields over the northwestern quadrant of the mesonet, seemed to indicate that a downburst occurred in this area. The anomalously low values of EPT accompanying the apparent downburst can not be explained by simple horizontal advection. Analysis of upper air data using all available soundings, indicate that the low values of EPT, detected by the surface mesonet, originated at mid-tropospheric levels. This potentially cold air was no doubt transported to the surface by the downburst(s).

The similarity model, which represents the downburst as an unsaturated penetrative thermal, was used to investigate the downward transport of air from upper levels. A cloud was formed by reversibly lifting the surface air represented in the Tuttle sounding. This cloud was assumed to be the environment of the penetrative thermal. Air of the lowest EPT which was found at the 430 mb level in the sounding was used to specify the initial conditions of the thermal.

The model was run for various cloud liquid water distributions. It was shown that the thermal of initial radius R_c (the critical radius above which the thermal remained unsaturated through its descent), released into the pseudo-adiabatic cloud, attained the maximum fall depth. Runs were also made in which the cloud liquid water was distributed evenly from the level of entrainment of environmental air to the surface. Experiments were also run in which the effects of precipitation were accounted for by reducing the cloud liquid water. It was shown that this decreased cloud liquid water content resulted in a decrease in the fall depth of the thermal, presumably due to decreased evaporation. These results are quite insensitive to the initial fall velocity of the thermal.

The rate at which the thermals' buoyancy increases is generally faster for smaller cloud liquid water contents. Again, this showed the direct effect of evaporation on the thermal. The vertical velocities are affected simiarly. The EPT traces are qualitatively similar to the traces corresponding to the buoyancy, indicating dilution during descent.

We feel that the downburst actually originated west of the mesonet where cooler air was present at mid-levels. On this premise, we adjusted the initial conditions of the thermal to reflect the EPT of 315.4 degrees K (approximately 6 degrees K cooler than the previous thermals'), which corresponded to the EPT recorded by the surface mesonet during the time of the downburst. Similar runs were made using the new initial thermal with the same cloud properties. The results are qualitatively the same when compared with those of the previous runs, but there are differences in the magnitudes of the results. The maximum fall depths are generally greater in the second set of runs, coming to within 300 m of the surface. The maximum vertical velocities of the descending thermals were approximately twice as strong as those of the first set of results.

The thermal initialized with the lower value of EPT attained the greatest fall depth but still fell short of reaching the surface. Following the ideas outlined in Emanuel (1981), we split the thermal into smaller entities at the level at which the buoyancy changed sign. The split thermal reached the surface in the case in which the maximum amount of cloud liquid water was available in the boundary layer. The increased evaporation enabled the thermal to reach the surface. The vertical velocities associated with these thermals, at the point of contact with the surface, were, however, rather weak.

The penetrative downdraft mechanism has difficulty accounting for some of the properties of the observed downburst in this case. It seems more likely that evaporation of falling precipitation into a relatively undiluted, unsaturated downdraft is responsible for the large velocities and low temperatures observed at the surface. There remains the problem of explaining the relaltively small space and time scales of the downburst. This, together with a description of the detailed dynamical behavior of downbursts, constitute possible topics for further research.

ACKNOWLEDGEMENTS

I first want to express my appreciation and thanks to Dr. Kerry Emanuel for his patience and guidance during my course of research here at M.I.T.

I thank Dr. Frederick Sanders for his fine teaching, in the synoptic field of meteorology, which helped me in my research.

Thanks go out to William Bumgarner, J.T. Lee, Peter Ray and Les Showell, all from the National Severe Storms Laboratory, for the data that they supplied which enabled the research for this thesis to be undertaken.

Many thanks to Marilyn Wolfson for her support and helpful discussions.

Special thanks go out to Bradley Colman and Frank Colby for what they have given of themselves during my stay at M.I.T.

I Thank Stephen Garner and Thomas Nehrkorn for their helpful conversations.

Final thanks are to my parents, for without their support none of this work would have been possible.

REFERENCES

Byers, H.R., and R.R. Braham, Jr., 1949: The thunderstorm, govt. printing office, Washington D.C., 287 pp.

Emanuel, K.A., 1981: A similarity theory for unsaturated downdrafts within clouds. J. Atmos, Sci. 38, 1541-1557

Forbes, G.S., and R.M. Wakimoto, 1981: A concentrated outbreak of tornadoes, downbursts, and microbursts on 6 August 1977. Submitted to Mon. Wea. Rev.

Fujita, T.T., 1971: Proposed characterization of tornadoes and hurricanes by area and intensity. SMRP Research Paper 91, University of Chicago.

_____, 1976: Spearhead echo and downburst near the approach end of a John F. Kennedy Airport runway, New York City. SMRP Research Paper 137, University of Chicago.

_____, 1978: Manual of downburst identification for project NIMROD. SMRP Research Paper 156, University of Chicago.

_____, 1981: Tornadoes and downbursts in the context of generalized planetary scales. J. Atmos. Sci., 38, 1511-1534.

_____, and H.R. Byers, 1977: Spearhead echo and downburst in the crash of an airliner. Mon. Wea. Rev., 105, 129-146.

_____, and F. Caracena, 1977: An analysis of three weather-related aircraft accidents. Bull. Amer. Met. Soc. 58, 1164-1181.

Morton, B.B., G. Taylor and J.S. Turner, 1956: Turbulent gravitational convection from maintained and instantaneous sources. Proc. Roy. Soc. London,. A234, 1-23.

Wolfson, M.M., 1983: Doppler radar observations of an Oklahoma downburst. Master of Science Thesis, Massachusetts Institute of Technology.